Dynamic Analysis of Spatial Structures

Session Organizer: Su-Duo XUE (Beijing University of Technology)

Plenary Lecture
Analysis and design of materials and structures for attenuating vibration & acoustic response
Gregory M. HULBERT, E. M. DEDE, C. YILMAZ, Z.-D. MA, Noboru KIKUCHI (Univ. of Michigan)

Keynote Lecture
Seismic risk analysis of large lattice dome supported by buckling restrained braces
Shiro KATO, Shoji NAKAZAWA (Toyohashi University of Technology)*

A parameter study on dynamic buckling of spatial arch trusses under seismic action
Hai-Wang LI, Jian-Xian LI, Fei ZHI, Fu MA, Dong-Qi QIN (Taiyuan University of Technology)*

Static elasto-plastic analysis of long-span rigid spatial structures under vertical earthquake
Yongfeng LUO (Tongji University), Muwang YANG (East China Normal University)*

Problems in the research of multi-dimensional and multi-support seismic analysis
Pengfei ZHAO, Jihong QIAN, Rongwei TANG (China Academy of Building Research)*

Dynamic field test on elliptical suspen-dome
Jie QIN, Bin SHEN, Guoli LI (Beijing Building Construction Research Institute)*

Simulating blast effects in steel lattice structures
Emily LEIGH, Christopher EARLS (Cornell University)*

Dynamic analysis of single layer lattice shell with BRBs
Xiuli WANG, Jiyun CHEN, Chang WU (Lanzhou University of Technology)*

Nonlinear dynamic analysis of space frame structures
Chung-Yue WANG (National Central University, Taiwan), Ren-Zuo WANG (National Center for Research on Earthquake Engineering, Taiwan)*

Dynamic behaviors of two large spatial structures
Jinzhi WU, Yigang ZHANG, Xiaobing GENG (Beijing University of Technology)*

Investigation into the dynamic behaviour of double layer tensegrity systems
Behzad SHEKASTEHBAND, Karim ABEDI (Sahand University of Technology, Tabriz)*

Keynote Lecture
Advances on seismic isolation in spatial structures
Su-Duo XUE, Xiong-Yan LI (Beijing University of Technology)*

Dynamic analysis of cable roof networks under transient wind
Sayed Ali GHAFARI OSKOEI, Ghyslaine McCLURE (McGill University)*

Wind-induced responses of Beijing National Stadium
Qing-Shan YANG, Yu-Ji TIAN (Beijing Jiaotong University)*

Theoretical analyses for wind vibration response of reticulated shell structures
De-min WEI, Jian-feng BIAN (South China University of Technology)*

For multiple-author papers:
Contact author designated by *
Presenting author designated by underscore

Proceedings of the 6th International Conference on
Computation of Shell and Spatial Structures
IASS-IACM 2008: "Spanning Nano to Mega"
28-31 May 2008, Cornell University, Ithaca, NY, USA
John F. ABEL and J. Robert COOKE (eds.)

Analysis and design of materials and structures for attenuating vibration and acoustic response

Gregory M. HULBERT*, Ercan DEDE, Cetin YILMAZ, Zheng-Dong MA, Noboru KIKUCHI

*University of Michigan
Ann Arbor, Michigan 48109-2125
Hulbert@umich.edu

Abstract

The ability to design to design and manufacture materials with complex structure and novel material response offers the opportunity to consider the control of the dynamic response of structures. This problem is well suited for a multi-scale approach in which the material characteristics and material layout are considered as part of the structural analysis and design problem.

Three approaches towards the design of band-gap materials and structures are presented and representative materials and structures are shown. In addition to material design employing Bragg scattering, the use of compliant mechanisms in sandwich structures is demonstrated. Lastly, inertial amplification is shown to provide a third method of inducing band-gap phenomena into materials and structures using embedded amplification mechanisms.

1. Introduction

The importance of designing structures with desired dynamic response characteristics is increasing, particularly in the ground vehicle industry. This is driven by customer demands for quiet vehicles and for well-tuned ride characteristics. In addition, safety requirements also are impacted by the dynamic response of materials, especially for military vehicles. Competing with these requirements is the continuing need to reduce the weight of vehicles to improve fuel economy. To this end, significant research has been directed towards the design of new composite materials.

Of particular focus in the present work is to construct systematically materials that enable structures to have designed vibration or acoustic response (spectral gaps) or to have significantly reduced response in desired frequency bands. Using a multi-scale approach, the desired structural response can be obtained by careful design of the material response.

Spectral gaps in the band structure of periodic media have been an ongoing research endeavor since the 1950s. In the last decade, there has been growing interest in computing and designing the phononic band structure of 2D and 3D periodic systems comprising various materials. Of particular focus has been obtaining complete phononic band gaps, which forbid the propagation of elastic or acoustic waves regardless of mode or wave vector. Practical applications of these systems include mechanical filters, sound and vibration isolators, and acoustic waveguides.

The two different widely published means of generating phononic band gaps in periodic media are Bragg scattering and local resonances. In Bragg scattering, a gap appears due to destructive interference of the wave reflections from the periodic inclusions within the media. Band gaps can also be generated via local resonators, which impede wave propagation around their resonance frequencies. A third approach towards phononic band gap generation is possible in which the effective inertia of the wave propagation medium is amplified via embedded amplification mechanisms. We classify this alternate approach as inertial amplification.

These three approaches towards the design of band-gap materials and structures are presented and representative materials and structures are shown. In addition to material design employing Bragg scattering, the use of compliant mechanisms in sandwich structures is demonstrated as a novel application of local resonances. Lastly, inertial amplification is shown to provide a third method of inducing band-gap phenomena into materials and structures using embedded amplification mechanisms.

2. Bragg scattering

Wave propagation in heterogeneous media is dispersive, i.e., the media causes an incident wave to decompose into multiple waves with different frequencies. A medium with periodic heterogeneity has distinct frequency ranges in which waves are either effectively attenuated or allowed to propagate. These frequency ranges are referred to as *band-gaps* (or stop bands) and *bands* (or pass bands), respectively, and are attributed to mechanisms of wave interference within the scattered elastic field, known as Bragg scattering. From a practical perspective, it has been shown that under certain conditions bounded structures formed from periodic materials can exhibit similar frequency-banded wave motion characteristics. By controlling the layout of constituent material phases and the ratio of their properties within a unit cell, a periodic composite can be designed to have a desired frequency band structure (the size and location of stop bands and pass bands). Figure 1 depicts various designs of a bi-material unit cell that exhibit different frequency band-gap responses. In Hussein *et al*. [1], an optimization problem was constructed to identify unit cell topologies that could maximize the bandwidth of the stop-band behavior across a broad frequency response domain.

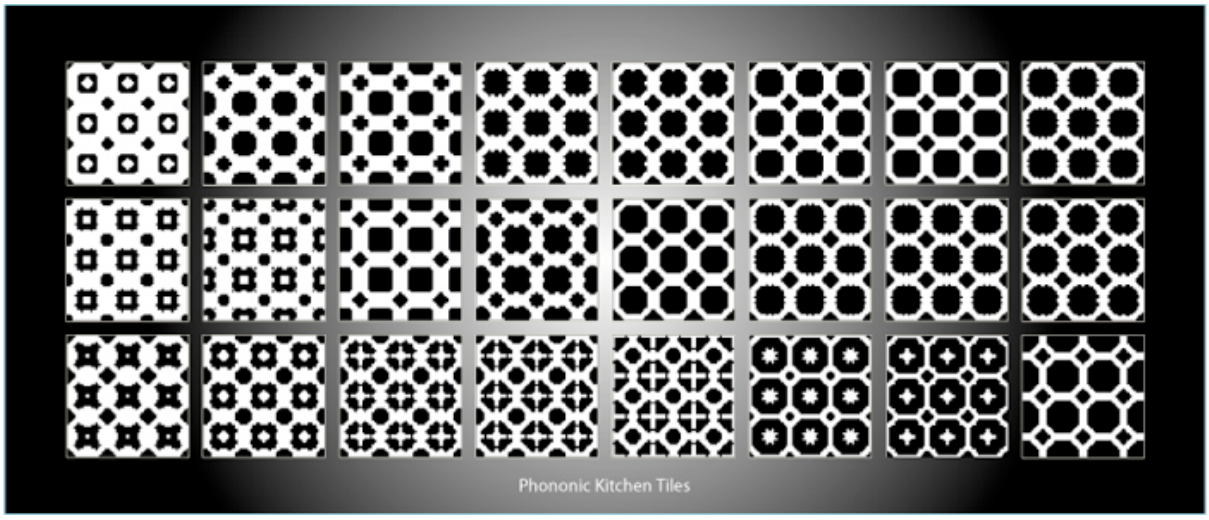

Figure 1: Examples of bi-material layouts to optimize phononic band-gaps using Bragg scattering (courtesy of Prof. Mahmoud I. Hussein)

3. Integral compliant mechanisms

The design of structures to mitigate structural vibration and acoustic response in mid-frequency spectrums (1-10 kHz) often has relied upon periodic lattices and structures, in particular, sandwich structures. The high stiffness-to-weight ratio and mid-frequency isolation attributes of sandwich structures both are attractive for the design of practical engineering structures. We have explored the novel use of compliant mechanisms as the core topology to attenuate mid-frequency structural response of sandwich structures; see, e.g., Dede and Hulbert [2]. While compliant mechanisms have been an active research field for the past 20 years, their application as a building block for vibration attenuation of sandwich structures presents a new application field. Figure 2 depicts an optimized compliant cell unit topology and a sandwich structure constructed from an assembly of the unit cells. The ability to optimize the compliant mechanism topology is described in Dede and Hulbert [2].

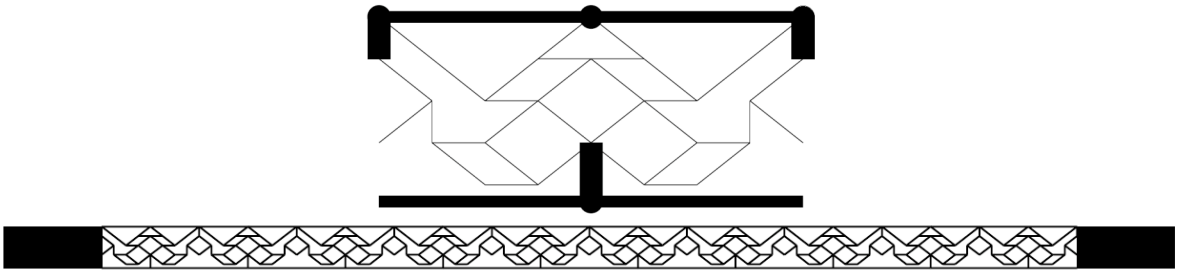

Figure 2: A reduced unit cell compliant mechanism topology (top); compliant sandwich structure comprising ten parallel unit cells (bottom).

4. Inertial amplification

A significant and practical challenge is to design systems that possess wide, low-frequency band-gaps. The lowest frequency gap due to Bragg scattering is of the order of the wave speed (longitudinal or transverse) of the medium divided by the lattice constant. Thus, a low-frequency Bragg gap requires low wave speeds (i.e., heavy inclusions in a soft medium) or a large lattice constant. On the other hand, by choosing low resonator frequencies, one can place local resonator induced band-gaps at much lower frequencies than that can be obtained by Bragg scattering. Low-frequency local resonances can be realized by embedding rubber-coated dense metal spheres or cylinders in an epoxy matrix. However, to obtain wide band-gaps at low frequencies, large volume filling fractions are required. Since the average density of the coated inclusions, e.g., rubber and dense metal, is more than an epoxy matrix, large volume fractions imply even larger mass fractions. Consequently, to obtain wide band-gaps at low frequencies, heavy resonators are needed that form a large fraction of the overall mass of the medium. Alternatively, by amplifying the effective inertia of the wave propagation medium using embedded amplification mechanisms, it is possible to circumvent the disadvantages described.

One of the first designs that made use of amplified effective inertia employs a single stage vibration isolator consisting of a levered mass in parallel with a spring. Such systems are used to isolate massive objects from vibrations. The lever in the system generates large inertial forces by amplifying the motion of a small mass, which in turn effectively increases the inertia of the overall system by lowering its resonance frequency. Furthermore, the isolator also introduces an anti-resonance frequency when the inertial force generated by the levered mass cancels the spring force. In Yilmaz *et al*. [3], this inertial amplification concept is utilized to generate band-gaps in infinite periodic systems. Their simple yet effective geometry allows them to be easily embedded into two or three-dimensional lattices, as illustrated in Figure 3. It is shown that the widest low-frequency band-gaps are obtained when most of the mass within the lattice is concentrated on very stiff amplifiers that can generate large amplifications. However, with smaller mass fractions on amplifiers, wide low-frequency band-gaps can still be obtained, provided that amplifiers are moderately stiff and can generate reasonably large amplifications. This is in contrast to obtaining wide low-frequency gaps via local resonators, which require heavy resonators that form a large fraction of the overall mass of their unit-cell. Moreover, unlike Bragg scattering, wave speeds and the lattice constant do not limit the lower frequency limit of a band-gap. Hence, this alternative method of generating band-gaps is particularly attractive for low-frequency applications.

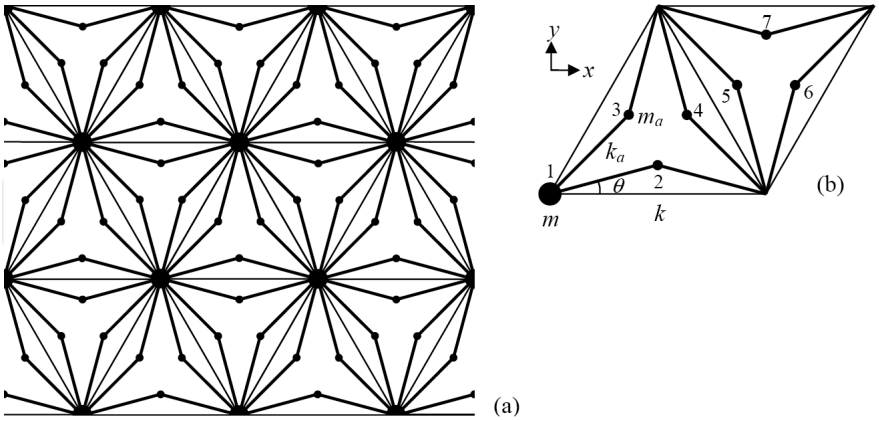

Figure 3: The infinite periodic lattice with inertial amplification (a); its irreducible unit cell (b).

References

[1] Dede EM, Hulbert GM. Analysis, design and optimization of structures with integral compliant mechanisms for mid-frequency response. *International Journal for Numerical Methods in Engineering* 2008; **73**: 470-492.

[2] Hussein MI, Hamza K, Hulbert M, Saitou K. Optimal synthesis of 2D phononic crystals for broadband frequency isolation. *Waves in Random and Complex Media* 2007; **17**: 491-510.

[3] Yilmaz C, Hulbert GM, Kikuchi N. Phononic band gaps induced by inertial amplification in periodic media. *Physical Review B* 2007; **76**: 054309.

Proceedings of the 6th International Conference on
Computation of Shell and Spatial Structures
IASS-IACM 2008: “Spanning Nano to Mega”
28-31 May 2008, Cornell University, Ithaca, NY, USA
John F. ABEL and J. Robert COOKE (eds.)

Seismic risk analysis of large lattice dome supported by buckling restrained braces

Shiro KATO*, Shoji NAKAZAWA

*Professor, Toyohashi University of Technology
Tempaku, Toyohashi, 441-8580, Japan
kato@tutrp.tut.ac.jp

Abstract

A method to compare the effectiveness of several bracing systems for a large dome is discussed based on a seismic risk analysis. In order to evaluate the risk depending on an adopted bracing system, a functional loss burdened to the dome structure due to earthquakes is calculated, depending on the type of adopted bracing system and the magnitude of base shear coefficient for design. The procedure of calculation utilizes a simple event tree modelling, where loss is counted considering the damages to structural members, non-structural walls and ceilings. Based on a simple calculation, an example of decision based on the evaluation is illustrated for selection of one bracing system from studied anti-seismic reinforcement methods.

1. Introduction

Large domes have been constructed as sport halls, exhibition halls and other similar facilities under which people gathers for certain purposes. Sport halls for communities and schools are typical ones as those of medium size. They are also considered to serve as refuges where people within community are to live instantly for certain duration in case of large earthquakes or disasters. The Houston Steel Dome and school sports halls in Kobe are well known to have served as those buildings.

The present study focuses on the seismic performance of this kind of halls, and discusses on a design demand for this kind of structures based on seismic risk analysis.

2. Geometry of Dome

First, a dome with a diameter of 100 meters is assumed for analysis in the present study as a sport hall of medium size in a medium city. The structure is given in Fig.1, where a single layer steel lattice roof with a ceiling attached is supported by a series of walls composed of diagonal earthquake resistant bracing elements.

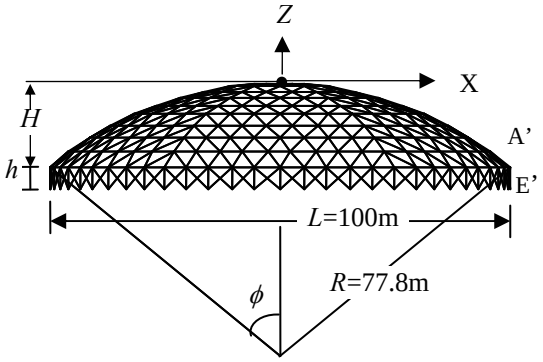

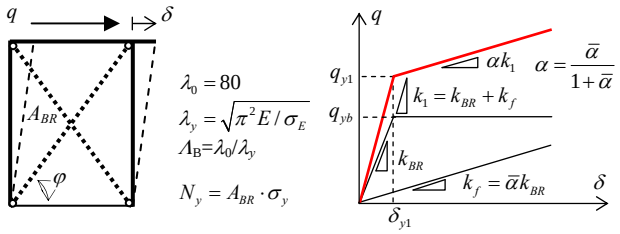

Replacement of brace hysteresis into equivalent bi-linear rule

Figure 1 A steel single layer lattice dome with a large area of ceiling, being supported by earthquake resistant braces.

The height of the wall of substructure is 500cm for H. Several types of bracing elements are assumed for comparison to investigate the effectiveness of their components to reduce the damage to the total structure serving refuges after big earthquakes. The data is given in Table.1. One structure is assumed based on a combination between Dome A or B depending on brace type given in Table 2. For example, Dome (A Un 0.3) means a structure with characteristics of Dome A and unbonded brace (buckling restrained brace) of $\alpha_{y0}=0.2$, while Dome (A Slip 0.2) means a structure of Dome A and Slip type brace of $\alpha_{y0}=0.2$.

Table.1 Design dead load and earthquake load for ultimate limit

	design loads as dead load	design loads as earthquake	characteristics
Dome A	two times the dead load	no consideration	Total weight for structures Wt=1770tf, H=500cm, $\cos\phi$ =0.729, ℓ_b = 532cm
Dome B	two times the dead load	0.6 as a base shear coefficient	

Table.2 Bracing elements

	design base shear coefficient for braces α_{y0}	yield stress σ_y	$A_{eq}(cm^2)$	$K_{BR}(tf/cm)$	$\kappa=K_F/K_{BR}$	story drift at first yield Δ_y (cm)
nnbonded type braces (bi-linear type)	0.2	$235N/mm^2$	2.811	11.78	0.2	0.834
	0.3		4.216	17.67		0.834
	0.4		5.622	23.56		0.834
slip type braces	0.3		4.216×2	17.67		0.834

3. Earthquake motions applied to risk analysis

Twelve artificial earthquake motions are prepared based on the design seismic response spectrum of Japan Building Code using phases drown from twelve recorded earthquake accelerations. The intensity of each artificial earthquake motion is defined as serviceability, repair and ultimate limit level, corresponding respectively $\lambda_E=1$, 3 and 5. As a rough average, the peak acceleration for $\lambda_E=1$ corresponds to 100cm/s^2.

4. Criteria for loss of function

Loss of functions is assumed based on the following conditions as given in Table.3, although the judgment of loss is fairly difficult. Two parts within a structure are classified for damage. One is the roof structure including ceilings on the dome. The other one is the wall composed of braces and wall finishing. The damage ratio for

Table.3a Assumption of failure limit for dome composed of steel reticular dome and ceilings: δ_{DV1}=12cm, δ_{DV2}=18cm, $A_{DH1}=A_{DV1}$=800cm/s2, $A_{DH2}=A_{DV2}$=1600cm/s2,

Damage or failure limit state	Maximum response limit over which loss of function follows due to the response
A No damage	The maximum vertical displacement δ_{DV} ; $\delta_{DV}\le\delta_{DV1}$,and maximum vertica acceleration response A_{DV} ; $A_{DV}\le A_{DV1}$, and maximum horizontal acceleration response A_{DH} ; $A_{DH}\le A_{DH1}$.
B Moderate	Not A, and Not C
C Severe damage	The maximum vertical displacement δ_{DV} ; $\delta_{DV}\ge\delta_{DV2}$,and maximum vertica acceleration response A_{DV} ; $A_{DV}\ge A_{DV2}$, or maximum horizontal acceleration response A_{DH} ; $A_{DH}\ge A_{DH2}$.

Table.3b Condition of failure for wall composed of braces and finishing $\delta_{SH1}=2.5$cm, $\delta_{SH2}=5.0$cm

Damage or failure state	Maximum response limit over which loss of function follows due to the response
A No damage	The horizontal displacement at top of wall δ_{SH} ; $\delta_{SH}\le\delta_{SH1}$:
B Moderate	Not A, and Not C
C Severe damage	The horizontal displacement at top of wall δ_{SH} ; $\delta_{SH}\ge\delta_{SH2}$:

Table.4 Ratio of Loss of function: Evaluation Type Ev1(Evaluation Type Ev2)

Walls and braces / Dome and ceilings		Damage or failure state		
		A	B	C
Damage or failure limit state	A	0	0.50	1.00
	B	0.50	0.50 (0.75)	1.00
	C	1.00	1.00	1.00

each part is assumed as shown in Table.3a for dome and ceilings and in Table.3b for wall finishing and braces. Two types of evaluation, Ev1 and Ev2, are performed based on Table.4. The difference is only the combination of Bs for wall and roof loss evaluation. The ratio in case of Evaluation Type 2 is given in the bracket in Table.4.

4. Results of function loss

The full loss of function is defined as 1.00. Fig.2 shows how the total loss depends on the seismic intensity for several domes. The marks, blank, semi-solid, and complete solid squares, illustrate respectively full functional, half functional, and no functional states. Fig.2a is given for the case of Dome (B Un 0.2) while Fig.2b for Dome (B Un 0.3) and Fig.2c for Dome (B Un 0.4). Fig.3 is the result for Dome (B Un 0.3) but based on two criteria as shown in Table.4. Ev1 and Ev2 correspond to the evaluation Ev1 1 and Ev2.

Comparison of those three results in Figure 2 together with Figure 4 reveals that the case of Dome (B Un 0.2) is under the most damage and that any dame can serve as a refuge without any loss of function only in case of serviceability limit level, and that almost all of them can not serve in case of seismic intensity larger than 4 for λ_E . Surprisingly, the dome (B Un 0.4) will not more effective than (B Un 0.3), although the seismic capacity of the unbonded braces of the dome (B Un 0.4) is higher than (B Un 0.3). The reason attributes to a fact that the high strength of shear wall much amplifies the vertical response within a roof due to anti-symmetric vibration. Figure 3 implies that the importance and caution for evaluation system to medium damage in case of medium seismic intensity, since the evaluation varies depending on the evaluation system.

Figure 5 shows the loss of function for domes installed with ordinary braces of slip type hysteretic loop in case of 0.3 for α_{y0} in Table.2. Its performance will be finer than Dome (B Un 0.2). The reason seems to be a tendency that the lower base shear coefficient gives a large horizontal displacement at the top of wall leading a larger shear deformation to walls within the substructure.

Figures 6 and 7 show the comparison of function loss between unbonded braces and ordinary slip type braces considering the damage ratio to domes of superstructure and walls of substructure. As a general tendency, it might be judged that loss of function is smaller in case of Dome (B) than Dome (Slip), and that domes and ceilings in case of Dome (Slip) are more vulnerable to earthquake motions. If the loss of function is counted as financial problems for construction and repair, the economical loss will be up much higher in case of Dome (Slip), since the repair work for domes and ceiling will be required costly due to works at site and due to a wide area of ceilings.

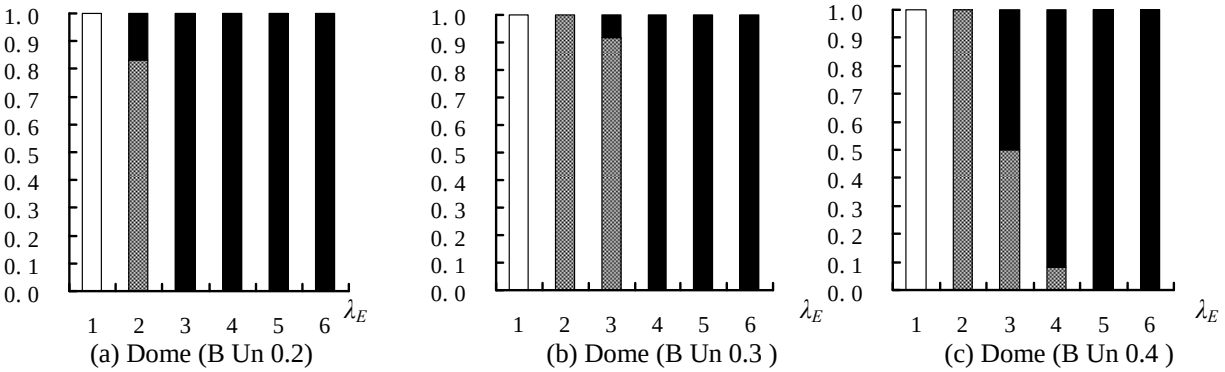

(a) Dome (B Un 0.2) (b) Dome (B Un 0.3) (c) Dome (B Un 0.4)

Figure 2 Loss of function: Ev1

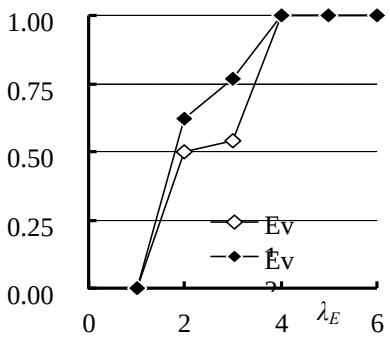

Figure 3 Loss of function for Dome (B Un 0.3)

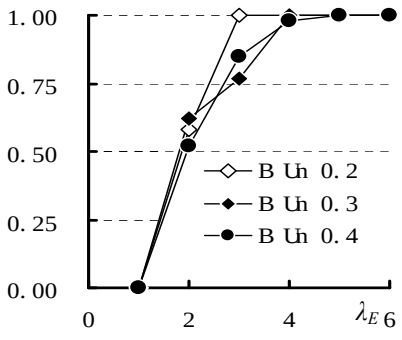

Figure 4 Loss of function for Dome (B): Ev1

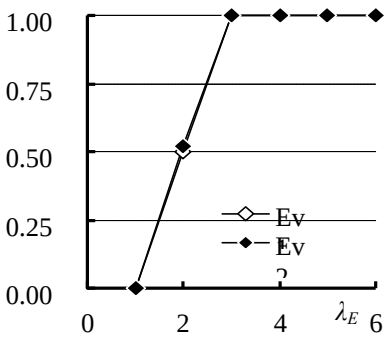

Figure 5 Loss of function for Dome (B Slip 0.3)

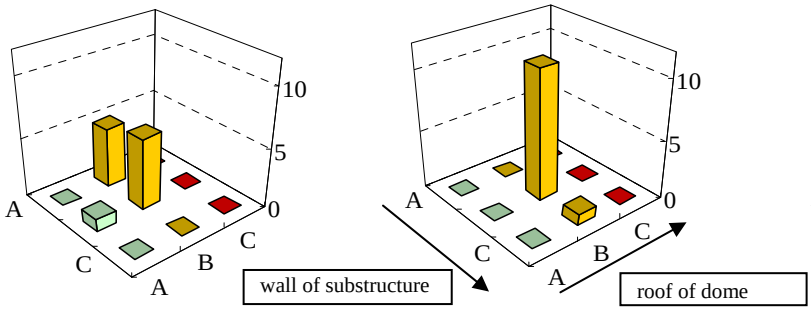

(a) $\lambda_E = 2$ (b) $\lambda_E = 3$ (c) $\lambda_E = 4$

Figure 6 Loss of function for Dome (B Un 0.3): Ev1

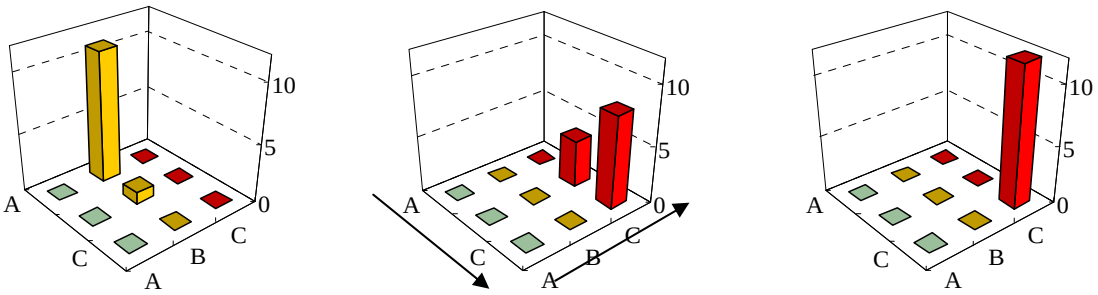

(a) $\lambda_E = 2$ (b) $\lambda_E = 3$ (c) $\lambda_E = 4$

Figure 7 Loss of function for Dome (B Slip 0.3): Ev1

Although the results in case of Dome (A) are not shown here, the dome was investigated with a confirmation that the structure of dome itself would collapse under moderate earthquake motions.

Comments

At present, engineers may access very effective FEM tools for structural dynamics as well as management analysis tools, and not only analysis for cost performance but also for effectiveness as refuges will be highly required in near future with respect to spatial structures for sport halls and similar buildings in strong seismic areas.

Acknowledgement

The authors would like to appreciate Drs. S D Xue and T Takeuchi for their collaboration for the present study. Also the first author is grateful for the partial supports as a Grand-in-Aid under grant No.(C)18560546 given by the Ministry of Education, Science, Sports and Culture of Japanese Government.

Proceedings of the 6th International Conference on
Computation of Shell and Spatial Structures
IASS-IACM 2008: "Spanning Nano to Mega"
28-31 May 2008, Cornell University, Ithaca, NY, USA
John F. ABEL and J. Robert COOKE (eds.)

A parameter study on dynamic buckling of spatial arch trusses under seismic action

Hai-wang LI*, Jian-xian LI, Fei ZHI, Fu MA, Dong-Qi QIN

*Professor, Department of Civil Engineering, Taiyuan University of Technology
79, Yingzexi Street, Taiyuan, 030024, China
lhwtut@126.com

Abstract

In this paper the dynamic response including buckling of spatial arch trusses with different parameters under earthquake is studied through ANSYS with geometric and material nonlinearity taken into consideration. The results show that: The ratio of their dynamic buckling bearing capacity is about 1:0.74:0.55 correspondently under El Centro, Ling-He and man-made seismic wave actions; the bearing capacity of the truss under vertical seismic wave is only 57.5% of that under horizontal seismic wave under El Centro seismic wave. The influences of the cross section height including 2m, 3m and 4m under vertical man-made waves are discussed when other conditions keep the same, and the ratio of their bearing capacity is about 1.00:1.10:1.23 correspondently. The influences of the rise ratios including 0.1, 0.2 and 0.3 under vertical El Centro seismic wave are discussed when other conditions keep the same, and the dynamic buckling to the rise ratio of 0.1 occurs while the strength failure to the rise ratio of 0.2 and 0.3.

1. Introduction

Large-span spatial arch trusses have been widely used in buildings like exhibition halls, waiting (departure) halls, gymnasiums and bridge systems. Their safety under severe earthquake is a big concern around the world. Although related researches on their normal behaviors have been carried out widely, but their dynamic response and failure mechanism under severe earthquake is still needed to be studied further. Paper [1] studied dynamic buckling of a spatial arch truss under seismic action; paper [2] studied dynamic buckling of spatial arch trusses under impulse loadings. In this paper the influences of the parameters on the dynamic response including buckling of spatial arch trusses under earthquake are carried out through ANSYS with geometric and material nonlinearity taken into consideration in detail.

2. Computation model and its material

The basic computation model is an 80m span spatial arch truss used in an entertainment center built in Taiyuan, China, with the rise of 8m, triangle cross section height of 2m and the width between the two upper chords of 2m, as shown in Fig.1. Rod cross sections are adopted as $\Phi 203\times 16$, $\Phi 168\times 6$, and $\Phi 68\times 3$ corresponding to the upper chords, the low chords, the oblique web members between the upper and the bottom chords and the horizontal web members between the two upper chords respectively. Its upper chord boundary nodes are all pin ended. Each rod of the trusses is divided into 2 Pipe20 elements with 8 integral points in their cross section (as shown in Fig.2), while the concentrated mass from whole dead load and half snow load as Mass21 in the

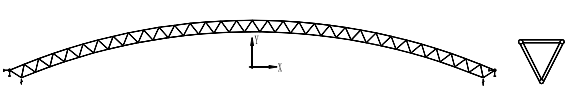

Fig.1 Basic computation model

Fig.2. Integral points of the rod cross section

numerical computation with ANSYS. The material adopts bilinear elastic-plastic hardening material model, with density 7850Kg/m^3, elasticity modulus 2.06GPa, tangent modulus 6.18GPa, the Poisson ratio 0.3, and the yield strength 235MPa. The damp is taken as Rayleigh with the damping ratio ζ =0.02 and the relevant parameter α and will be calculated according to the trusses' natural vibration frequencies. The man-made, Linghe and El Centro waves are chosen as seismic waves applied to the trusses. The parameters studied are shown in the Table 1.

Table 1 Parameter cases studied

Case	Span (m)	Cross section height(m)	Rise to span	Type of seismic wave	Input direction of seismic wave
1	80	2	0.1	El Centro	vertical
2	80	2	0.1	Linghe	vertical
3	80	2	0.1	Man-made	vertical
4	80	2	0.1	Man-made	horizontal
5	80	3	0.1	Man-made	vertical
6	80	4	0.1	Man-made	vertical
7	80	2	0.2	Man-made	vertical
8	80	2	0.3	Man-made	vertical

3. Results and analysis

3.1 The process of dynamic response and buckling of the spatial arch truss under seismic wave

The computations are done first on the dynamic response of the truss on the basic computation model (case 1). The results show that when the acceleration amplitude increases to 2990 gal, the maximum displacement

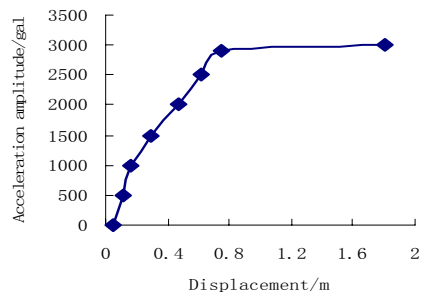

Fig.3 Displacement −acceleration amplitude curve of the center node

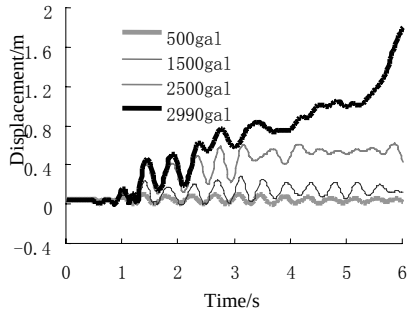

Fig.4 Displacement history curve of the center node

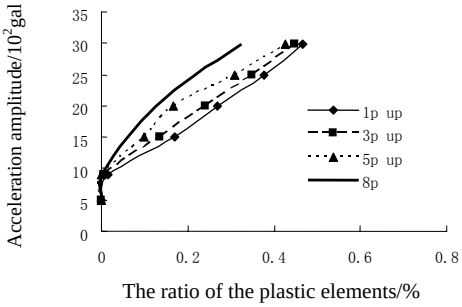

Fig.5 The ratio curves of the plastic elements with different integral points entering yield stage

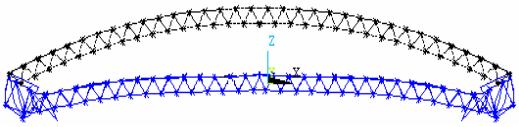

Fig.6 Dynamic buckling deformed shape of the arch truss (5 times)

response of the mid-span node abruptly rises as shown in Fig.3; the displacement history curve of the mid-span node diverges as shown in Fig.4; the ratio curves of the plastic elements with 8 integral points, more than 5 integral points and 3 integral points and 1 integral point entering yield stage in their cross section are shown in Fig.5, and so that the truss buckles judging from Lyapunov's B-R dynamic buckling criteria adopted, as shown in Fig.6.

3.2 Influences of the parameters on Dynamic Buckling

3.2.1 Seismic wave types

The influences of the types of seismic waves including El Centro, Ling-He and man-made seismic wave are discussed with parameters adopted by case 1 to case 3 shown in Table 1. The curves of their maximum displacement responses of the mid-span node with acceleration amplitude are shown in Fig.7. The ratio of their dynamic buckling bearing capacity is about 1:0.74:0.55 correspondently. And the ratios of the elements with 8 integral points, more than 5 integral points and 3 integral points and 1 integral point entering yield stage in their cross section are shown in Table 2.

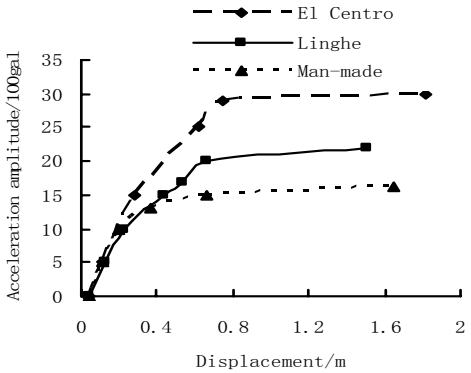

Fig.7 Displacement −acceleration amplitude curve of the center node with different seismic waves

Table 2 Plastic element ratios when dynamic buckling

Seismic wave	Dynamic buckling bearing capacity (10^2gal)	The ratio of the plastic elements with different integral points entering yield stage (%)			
		1p up	3p up	5p up	8p
El Centro	29.9	46.5	44.8	42.5	32.5
Linghe	22.0	44.0	42.5	37.0	27.4
Man-made	16.3	42.7	41.3	32.4	24.8

3.2.2 Input direction

The influences of the input directions including horizontal input and vertical input are also studied on the

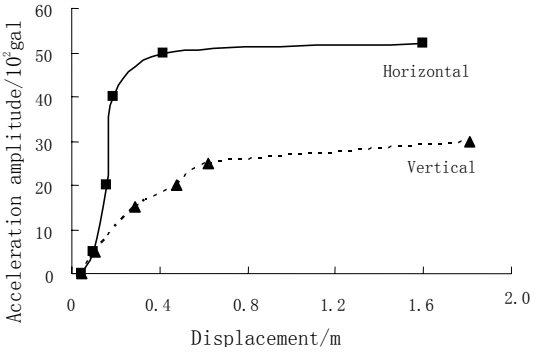

Fig.8 Displacement −acceleration amplitude curve of the center node with different input directions

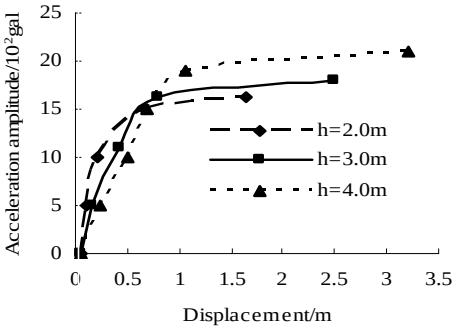

Fig.9 Displacement −acceleration amplitude curve of the center node with different truss heights

Table 3 Plastic element ratios when dynamic buckling

Seismic wave	Dynamic buckling bearing capacity (10^2gal)	The ratio of the plastic elements with different integral points entering yield stage (%)			
		1p up	3p up	5p up	8p
Vertical	29.9	46.5	44.8	42.5	32.5
Horizontal	52.0	32.8	31.4	27.4	22.0

dynamic responses of the truss with parameters adopted by case 3 and case 4 shown in Table 1. The curves of their maximum displacement responses of the mid-span node with acceleration amplitude are shown in Fig.8. The result shows that the dynamic buckling bearing capacity of the truss under vertical seismic wave is only 57.5% of that under horizontal seismic wave. And the ratios of the plastic elements with different integral points entering yield stage in their cross section are shown in Table 3 when buckling.

3.2.3 The cross section height

The influences of the cross section height including 2m, 3m and 4m under vertical man-made waves are discussed with parameters adopted by case 3 and case 5 and case 6 shown in Table 1. The curves of their maximum displacement responses of the mid-span node with acceleration amplitude are shown in Fig.9. The ratio of their dynamic buckling bearing capacity is about 1:1.10:1.23 correspondently. And the ratios of the plastic elements with different integral points entering yield stage in their cross section are shown in Table 4.

Table 4 Plastic element ratios when dynamic buckling

Cross section height(m)	Dynamic buckling bearing capacity (10^2gal)	The ratio of the plastic elements with different integral points entering yield stage (%)			
		1p up	3p up	5p up	8p
2.0	16.3	42.7	41.3	32.4	24.8
3.0	18.0	44.8	43.0	41.0	38.0
4.0	20.0	47.0	45.7	42.7	40.0

Table 5 Plastic element ratios when dynamic buckling or strength failure

Rise to span	Dynamic bearing capacity (10^2gal)	The ratio of the plastic elements with different integral points entering yield stage (%)			
		1p up	3p up	5p up	8p
0.1	16.3 (buckling)	42.7	41.3	32.4	24.8
0.2	43.0 (strength failure)	44.0	42.8	38.6	25.7
0.3	70.0 (strength failure)	45.0	40.6	33.4	27.0

3.2.4 The rise ratios

The influences of the rise ratios including 0.1, 0.2 and 0.3 under vertical man-made seismic wave are discussed with parameters adopted by case 6 to case 8 shown in Table 1. The curves of their maximum displacement responses of the mid-span node with acceleration amplitude are shown in Fig.10. The dynamic buckling to the rise ratio of 0.1 occurs while the strength failure to the rise ratio of 0.2 and 0.3. The strength failure in this study occurs judging from the standard that the strain of the first integral points of the plastic elements exceeds the strain limit of steel (adopted as 20%). And the ratios of the plastic elements with different integral points entering yield stage in their cross section are shown in Table 5 when buckling or strength failure.

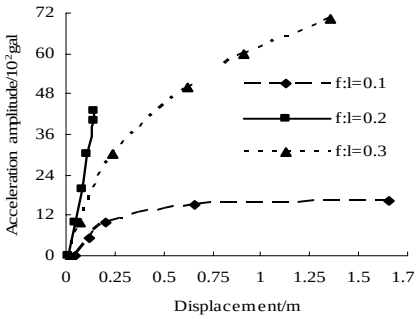

Fig.10 Max. displacement -acceleration amplitude curve of the center node with different rise ratios

References

[1] Fu Ma, Haiwang Li, Dongqi Qin. A study on dynamic buckling of spatial arch trusses under seismic action. In the *International Symposium on New Olympic, New Shell and Spatial Structures* (IASS-APCS2006), Beijing, 2006, 10:364-365.

[2] Haiwang Li, Chunyan Li, Dongqi Qin. A study on dynamic buckling of spatial arch trusses under impulse loadings. In the *International Symposium on New Olympic, New Shell and Spatial Structures* (IASS-APCS2006), Beijing, 2006, 10:366-367

Proceedings of the 6th International Conference on
Computation of Shell and Spatial Structures
IASS-IACM 2008: "Spanning Nano to Mega"
28-31 May 2008, Cornell University, Ithaca, NY, USA
John F. ABEL and J. Robert COOKE (eds.)

Static elasto-plastic analysis of long-span rigid spatial structures under vertical earthquake

Yongfeng LUO*, Muwang YANG

*College of Civil Engineering, Tongji University, 1239# Siping Road, Shanghai, 200092, China
yfluo93@mail.tongji.edu.cn

Abstract

Long-span structures are one of the most rapidly developing structure systems. It is found widely in modern buildings, especially in large-scale and public buildings. The dynamic characteristics and the seismic behavior of the structures are usually complex and different from tall buildings. The current design methods for the seismic resistance of the long-span structures are not reasonable. However, available simplified seismic analysis methods for the long-span structures have not been found till now. Few research references about static analysis methods of seismic responses of the long-span spatial structures are reported. The current static elasto-plastic analysis method, named push-over method, is widely adopted in the seismic analysis of tall buildings. Whereas the fundamental vibration mode of the long-span spatial structures is usually vertical deformation, the push-over method does not suit for the seismic analysis of the long-span spatial structures any more. In current actual engineering analysis, the time history analysis method is an only method used in various types of the long-span structures for seismic analysis to predict the structural dynamic response and behavior. Then the great deal of time consumption makes it difficult to use.

According to the dynamic characteristics of the long-span spatial structures and based on the principle of the push-over method, a new static elasto-plastic analysis method, named "push-down" method, is proposed in this paper. The vertical elasto-plastic capacity spectrum and demand spectrum are established. Two types of vertical load patterns are also proposed. At the same time, the fundamental mode pattern of vertical loads and the multi-mode pattern of vertical loads used in push-down method are derived. The application range and computational steps of the push-down method in the long span rigid spatial structures are given. A simple numerical example is conducted and presented. The validity and the accuracy of the method are verified.

1. Introduction

Few researches about static elasto-plastic analysis methods of vertical seismic response of long-span spatial structures have been found till now. The time-history method is usually adopted in the seismic analysis of the actual spatial structures now. The static elasto-plastic analysis method, named push-over method (FEMA273 [1]), is widely adopted in the seismic analysis of the regular tall-buildings, in which the first natural vibration mode is horizontal deformation. Whereas the fundamental vibration mode of the long-span spatial structures is vertical deformation, the push-over method does not suit for the long-span spatial structures any more. Therefore, the research of static elasto-plastic analysis methods of long-span spatial structures under vertical earthquake becomes a new subject.

A new static elasto-plastic analysis method, named 'push-down method' (Muwang Yang [3]), is proposed in this paper. It's named since the seismic responses of the long-span spatial structures under the certain mode patterns of vertical loads are analyzed. The transformation formula of the vertical elasto-plastic capacity spectrum and demand spectrum are established. At the same time, the fundamental mode pattern of vertical loads and the multi-mode pattern of vertical loads used in push-down method are derived. It suits for the spatial structures in which components can be all modeled by beam elements or beam-column elements.

2. The principle of push-down method

2.1 Basic assumptions

- Plane cross-section assumption is used in structure members.
- The effect of shearing deformation of members is neglected.
- Tension stresses and forces are defined to be positive. Clockwise rotations are defined to be positive.
- No separation between steel and concrete in the composite members.

2.2 The patterns of vertical loads

2.1.1 The fundamental mode pattern of vertical loads

The mode pattern vector of vertical loads is the same as the vector of the fundamental vibration mode. The formula is shown as

$$\{P\} = \{\phi_1\}V_0 \tag{1}$$

Where, $\{P\}$ is the pattern vector of the vertical loads, $\{\phi_1\}$ is the vector of the fundamental vibration mode, V_0 is the vertical increment shear force of the structure.

2.1.2 The multi-mode pattern of vertical loads

Several vibration modes are selected as the mode patterns of the vertical loads since they are all dominant modes of the vibration. The push-down method is conducted for each mode pattern. The final results of the push-down method of the multi-mode pattern of vertical loads can be obtained by a combination method, SRSS (Square Root of Sum of Squares). Each mode pattern of vertical loads can be described as

$$\{P_j\} = \{\phi_j\}V_0 \tag{2}$$

Where, $\{P_j\}$ is the pattern vector of vertical loads corresponding to the vibration mode j, $\{\phi_j\}$ is the vector of vibration mode j.

2.3 The push-down method of the fundamental mode pattern of vertical loads

2.3.1 Vertical capacity spectrum

For the long-span spatial structures that the fundamental vibration mode is vertical and dominant deformation, the relationship curve between the vertical force excited by earthquake and the displacement of the control joint can be transformed into the relationship curve between the spectrum acceleration and the spectrum displacement of a system with a single degree of freedom (Shuwei Geng *et al*. [4]). The transformation formulas are

$$S_d = \frac{u_v}{\Gamma_1 u_{v,1}} \qquad S_a = \frac{V_v}{M*} = \frac{V_v}{\alpha_1 M} \tag{3}$$

Where, u_v is the displacement of the control joint. Γ_1 is the modal participant coefficient of the fundamental mode. $u_{v,1}$ is the displacement of the control joint with the largest shape value in the fundamental mode. V_v is the total of vertical shear. α_1 is mass participant coefficient of the fundamental mode. M is the mass of structure.

2.3.2 Vertical demand spectrum

The vertical elastic spectrum acceleration and spectrum displacement (LU Xi-lin *et al*. [2]) in ADRS format is

$$S_{ae} = \alpha_{v\max} g \qquad S_{de} = \frac{T^2}{4\pi^2} S_{ae} g \tag{4}$$

The vertical elasto-plastic spectrum acceleration and spectrum displacement (Vidic T *et al*. [5]) are

$$S_{ap} = S_{ae} / R_v \qquad S_{dp} = \frac{\mu S_{de}}{R_v} = \frac{\mu}{R_v}\left(\frac{T}{2\pi}\right)^2 S_{ae} \tag{5}$$

Where, S_{ae} is the vertical elastic spectrum acceleration, S_{ap} is the vertical elasto-plastic spectrum acceleration, S_{de} is the vertical elastic spectrum displacement, S_{dp} is the vertical elasto-plastic spectrum displacement.

2.3.3 Calculating the performance point

When the capacity spectrum curve of the structure and demand spectrum curve of certain seismic intensity are drawn in the same chart, the intersection point is named performance point (figure 1). The corresponding displacement of the performance point is the spectrum displacement. This spectrum displacement can be converted into the displacement of control joint. The distribution of plastic hinges, the joint displacements and the structure deflection can be obtained meanwhile. Then the seismic resistance evaluation of the structure can be achieved. If there is no intersection point, the analysis must be retried for satisfying seismic performance.

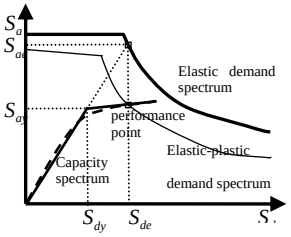

Figure 1: The performance point of the structure

2.4 The push-down method of the multi-mode pattern of vertical loads

If the effects of higher order vibration modes can not be neglected, the push-down method of the multi-mode pattern of vertical loads should be adopted.

2.4.1 The principles of push-down method of the multi-mode pattern of vertical loads

The relationship curve between the vertical force excited by earthquake and the displacement of the control joint can be transformed into the relationship curve between the spectrum acceleration and the spectrum displacement.

$$S_{d,no} = \frac{u_{v,no}}{\Gamma_{no} u_{no}} \qquad S_{a,no} = \frac{V_{v,no}}{M^*} = \frac{V_{v,no}}{\alpha_{no} M} \tag{6}$$

Where, $u_{v,no}$ is the vertical displacement of the control joint under the mode pattern of the vertical loads corresponding to mode *no*. Γ_{no} is the modal participant coefficient of the mode *no*. u_{no} is the vertical displacement of the control joint with the largest shape value corresponding to mode *no*. $V_{v,no}$ is the total vertical shear of mode *no*. α_{no} is modal mass coefficient of mode *no*. M is the mass of the structure.

After the performance point corresponding to each mode pattern of vertical loads is obtained, the displacement of the structure under vertical loads of pattern mode *no* is shown as follows

$$u_{vn} = \Gamma_n \phi_n S_{d,no} \tag{7}$$

Where

$$\Gamma_n = \frac{\phi_n^T mi}{\phi_n^T m \phi_n} \tag{8}$$

Through the mode combination (SRSS method), the forces and the displacements of the structure can be calculated

$$R_e = \left(\sum_{n=1}^{j} R_{no}^2 \right)^{1/2} \tag{9}$$

Where, j is the number of mode. R_{no} is the response of the structure corresponding to mode *no*.

2.4.2 The computational steps of the push-down method with the multi-mode pattern

The main computational steps of the push-down method with the multi-mode pattern of vertical loads are:

- After the push-down analysis under each pattern of the vertical loads, develop the relationship curve between the vertical shear force of supports excited by earthquake and the displacement of the control joint.
- Calculate the modal participant coefficient Γ_j and the modal equivalent mass M_j.
- Obtain the corresponding elastic spectrum acceleration.
- Calculate the strength reduction coefficient R_v and ductility coefficient μ of the structure under the different ground site and the seismic intensity. Transform the vertical elastic demand spectrum into the vertical elasto-plastic demand spectrum.
- For each pattern of vertical loads, solve the vertical target displacement S_{dpn}
- Bi-linearize the capacity spectrum curve, find the performance point.
- Calculate the displacement of the control point. Through the modal combination method, the final displacement of the structure under the multi-mode pattern of the vertical loads can be obtained.

3. The numerical example

A single-layer reticulated shell (Figure 2) is computed. The members are H400×200×10×14 in radial and H300×150×6×10 in circumferential. Steel is Q345B. The dead load is $0.5kN/m^2$ and the live load is $0.5kN/m^2$. All supports are hinged. The mass coefficients of mode 4 and mode 10 are 0.669 and 0.257 respectively. The dynamic characteristics of the shell can mainly be expressed by mode 4 and 10. The push-down analysis of the multi-mode pattern of vertical loads should be adopted. The results are listed in table 1.

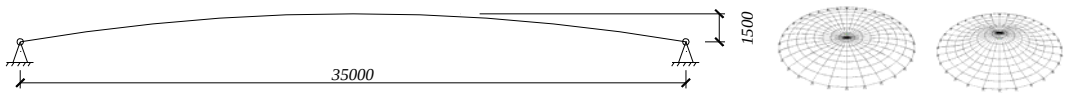

model 4 mode 10

Figure 2: The reticulated shell and the vibration modes

Calculating method	Push-Down	Artificial ground motion 1	Artificial ground motion 2	Artificial ground motion 3
The displacement of control joint (mm)	21.70	19.5	20.2	19.1

Table 1: The numerical results

4. Conclusion

A static elasto-plastic seismic analysis method for rigid long-span spatial structures, named push-down method, is proposed in this paper. The validity and the accuracy of the method are verified by a simple example. This new method can be simply used to evaluate the seismic performance of rigid long-span spatial structures in which the dominant vibration modes are mainly vertical deformation.

References

[1] FEMA273, NEHRP. Guidelines for the seismic rehabilitation of buildings. Federal Emergency Management Agency. Washington, D. C., 1997

[2] LU Xi-lin, ZHOU Ding-song. Ductility demand spectra and inelastic displacement spectra considering soil conditions and design characteristic periods, Earthquake Engineering and Engineering Vibration. 2004, 24(1): 39-48

[3] Muwang Yang. Static Elasto-plastic Analysis of Long-Span rigid Spatial Structures under Vertical Earthquake. The dissertation for doctor degree, Tongji University, 2007

[4] Shuwei Geng, Xianxin Tao. The ratios of vertical to horizontal acceleration response spectra. Earthquake Engineering and Engineering Vibration. 2004. 24(5):33-38

[5] Vidic T, Fajfar P. Consistent inelastic design spectra: strength and displacement. Earthquake Engineering and Structural Dynamics, 1994, 24(5): 507-521

Proceedings of the 6th International Conference on
Computation of Shell and Spatial Structures
IASS-IACM 2008: "Spanning Nano to Mega"
28-31 May 2008, Cornell University, Ithaca, NY, USA
John F. ABEL and J. Robert COOKE (eds.)

Problems in the research of multi-dimensional and multi-support seismic analysis

Pengfei ZHAO*, Jihong QIAN, Rongwei TANG

*China Academy of Building Research.
No 30 Beisanhuandonglu, Beijing100013, China
E-mail: zhaopengfei@cabrtech.com

Abstract

With the development of analysis hardware and software, more and more subjects on the multi-dimensional and multi-support seismic analysis have been carried out. The main goal of this paper is to discuss some problems in this research field based on summarizing the structure seismic methods. These methods are divided into determinate analysis and indeterminate analysis, or into simple support and multi-support. Due to wide application scope, the response spectrum is discussed with the multi-dimensional ground motion as emphases problem. The problem of what research work should be carried out in each seismic analysis method, is proposed respectively.

1. Introduction

The seismic problems can be divided into the following parts:

- According to seismic analysis method
  - determinate analysis
    - time-history method
    - response spectrum method
  - indeterminate analysis
    - stationary random analysis
    - nonstationary random analysis
- According to describing method of ground motion
  - simple-support
    - single-dimensional input
    - multi-dimensional input
  - multi-support
    - single-dimensional input
    - multi-dimensional input

figure 1 Summary of seismic analysis method

1.1 Earthquake input

Actually, many problems, such as the earthquake mechanism, the characteristic of earthquake wave and so on, are the bases of the structure seismic research. In this field, following need to be perfected:

A. Providing considering the earthquake wave in multi-dimension simultaneously, the ground motion model and corresponding coherency effect will play important roles in structure response. However, we have not satisfied research result in this field.

B. It is beyond all doubt that the rotational component of ground motion is one of substantial factors for destroying structures. But so far there is no even one rotational component record

1.2 Structure model

In general, it is a mature technique for setting up structure finite element model. In this filed, the valuable parts is the research on material characteristic on plastic phases.

1.3 Seismic response analysis

The methods used in seismic analysis can be summed up as figure 1.

Now, we discuss the methods in figure 1 respectively.

2. Discuss on seismic analysis methods

2.1 Time history method

The advantage of this method is common and audio-visual, while the disadvantage is that its result is specific and individual. It is difficult to make innovations in this field.

The available points in this method are to search some roles by a great lot of calculations and analysis and we think there is little innovation space.

2.2 Response spectrum method

It is no doubt that the response spectrum method is ones applied most, with the advantage that it is simple and has parameters with statistical sense. At present, the response spectrum in codes can only be used in the situation of one dimension and single-point excitation.

As the matter of fact, the response spectrum method is closely linked with stochastic vibration theory. According to the theory, the ground motion is assumed to be stationary stochastic process and the power spectral density of any structure seismic response z is:

$$S_z(\omega) = \sum_{p}^{m} \sum_{q}^{m} \sum_{i}^{n} \sum_{j}^{n} \phi_{iz} \phi_{jz} \gamma_{ip} \gamma_{jq} H_i^*(\omega) H_j(\omega) S_{pq}(\omega) \qquad (1)$$

In which, ϕ_{iz}, ϕ_{jz} ——the magnitude of z in mode i and j;

p, q ——earthquake wave direction;

m, n ——the number of earthquake wave directions and modes taken into account;

γ_{ip}, γ_{jq} ——the participant factors of mode i in p direction and mode j in q direction;

$H_{i(j)}(\omega)$ ——the frequency transform function of mode i (j);;

$S_{pq}(\omega)$ —— the cross power spectral density of ground motion in p and q direction.

By Flourier transform method, the self-correlation function $R_x(0)$, namely variance σ_Z^2 of response z can be gotten based on the power spectral density:

$$\sigma_Z^2 = R_x(0) = \int_{-\infty}^{\infty} S_Z(\omega) d\omega \qquad (2)$$

The peak value of response z - $z_{\max}$ can be gotten by multiplying square σ_z with peak value factor γ:

$$z_{\max} = \gamma \, \sigma_z \qquad (3)$$

The peak value factor γ is related with specified exceeded probability. It is noted that the peak value of response $z_{\max}$ is actually the concept of response spectrum.

The formula（1）can be simplified by the following steps: at first do integral at left and right sides simultaneously with $d\omega$; then designate ρ_{ij}^{pq} as the coherency coefficient of mode i , j in the direction p and q.

$$\rho_{ij}^{pq}=\frac{\int_{-\infty}^{\infty}H_i^*(\omega)H_j(\omega)S_{pq}(\omega)d\xi}{\sqrt{\int_{-\infty}^{\infty}\left|H_i(\omega)\right|^2 S_{pp}(\omega)d\omega}\cdot\sqrt{\int_{-\infty}^{\infty}\left|H_j(\omega)\right|^2 S_{qq}(\omega)d\omega}} \quad (4)$$

In which, $S_{pp}(\omega)$, $S_{qq}(\omega)$ are ground motion power spectral in p, q direction.

The denominator of formula（4）is actually the product of $\sigma_{ip}\cdot\sigma_{jq}$, i.e., the response square variance of mode i in p direction and mode j in q direction.

So, formula (2) can be written as:

$$\sigma_z^2=\sum_p^m\sum_q^m\sum_i^n\sum_j^n\phi_{iz}\phi_{jz}\gamma_{ip}\gamma_{jq}\rho_{ij}^{pq}\sigma_{ip}\sigma_{jq} \quad (5)$$

If assuming the peak value factors of σ_z, σ_{ip} and σ_{jq} are equal, formula（5）can be transferred as:

$$S_z=\sqrt{\sum_p^m\sum_q^m\sum_i^n\sum_j^n\rho_{ij}^{pq}S_{ip}S_{jq}} \quad (6)$$

In which, S_{ip}, S_{jq} are the magnitude of response z of mode i in direction p and mode j in direction q, based on the response spectrum of single dimension.

Actually, formula （6）is CQC expression, and includes two sense of combination: one is the combination of response values of each mode; the another is the combination of response values of each ground motion direction.

The following research in the multi-dimension response spectrum field should be done:

① Propose new power spectral density matrix of ground motion or improve old ones, in which the emphasis is power spectral and cross-spectral density function of rotation component.

② When considering the rotational component of ground motion, how to calculate the participant factors of each mode γ_{ip}.

③ Simplify the calculation of the coherency coefficient ρ_{ij}^{pq}.

④ Connect the multi-dimensional response spectrum with the single-dimensional one in the national code.

⑤ Make comparison between the results of the multi-dimensional response spectrum analysis and time-history analysis.

⑥ Based on the large number of multi-dimensional seismic analysis results, the rough law of long-span structures seismic response can be mastered.

So, in the research on the multi-dimensional response spectrum, the problems ①, ③ and ④ above mentioned should be paid more attention to. And that, the most important core one is problem ①, i.e., the input model of earthquake wave.

2.3 Indeterminate method

The combination of stochastic theory with seismic analysis reveals the essence of contradiction profoundly. Moreover, the pseudo-excitation method has provided a powerful tool for stochastic seismic analysis.

In the past, the nonstationary characteristic is only focused on the intensity of ground motion, but the frequency spectrum varies as well, to which should be paid more attention in the future. Otherwise, it has not been studied for applying indeterminate method to high buildings.

We think the following research contents can be carried out firstly:

A. Multi-dimensional ground motion input (including rotational components);

B. Attempt to apply the indeterminate method to high buildings;

C. Considering the nonstationary characteristic of ground motion in the intensity and frequency spectrum simultaneously..

3. Discuss on describing method on ground motion

2.1 Single-dimensional and single-support input

Most work is based on this input assumption and we think there is no space available to do more research.

2.2 Multi-dimensional and single-support input

There is no difficult in time-history based on this input, however we have no rotation component record of earthquake. And the pseudo-excitation method is effective to solve this problem.

2.3 Multi-dimensional and multi-support input （not considering rotation component of ground motion）

Due to actual ground motion research level, we think there are two difficulties in considering rotational component of ground motion when carrying out multi-dimensional and multi-support seismic analysis. The first one, at present, the "rotational component" is all derived from translation component by some theories and hypothesis. In this case, it is nonsense to take rotational component with translation component simultaneously. The second one, when the rotation problem is discussed, a corresponding rotation axis is proposed and the rotation angle and corresponding acceleration of each point are assumed to be the same; then we can not imagine the following situation: each point has different rotation angle and acceleration but with the same rotation axis.

3. Conclusion

(1) At present, the common and proper software on the time-history analysis considering multi-support and multi-dimensional excitation, has not been found.
(2) The research objects on the response spectrum method include:
A. considering simple-support and multi-dimensional input simultaneously.
B. considering multi-support and multi-dimensional input (but not including rotational component) simultaneously.
C. considering arrival angle of earthquake wave.
(3) The stochastic analysis study should solve the following problems:
A. when the multi-dimensional and simple-support excitation is considered, how to use stochastic method.
B. how to consider the nonstationary characteristics of the frequency spectrum of ground motion.
(4) When doing research work on multi-dimensional and multi-support input, the rotation component of ground motion can not be taken into account.

References

[1] Hughes TJR. The Finite Element Method: Linear Static and Dynamic Finite Element Analysis (2nd edn). Dover, 2000.

[1] MOUNIR BERRAH, EDUARDO KAUSEL. Response Spectrum Analysis of Structures Subjected to Spatially Varying Motions. *Earthquake Engineering and Structural Dynamics* 1992; 21: 461-470.

[2] MIHAILO D. TRIFUNAC, MARIA I. TODOROVSKA. Response Spectra for Differential Motion of Columns. *Earthquake Engineering and Structural Dynamics* 1997; 26: 251-268.

[3] Ernesto Heredia-Zavoni, Erik H. Vanmarcke. Seismic Random-Vibration Analysis of Multisupport-Structural Systems. *Journal of Engineering Mechanics.*1994, 5.

[4] ALYS. NAZMY, AHMED M. ABDEL-GHAFFAR. Effects of Ground Motion Spatial Variability on the Response of Cable-Stayed Bridges. *Earthquake Engineering and Structural Dynamics* 1992; 21: 1-20.

[5] JIAHAO LIN, JIANJUN LI, WENSHOU ZHANG. Random Seismic Responses of Multi-Support Structures in Evolutionary Inhomogeneous Random Fields. *Earthquake Engineering and Structural Dynamics* 1997; 26: 135-145.

[6] ASPASIA ZERVA. Seismic Ground Motion Simulations from a Class of Spatial Variability Models. *Earthquake Engineering and Structural Dynamics* 1992;21: 351-361.

Proceedings of the 6th International Conference on
Computation of Shell and Spatial Structures
IASS-IACM 2008: "Spanning Nano to Mega"
28-31 May 2008, Cornell University, Ithaca, NY, USA
John F. ABEL and J. Robert COOKE (eds.)

Dynamic field test on elliptical suspen-dome

Jie QIN*, Bin SHEN, Guoli LI

Beijing Building Construction Research Institute
No.34 Fuxing Road, Beijing 100039, China Phone +86-10-88223703
E-mail: qjcumt@263.net

Abstract

To study the dynamic characteristics of elliptical suspen-dome, a 6.7m-long-axis and 5.1m-short-axis model was made. Compared with the result between the test and calculation, the elliptical Suspen-dome is a self-vibration frequency-intensive structure. The elliptical Suspen-dome's mode is complex, mainly in the vertical vibration mode. Test results of self-vibration frequency are similar to that in calculation. Mode also tallies with the calculation result.

1. Introduction

Based on the concept of tensile-integrity and cable dome, Japanese engineers, M.Kawaguchi and M.Abe[1] , proposed suspen-dome as a new structure in 1993 and then the systematic research was carried out by M.Kawaguchi's group. In China, the researches mostly centralize in Tianjin University[2], Beijing University of Technology, Zhejiang University and Tsinghua University. The completed model tests were all circular forms and not involved in elliptical one and most of tests were not related to dynamic field. Thus the study of dynamic characteristics on elliptical suspen-dome appears necessary and im portant.

2. Model design

In this paper the design of a typical flat elliptical suspen-dome test model. The model had a 6.7m-long-axis, 5.1m-short-axis and 0.656m-rise single-layer truss dome. The length of struts was 0.3m in outer three layers and 0.25m in the other two layers. The steel pipes(φ18×1.2 andφ8×1) were used for the truss members and struts, and the steel cables(φ5 and φ4) were used for radial and hoop cables (the hoop cables in the outer four layers used φ5 and all the rest used φ4). For the convenience of welding and loading, the hoop pipes in innermost layer used a steel plate with 60mm height and 6mm thickness.

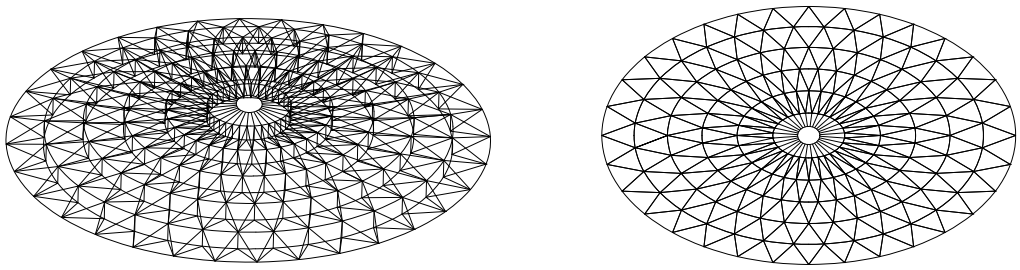

3D-view The floor plan

Figure 1. The test model

2.1. The upper part of the structure production: elliptical dome upper planar single-string network is ellipsoid shell surface, so many kinds of bars, of varying lengths, to the ring of a five-length type, there are radial length of more than 100 kinds of types. It would bar the expected length of the high demand, and error control in about 2 mm. Single-node network shell used welding, ball joints 100 mm in diameter and weighing about 0.9 Kg.

2.2 The lower part of the structure of cable-system production: As the test conditions, such as various reasons, rod and monolayer between shells also used welding, welding requirements with the monolayer shells welding, the most important requirement is a certain guarantee Vertical rod. There are also many types of radial cable, the expected size also very accurate. Cable and cable radial ring, ring and radial cable and rod and rod between cables used hinged.

2.3 Node production: elliptical dome plane string nodes associated with complex. Node structural components of the transmission link internal forces. The whole model is the key point of the design problem. Dome string of these types of nodes a preliminary discussion, and put forward a number of practical forms of the node structure. Liu Xiliang also in the Tianjin Development Zone Business Centre hall, Kunming Park Plaza lighting the top, was designed by Xu Bin badminton Museum of Anshan in the form of a node. Following on the test model used by the node types are introduced.

2.4 Support design: Bound situation on the border of the seismic properties of very significant. Structure in the practical application, in order to take into account the seismic capacity. It will adopt flexible boundary conditions. Suspen-dome structure is usually the case which be used in the horizontal radial stiffness of the spring with a certain bearing. Therefore, the boundary conditions can be roughly divided into three categories: radial sliding bearings, springs and bearings fixed hinge bearings. This test hinge bearing a fixed form. First, the ball joints and pipe welding, then welded steel pipe at the bottom of a small plate, the end plate and the two edges ring beam welding.

3. Self-vibration frequency and mode equation

3.1. Find the structure self-vibration frequency and mode equation through the technology of sine wave sweeping frequency

Data of test shows the results of the self-vibration frequency and mode equation. The mode scale, material properties, loads and supports are accord with test condition. Compared with the results between test and theory calculation, every mode in the test is also found in the theory calculation. The self-vibration frequency in the test is close to that in the theory calculation. It's because of the error in the model making, error in the test, error in the measurement, condition of the test, etc. In a word, the measurement of the self-vibration frequency is exact.

3.2. The frequency sweeping by the white noise, different nodes acceleration spectrum chart is achieved in different nodes.

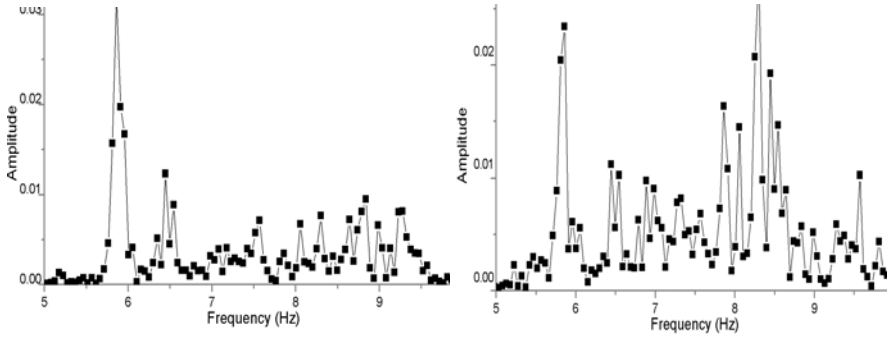

Ch37 vertical acceleration spectrum chart Ch38 vertical acceleration spectrum chart

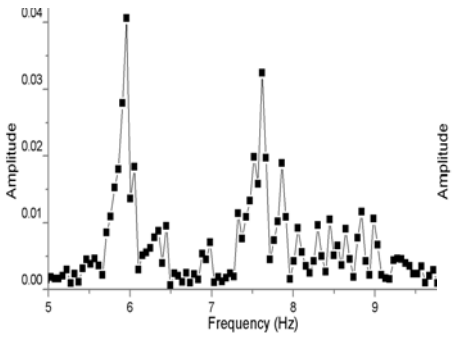

Ch39 vertical acceleration spectrum chart

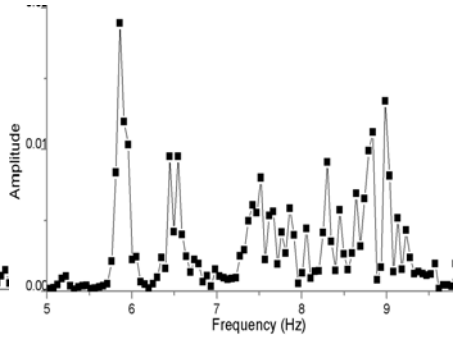

Ch45 vertical acceleration spectrum chart

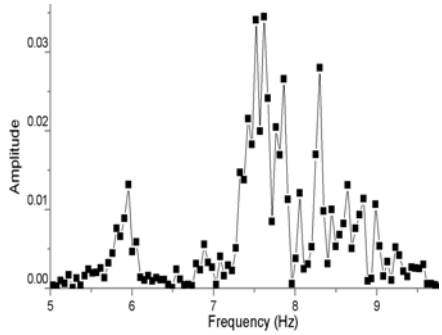

Ch46 vertical acceleration spectrum chart

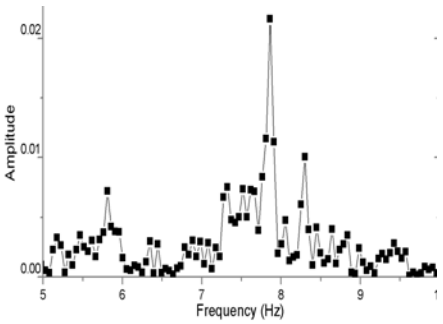

Ch53 horizontal acceleration spectrum chart

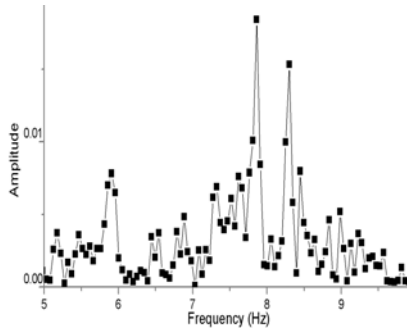

Ch54 horizontal acceleration spectrum chart

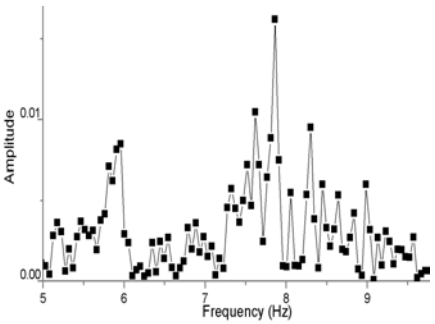

Ch55 horizontal acceleration spectrum chart

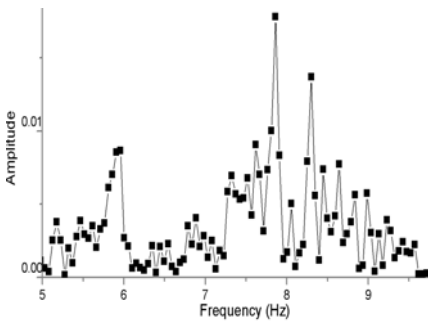

Ch61 horizontal acceleration spectrum chart

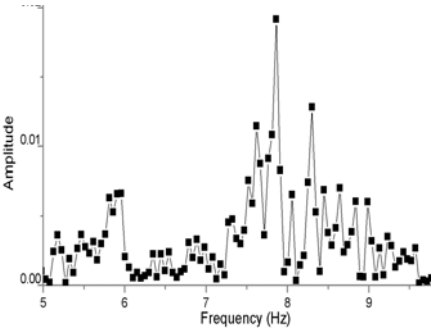

Ch62 horizontal acceleration spectrum chart

Figure.2 acceleration spectrum chart

Figure 2 shows the main mode is different in different nodes. Some main mode is different in different nodes, the same direction; other main mode is same in different nodes, the same direction. The frequency distribution is very intensive. And the first mode is not always the main mode in this structure. In most of structures, first vibration mode is the main mode. It also reminds us, in the subsequent design of the project to pay special attention to the structure of cylindrical shell net frequency analysis to find main mode. According to the local conditions, adjusting the seismic design is very important, to avoid very obvious resonance of the structure and to reduce earthquake hazards.

Figure 2 shows the former 1 frequency through the acceleration spectrum chart.

Tab.1 the former 6 frequencies

Number of frequency		1	2	3	4	5	6
frequency /Hz	Sine wave	5.99	6.17	6.80	7.35	——	9.09
	White noise	5.96	6.44	6.88	7.88	8.30	8.99
Difference of two way		0.5□	4.2□	1.1□	6.7□	——	1.1□

Tab.2 the former 20 frequencies by calculation

Number of frequency	1	2	3	4	5	6	7	8	9	10
frequency /Hz	6.54	6.68	7.38	7.85	7.90	8.42	8.49	8.78	8.86	9.17
Number of frequency	11	12	13	14	15	16	17	18	19	20
frequency /Hz	9.33	9.40	9.47	9.50	9.60	9.91	9.97	10.00	10.01	10.31

Table 1 shows the results is similar between the frequency sweeping by the white noise and sine wave sweeping. Table 2 shows the former 20 frequencies by calculation. The frequency distribution is very intensive in the form; the results of the test measurement are similar with that by calculation.

4. Damping ratio

Damping is the depletion of the energy system capacity. Attenuation method is used here for the structure of the damping ratio.

Through the above free signal attenuation obtained damping ratio, respectively: 0.0052, 0.0068, 0.0060, 0.0058, 0.0066, 0.0058, from the average, and seek structural damping ratio of 0.006

5. Model test results

Through test of the elliptical suspen-dome structure, self-vibration frequency, mode and damping ratio are achieved. Comparing with theoretical calculations, the following conclusions are achieved:

1. The elliptical suspen-dome is a self-vibration frequency-intensive structure.

2. The elliptical suspen-dome's mode is complex, mainly in the vertical vibration mode.

3. Test results of self-vibration frequency are similar to that in calculation. Mode also tallies with the calculation result.

References:

[1] Mamoru Kawaguchi,Masaru Abe,Tatsuo Hatato,Ikuo Tatemichi,Satoshi Fujiwara,Hiroaki Matsufuji,Hiroyuki Yoshida and Yoshimichi Anma,ON A STRUCTURAL SYSTEM "SUSPEND-DOME",Proc. of IASS Symposium,Istanbul,1993□523□530.

[2] Xiliang Liu, Qinghua Han. The design and construction of frame structure. Tianjin: Tianjin University Press, 2004

Proceedings of the 6th International Conference on
Computation of Shell and Spatial Structures
IASS-IACM 2008: "Spanning Nano to Mega"
28-31 May 2008, Cornell University, Ithaca, NY, USA
John F. ABEL and J. Robert COOKE (eds.)

Simulating blast effects in steel lattice structures

Emily LEIGH*, Christopher EARLS

*School of Civil and Environmental Engineering
Cornell University, Ithaca, NY USA
ecl38@cornell.edu

Abstract

The occurrence of explosive loading on steel lattice structures may lead to extensive localized damage and collapse of the overall structural system. The current research presents a novel approach for characterizing blast-induced damage in individual steel components. The commercial finite element code ADINA is used for detailed shell-element-based collapse modeling of steel W-sections subjected first to explosive loading, and then to proportional moment-thrust load combinations in stress-resultant space. The resulting failure load combinations, derived from numerous separate collapse analyses of a damaged member, are used to define a failure surface that characterizes the effects of the shock loading in that component. Different steel sections, lengths, charge weights, and stand-off distances are considered, in order to populate a library of bounding surface plasticity models for use with more conventional frame finite element formulations.

1. Introduction

Recent world events have highlighted the importance of human threat to structures as a concern for structural engineers in the U.S. and many other parts of the world. Since this particular threat scenario is outside of the realm of common practice for civil structural engineers, it is important that an understanding of the unique loading features of the threat be considered. The shock wave created by an explosion can exert incident overpressure loading that is several orders of magnitude greater, and in directions different than the loads for which the structure has been designed if explosive threat has initially been ignored. The most effective blast mitigation strategy, the creation of adequate stand-off distance, is often not possible for certain structural geometries like a bridge through-truss, or the underside of a highway overpass. These types of exposed steel structures must be hardened to blast instead, a strategy that requires accurate and effective computational modeling of blast effects to determine adequate hardening approaches. The current research investigates explosive effects in steel lattice structures by numerically simulating blast loading on different individual components, and then examining the resulting damage by loading the component to failure. By producing failure surfaces that adequately capture the damage induced in various steel sections for different charge weights and locations, the current research provides an extensive library of explosive loading effects on common steel sections in a compact format.

2. Literature review

2.1 Air blast loading

Air blast loading can be modeled as an incident pressure field impinging on a structural surface, where the over-pressure time history follows a decaying exponential equation form. Equation parameters include maximum overpressure, arrival time, duration, and decay coefficient, where the values of these parameters depend on charge weight, W, and distance, R, from the point under consideration to the explosive source. Parameter values, determined from various sets of experimental blast data, are tabulated as a function of scaled distance, Z (e.g. $Z = R/W^{1/3}$), from a blast point. The parameter equations detailed by Kingery and Bulmash [7] are widely accepted, and serve as the basis for ConWep, a blast load code restricted to use by U.S. government agencies.

The current research employs alternate parameter equations from the open literature, and the resulting overpressure-time histories are comparable to those produced via the methodology of Kingery and Bulmash [7]. The blast load generation code written for use in this research includes parameter expressions by Brode [3], for reflected blast calculations, and parameter data and equations from Kinney and Graham [8], for free air blast overpressures as well as the remaining time and decay coefficient parameters.

2.2 Blast effects on structures

Relevant available literature on blast effects in steel structures focuses on frames and bridges. Baylot *et al.* [2] perform numerous finite element analyses of bridge beams subjected to blast and fragment loads, where charges are restricted to a location between the bottom flange and the underside of the deck at mid-span. Results from these analyses are used to postulate equation forms for prediction of blast resistance as a function of web height, and also web thickness, for hot-rolled sections and plate-girders. The current research is more generalized: charge location is unlimited and beams are stand-alone, without a deck in composite action with the top flanges.

Chen and Liew [4] investigate the behavior of single columns subjected to uniformly distributed blast loading and subsequent fire attack, focusing on the influence that blast loads have on the fire resistance of steel frame structures. The current research, despite the exclusion of fire effects, builds upon Chen and Liew [4] as it includes spatial variation in the explosive loading on steel members.

3. Approach

3.1 Mesh

Individual W-sections are represented by their midline geometry, and meshed with a single layer of shell elements of the appropriate thickness (equal to t_w or t_f). The nonlinear, finite strain MITC4 shell element from the ADINA element library is employed in the model (Bathe and Dvorkin [1]). The mesh density is 4 elements per flange outstand width $b_f/2$, and 16 elements per web height.

Cross-sectional distortion at support locations is restrained by placing very stiff beam elements along the middle lines of the end cross-sections. Moment releases are placed at the flange-web junctions, in the end nodes of the web beam elements only, to permit warping deformation of the flanges of the cross-section. Simple boundary conditions are applied, with the pin and roller located at the centroid of the cross-section, at opposite beam ends. A schematic of the geometry, end-treatment, and boundary conditions for this model is shown in Figure 1.

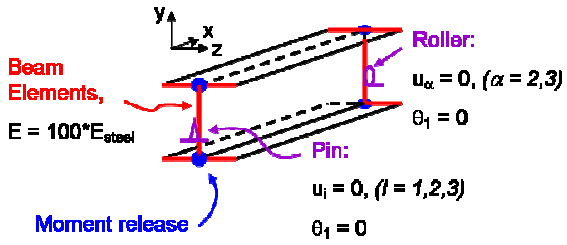

Figure 1: Model schematic

3.2 Material Model

A multilinear material model for A36 steel is used, where the stress-strain information, shown in Figure 2, consists of averaged results from a series of coupon tests (Frank [6]). Other material property values include modulus of elasticity E = 29500 ksi, Poisson's ratio ν = 0.3, and density ρ = 0.000735 lb-s^2/in^4 (0.284 lb/in^3).

Strain (in/in)	Stress (psi)
0.001432896	42,270.45
0.0160702	43,745.20
0.2688814	75,000.00

Figure 2: True stress-strain data, A36 steel

The model employs the constitutive relationship used by Drysdale and Zak [5] to model rate-dependent material effects. The initial yield stress, σ_y, is defined as a function of effective plastic strain rate, $\dot{\varepsilon}^p$, as

$$\sigma_y = \sigma_o \left[1 + b \ln\left(1 + \frac{\dot{\varepsilon}^p}{\dot{\varepsilon}_0} \right) \right], \tag{1}$$

where σ_o = static yield stress,

$\dot{\varepsilon}_0$ = transition strain rate,

b = strain rate hardening parameter.

Parameter values of $\dot{\varepsilon}_0$ = 0.0001/s and b = 0.043, which were obtained by fitting Eq. (1) to experimental data for mild steel (Drysdale and Zak [5]), are used in the models.

3.3 Loading

Model loading is accomplished in a two-step sequence: dynamic explosive loading is applied over a time scale of milliseconds, and then proportional moment-thrust loading is applied in a static collapse analysis.

Explosive overpressure loading is produced by the air blast load generation code written for this research, and is applied as nodal force-time histories for all nodes that are in direct line of sight to the explosion source point. The combined loading includes an axial load and two different sets of couples, representing major and minor axis bending, at each girder end. The loading sequence is shown in Figure 3.

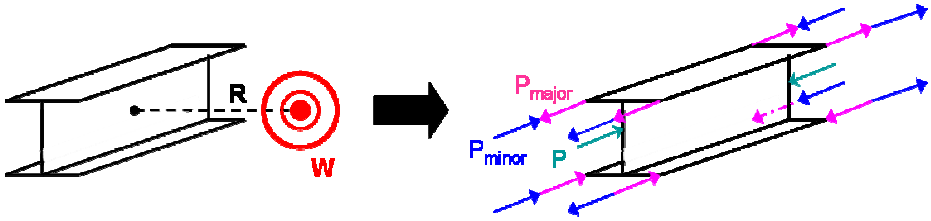

Figure 3: Loading sequence

Proportional load magnitudes are set to coincide with the activation of limit states. In order to generate adequate data to describe a failure surface, several separate collapse analyses of a damaged girder are carried out using different load combinations in stress-resultant space. Each load combination is described by a vector in stress-resultant space, $\lambda\{\alpha M_{py}, \beta M_{px}, \gamma P_{cr}\}$, shown in Figure 4. The load proportionality factor, λ, is the length of the vector, and α, β, and γ are constants that describe the loading vector direction with respect to the familiar metrics P_{cr} (critical buckling load), M_{px} (major-axis plastic moment), and M_{py}, (minor-axis plastic moment).

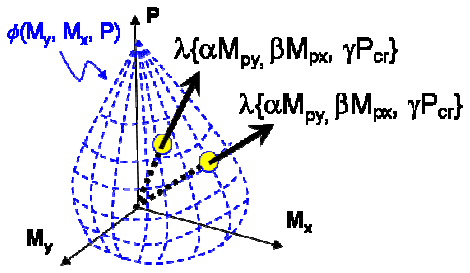

Figure 4: Methodology for determining failure points

4. Results

For clarity, the results presented here are limited to one explosion scenario: a W14x38 section, length L = 15 ft, is exposed to a blast, of charge weight W = 1000 lb, which is centered on the web height at mid-span a distance

R = 75 ft away. At this scaled distance, $Z = R/W^{1/3}$ = 7.5 ft/lb$^{1/3}$, the maximum reflected overpressure, P_r, is equal to 32.0 psi. A series of separate collapse analyses are carried out on the damaged beam to find points on the damaged yield surface in stress resultant space, shown for the first octant only in Figure 5. For reference, an Orbison failure surface, of the usual form for an undamaged section (McGuire *et al.* [9]), is also depicted in Figure 5.

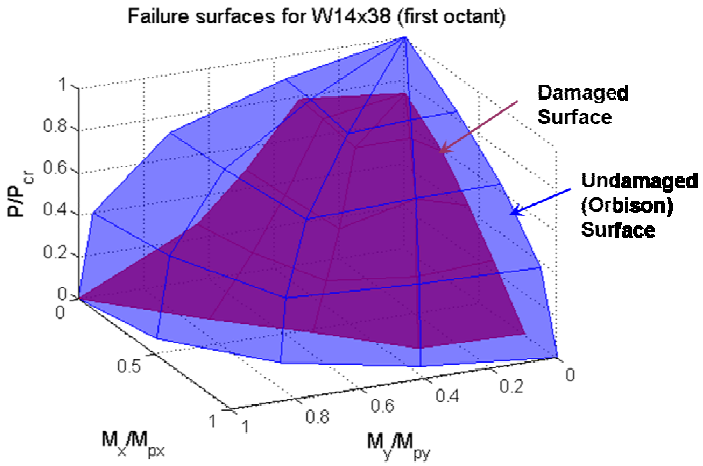

Figure 5: Approximations to damaged and undamaged failure surfaces

4. Conclusions

The current research contributes a new approach for constitutive modeling within the context of explosive response simulation. Future research will focus on incorporating the failure surfaces determined for individual blast-damaged steel sections into traditional frame finite element formulations, in order to build a computationally efficient tool for blast response calculation in steel lattice structures.

Acknowledgement

This material is based upon work supported under a National Science Foundation Graduate Research Fellowship.

References

[1] Bathe KJ and Dvorkin EN. A formulation of general shell elements—the use of mixed interpolation of tensorial components. *Computers & Structures* 1986; **17**(5-6): 871-879.

[2] Baylot JT, Ray JC, and Hall RL. Prediction method for response of steel bridge beams and girders to blast and fragment loads. *Transportation Research Record* 2003; **1827**: 69-74.

[3] Brode HL. Numerical solutions of spherical blast waves. *Journal of Applied Physics* 1955; **26**(6): 766-775.

[4] Chen H and Liew JYR. Explosion and fire analysis of steel frames using mixed element approach. *Journal of Engineering Mechanics* 2005; **131**(6): 606-616.

[5] Drysdale WH and Zak AR. A theory for rate-dependent plasticity. *Computers & Structures* 1985; **20**(1-3): 259-264.

[6] Frank, KH. Personal communication, Department of Civil, Architectural, and Environmental Engineering, University of Texas, Austin.

[7] Kingery CN and Bulmash G. Airblast parameters from TNT spherical air burst and hemispherical surface burst. Technical Report ARBRL-TR-02555. US Armament Research and Development Center, Ballistic Research Laboratory, Aberdeen Proving Ground, MD, April 1984.

[8] Kinney GF and Graham KJ. Explosive Shocks in Air (2nd edn). Springer-Verlag, 1985.

[9] McGuire, W, Gallagher, RH and Ziemian, RD. Matrix Strucutural Analysis (2nd edn). John Wiley & Sons, Inc., 2000.

Proceedings of the 6th International Conference on
Computation of Shell and Spatial Structures
IASS-IACM 2008: "Spanning Nano to Mega"
28-31 May 2008, Cornell University, Ithaca, NY, USA
John F. ABEL and J. Robert COOKE (eds.)

Dynamic analysis of single layer lattice shell with BRBs

Xiuli WANG*, Jiyun CHEN, Chang WU

School of Civil Engineering, Lanzhou University of Technology
287#, Langongping Road, Lanzhou, Gansu , PR China,730050
Email: wangxl@lut.cn

Abstract

The discussion how to reduce earthquake responses for a single layer lattice dome installed with buckling restrained braces has been carried out in this paper. The finite element analysis software ANSYS program is applied to analysis the 40m span single-layer oval shell and its parameters. In the model the sub-structure selects the reinforced concrete column so as to considering the effect to shell. The modes under natural vibration model are comparatively analyzed whether consider the Single-layer Oval Shell with sub-structure or not. 4 kinds of BRB arrangement mode will be put forward that is some sections of the same area are replaced by BRBs, and analysis the vibration reducing performance of the single-layer oval shell with BRBs. The results are showed that the effect of the Sub-structure can not be ignored and the shell structure vibration reducing effect is fine by rational arrangement of the BRBs.

1. Introduction

More and more reticular domes have been adopted in the large span structures because they can effectively cover a large area without column inside. The major stress character of the single-layer oval shell is the membrane stress. Because the latticed shell is thin under earthquake actions, the structure is easy to get the unstable destroy, the plastic of material is lower, so the analysis on the study and the research on the properties of the vibration reducing is very necessary. Buckling-Restrained Braces is a excellent energy dissipation structural brace consisting of a steel core plate surrounded by mortar and enclosed in a steel tube. A membrane called the un-bonding material, between the core plate and the mortar. Nuclear steel brace can reach full yield under tension and pressure, it takes on better ductility because of the stable and full hysteresis loop, BRBs with low yield stress and dissipate energy on the small displacement level. At present, the researches of these braces are concentrated on frame structure. However, there is a lack of knowledge of behavior of these braces for large span space construction. In this paper, take 40m span single-layer combined lattice shell under earthquake excitation as study subject. Nonlinear finite element method is applied, use software ANSYS program to model and analysis with parameters.

2. Model analysis

According to the ANSYS offered, Beam188 unit bas been selected for beam unit and Link8 has been adopted for the rod unit in this paper. The analysis of the single-layer oval shell with sub-structure is investigated. The gravity load of the roof concentrates on the joints with the Mass21 unit. The analytic model is following as Figure 1 shows. The constitutive relation of material uses the ideal elastic-plastic model. The yield criterion is the Von-Mises yield criterion; the joint form is rigid connection.

Calculate the first step of the reticular shell by synthesizing the mechanical characteristics of this structure and adopt 4 kinds of cross-section following as Table 1. This model contains three kinds of materials: Sub-structure: C30, E=3.0e10N/m^2, λ=0.3, dens=2500kg/m^3; Shell: Q 235B, E=2.1e11N/m2, λ=0.3, dens=7800kg/m^3; BRBs: E=2.1e11N/m^2, λ=0.3, dens=7800kg/m^3, f_y=100MPa. The reinforced concrete is use for sub-structure of the Oval Shell, the dimension of which is: column height is 15m, diameter is 900mm, span is 60m; the length of middle cylinder is 21m and the rise-span ratio is 1/4.

Table 1 Cross-section of Members (mm)

Number of member	Cross Section	Position Member
1	φ133X4.5	main ribs and subordination ribs
2	φ108X4.5	inclined rods
3	φ900	reinforced concrete column
4	φ108X4.5	BRBs

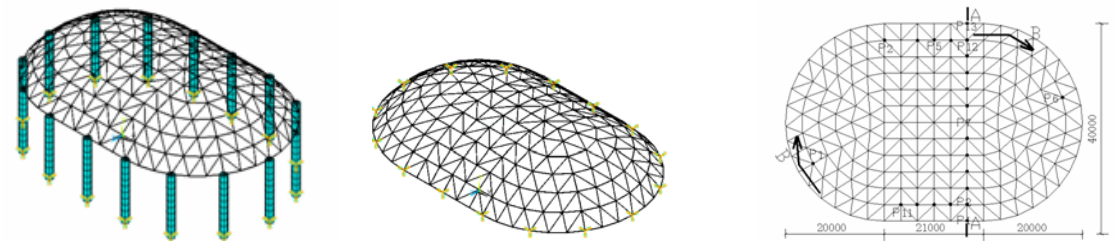

(1) Shell with sub-structure. (2) Shell without sub-structure. (3) Key nodes of the shell.

Figure 1: Geometric modal of the shell

3. Natural vibration analysis

The single-layer oval shell mode with sub-structure or without is established, which span is 40m and height-to span ratio is 1/4. The first fifty modes were analyzed through two calculations. Each natural frequency and mode can be seen Table 2. Under horizontal seismic load, it can be concluded that resistance capacity to deformation of sphere part is better and of cylinder part is weaker through mode analysis. Although the whole horizontal displacement of oval shell with sub-structure is large, the deformation is smaller compared the bar with the oval shell without substructure, in view of the cooperative effect and the earthquake energy consumption. Under vertical seismic load or combined loads, the coordination capability weakened, even the internal bars damaged more serious as a result of the sub-structure. Whether under the horizontal and vertical seismic loads or not, the cylinder of the single-layer oval shell has large motion trend. Because the oval shell possesses twofold attributions: spherical reticulated shell and cylindrical lattice shell, so we will input three dimensional earthquakes to study the structural respond to earthquake. Based on above analysis, the horizontal and vertical seismic loads cannot be neglected. Meanwhile, it shows that the effect of the substructure should be considered and the frequencies should be analyzed.

Table 2. Typical natural frequencies (Hz)

The first fifty modes	1	2	4	8	9	10	41	42	49	50
With sub-structure	0.3369	0.3536	0.44864	0.5314	0.5564	0.5944	1.2498	1.2698	1.3900	1.3976
Without substructure	0.3348	0.3429	0.3436	0.4950	0.5891	0.6044	1.2601	1.2783	1.3351	1.3418

4. Vibration reduction analysis

The response of a single-layer oval shell structure to earthquakes is a key issue to investigate. The core analysis of the paper is how to play a very good energy dissipation function with Buckling-Restrained-Brace. Input three dimensional earthquake to simulate seismic action on earthquake response analysis, earthquake intensity was given as degree 8,design acceleration of ground motion is 0.2g, peak acceleration was chosen 400GAL under strong earthquake ,time interval was assumed 0.02 second, sub step number was 10, the lasting time of the earthquake was assumed as 4 second.

4.1 Arrangements of BRBs

Oval shell is consists of spherical and cylindrical part. In order to guarantee the strength, rigidity and stability, transverse and vertical members are not fit to replace. Slant rod of the shell should be replaced equal section. As a result of less constraint and low rigidity, the model on the last ring without column joints is the maximum

displacements at peak point. Secondly, the maximum value of the nodal displacements and the stress mainly concentrates on the last second and three ring of the shell. On account of the particularity of oval shell, the position where the intermediate of the cylindrical reticulated shell and the joints are the key issue. Therefore, four kinds of arrangements are shown in Figure 2. The fifty frequencies had not significantly changed in before and after BRBS. BRB1 is used for equal section to replace the Slant rod of the bottom ring. Because sub-structure has no restriction affect on the part nodes, so that the nodes is the weakness of the seismic response. Accordingly, the other three arrangements emerged based on the first arrangement.BRB2 is used for equal section to replace the two transverse rib of Slant rod on the intermediate of cylindrical reticulated shell, BRB3 is used for equal section to replace the Slant rod between two transverse rib on the joints of the cylindrical reticulated shell and the spherical lattice shell, and BRB4 is used for equal section to replace the Slant rod between second ring-stiffened of the cylindrical reticulated shell.

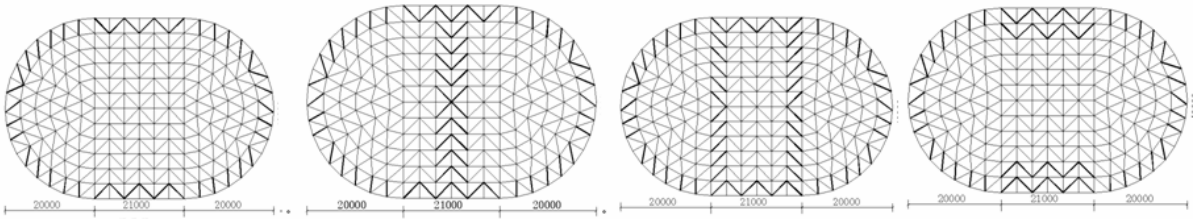

(1) BRB1 (2) BRB2 (3) BRB3 (4) BRB4

Figure 2: Arrangements of BRBs.

4.2 Displacement response

Figure 3 shows the displacement of the main nodes which are in the direction A-A and direction B-B. The internal force redistribution emerges with BRBS. The absolute value of positive and negative displacement decreases obviously. The amplitude of displacement fluctuates gentle and uniform relatively, it can be obtained that the arrangements of BRBs are reasonable. As can be seen from the data-table, the transverse direction A-A and ring direction B-B are geometric symmetry, but the node displacement distribution has no symmetry, the transverse displacement decreases gradually from the two side to the intermediate, the maximum displacements at peak point of the cylindrical ring direction is larger than of the spherical part, and that the largest displacement decreases greatly under the four kinds BRBS. Meanwhile the node displacement distributes more uniform; it can be showed that the seismic response has better effect. The largest node displacement is on the last second and three ring of the cylindrical part. The result further demonstrates the weakness of the oval shell. The contribution of the BRBs to the vertical displacement is relatively small, but the maximum displacements at peak point of the middle cylinder decrease greatly. The displacement with BRB1 and BRB3 is smaller than other support structure and original structure, BRB3 has better effect. BRB2 and BRB4 have less effect relatively on the nodes displacement decreases.

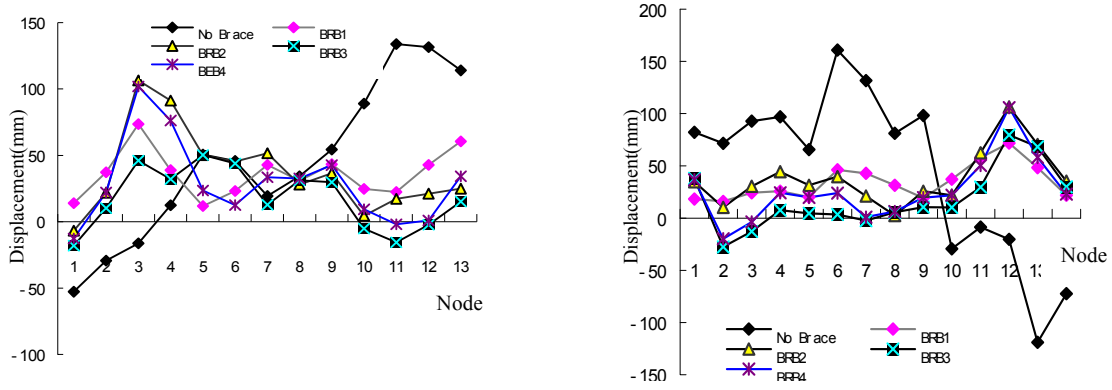

(1) direction A-A (2) direction B-B

Figure 3: The comparison of node displacement in transverse

4.3 Axial force response

Table 3 shows the maximum axial stress. From Table 3 it can be seen that the maximum tensile force response of the structure with BRBs decreases obviously and the maximum pressure force response has no remarkable change. BRB1 has the best effect on the decrease of the axial force, BRB3 is better, BRB4 and BRB2 are worse. Although it shows that the vibration reducing effect of BRBs to the shell is remarkable, there are also distinctive differences in seismic response of the quantity and the arrangements of BRBs.

Table 3. The comparison of maximal axial force BRB with sub-structure or not.

Arrangements / Maximal axial force	No-Brace	BRB1	BRB 2	BRB 3	BRB 4
Maximal tensile force FN/KN	151	129	107	112	134
Maximal pressure force FN/ KN	-196	-187	-216	-190	-207
Coefficient of tensile force vibration reducing K_+	1.0	0.85	0.71	0.74	0.89
Coefficient of force vibration reducing K_-	1.0	0.95	1.1	0.97	1.06

5. Conclusion

From the systematical analysis above, following conclusions can be obtained:

(1)The horizontal and vertical seismic loads can not be ignored and the effect of the sub-structure on the frequency should be considered. The modes under natural vibration should be analyzed as much as possible.

(2)As a result of the internal force redistribution, the maximum node displacement is in a certain range with kinds of arrangements of BRBs. The last ring of the sphere and second ring direction of the cylinder are two important position for structure reinforce and energy dissipation, the maximum displacements of the single-layer oval shell with sub-structure on the top of the structure should not be considered.

(3)Four kinds of BRBs arrangement has remarkable vibration reducing effect on the single-layer oval shell, the rate of maximum negative displacement reduce is about 25%, the axial force reduced at certain degree ,the rate of reduce is about 5%.

(4) From the analysis, it can be obtained that the influence of rise-span ratio, length-width ratio, initial geometric imperfection, temperature on the vibration reducing should be comprehensive considered. Therefore, the real condition should be fully taken into account, the structures considering vibration reducing with sub-structure remains to further study.

Acknowledgement

The authors are grateful for the supports of National Natural Science Foundation of China.(50678078) and Excellent Young expert Foundation of Lanzhou University of technology for the present research.

References

[1] Wang Xiuli, Wang Lei: Seismic response analysis of new type elliptical reticulated shell. *Earthquake Resistant Engineering and Retrofitting*. 2007, Vol.29(4)pp:31-36.

[2] S Kato, S Nakazawa, M Uchikoshi and Y Mukaiyama: Response Reducing Effect of Seismic Isolation. System Installed Between Large Dome and Lower Structure. Proceedings of APCS,2000,Vol.1,pp.323-330

[3] Xue Suduo, Cao Zi, Wang Jianning: Elastic-plastic seismic response of single layer cylindrical lattice shells. *Earthquake Engineering and Engineering Vibration*. 2002, Vol.22(1), pp.57-60.

[4] Cao Zi,Zhang Yigang. Seismic response characteristics analysis of seismic response. *Building Structure.* 1998. 28(8):40-43.

[5] Fan Feng, Shen Shizhao. Vibration reducing analysis of reticulated shells with viscous damper. *Earthquake Engineering and Engineering Vibration*. 2003. 29(4): 31-36.

Proceedings of the 6th International Conference on
Computation of Shell and Spatial Structures
IASS-IACM 2008: "Spanning Nano to Mega"
28-31 May 2008, Cornell University, Ithaca, NY, USA
John F. ABEL and J. Robert COOKE (eds.)

Nonlinear dynamic analysis of space frame structures

Chung-Yue WANG*, Ren-Zuo WANG**

* Department of Civil Engineering, National Central University
Chungli, 32054, Taiwan, R.O.C
cywang@cycu.edu.tw

* National Center for Research on Earthquake Engineering
Taipei 106, Taiwan, R.O.C.
rzwang@ncree.org.tw

Abstract

In this paper, a novel formulation for the nonlinear motion analysis of reticulated space frame structures is developed by applying a new concept of computational mechanics, named the vector form intrinsic finite element (VFIFE or V-5) method. The V-5 method models the analyzed domain to be composed by finite particles and the Newton's second law and Euler's equation of motion are applied to describe each particle's motion. By tracing the motions of all the mass particles in the space, it can simulate the large geometrical and material nonlinear changes during the motion of structure without using geometrical stiffness matrix and iterations. The analysis procedure is vastly simple, accurate, and versatile. The formulation of VFIFE type space frame element includes a new description of the kinematics that can handle large rotation and large deformation, and includes a set of deformation coordinates for each time increment used to describe the shape functions and internal nodal forces. A convected material frame and an explicit time integration scheme for the solution procedures are also adopted. Numerical examples are presented to demonstrate capabilities and accuracy of the V-5 method on the nonlinear dynamic stability analysis of space frame structures

1. Introduction

Nonlinear analysis methods developed since last century are used to study the behavior of structures with material and geometrical nonlinearities. Gallagher and Padlog (1963) first introduce the geometrical stiffness matrix into the nonlinear analysis of structure by considering the nonlinear strain terms in the formulation. Argyris et al. [1] have tried to modify the definition of bending moment to derive a modified geometrical stiffness matrix to satisfy the equilibrium requirement at each deformed state. Yang and Kuo [2] proposed a method to decompose the displacement of structural element into rigid body displacement and natural deformation displacement in each incremental step of the computation and this kind of decomposition can lead the geometrical stiffness matrix pass the rigid body motion test. It is well known that the core idea of the nonlinear analysis of structure is how to clearly identify the rigid body component and the deformation component in the motion. Recently, a novel computation method called as the vector form intrinsic finite element (VFIFE, simply called V-5) method was proposed by Ting et al. [3, 4] and Shi et al. [5]. The VFIFE method has been successfully applied to the nonlinear motion analysis of 2D frame (Wu et al. [6]) and the dynamic stability analysis of space truss structure (Wang et al. [7, 8, 9]). Due to some special characteristics of the VFIFE method, it is very easy to be applied to study the highly nonlinear dynamic behavior of a structure system from continuous to discontinuous states. In this paper, the theory of space frame element in VFIFE (Wang [10]) is briefly introduced.

2. Fundaments of the 3D Fame in VEFIFE

A novel computational method so called the Vector Form Intrinsic Finite Element is developed by Ting et al. (2004 a, b) to handle engineering problems with the following characters: (1) containing multiple deformable bodies and mutual interactions, (2) material non-linearity and discontinuity, (3) large deformation and arbitrary rigid body motions of deformable body. Since the conventional FEM based on variational method requires the total virtual work to be zero but does not require the balance of forces at nodes. These unbalanced residual forces will do some non-zero work under virtual rigid body motion and cause the inaccuracy and un-convergence of the calculation results. The computation procedure and some concepts of this VFIFE method are similar to the FEM. But the major difference is that the VFIFE does not apply the variational principle on the stress expressed equilibrium equations in its formulation. Instead, VFIFE maintains the intrinsic nature of the finite element method and makes strong form of equilibrium at nodes, the connections of members.

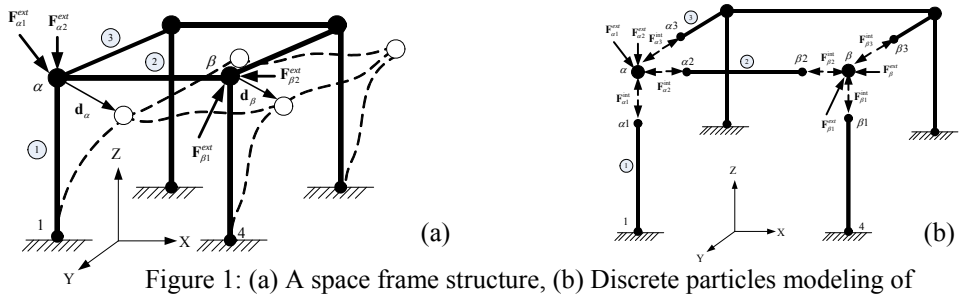

Figure 1: (a) A space frame structure, (b) Discrete particles modeling of space frame structure system by the VFIFE method.

In other words, the continuous bodies are represented by a set of mass points through lumped mass technique as shown in Fig. 1. Each mass point satisfies the law of mechanics, i.e. the conservation of linear and angular momentums. Similar to other well-developed VFIFE elements, a convected material frame and explicit time integration for the solution procedures are also adopted in the formulation of 3D frame element. The description of kinematics to discrete rigid body and deformation displacements, and a set of deformation coordinate for each time increment to describe deformation and internal nodal forces can be found in the thesis of Wang [2005a]. The formulation of space frame element in V-5 is an extension of the theories for space truss element. The correspondence between these two types of element can be identified from the work done by the authors (Wang et al. [7]). The basic modeling assumptions for the VFIFE method for 3D frame structures are essentially the same as those in classical structural analysis. A frame is constructed by means of prismatic members and joints. Members are subjected to forces and moments. The corresponding general internal forces $\hat{\mathbf{f}}^* = (\hat{f}_{2x}, \hat{m}_{1y}, \hat{m}_{1z}, \hat{m}_{2x}, \hat{m}_{2y}, \hat{m}_{2z})^T$ of the frame element in the deformation coordinate system can be derived by the principle of virtual work. From the static equilibrium equations, all the internal forces at the two nodes of the frame element can be calculated. After calculating all the internal forces of element nodes, one can sum over all internal forces $-\mathbf{F}_\beta^{\text{int}}$ and external forces $\mathbf{F}_\beta^{ext}$ applied on a rigid body particle β and obtain the following equation of motion without damping effect:

$$\mathbf{M}_\beta \ddot{\mathbf{d}}_\beta = \mathbf{F}_\beta^{ext} - \mathbf{F}_\beta^{\text{int}} \tag{1}$$

Where $\mathbf{M}_\beta$ is the general mass matrix and $\ddot{\mathbf{d}}_\beta$ is the general displacement vector of the particle β. In the present analysis, the explicit time integration technique is used to solve Eq. (1). Since the VFIFE method uses the motion and relative displacements of particles to identify the internal forces among them. This feature allows users to do the displacement control type excitation.

3. Numerical Examples

Example 1: Buckling of Space Frame Structure

Figure 2 shows a reticulated space frame structure composed of 12 members subjected to a vertical load P at its highest node. Each member has a cross sectional area $A = 0.9in^2$, principal mass moment of inertials

$I_2 = 0.2in^4$, $I_3 = 0.02in^4$, $J = 0.0331in^4$, Young's modulus $E = 4.398x10^5\ psi$ and shear modulus $G = 1.59x10^5\ psi$. This large deformation, post buckling problem has been studied by many researchers (Papadrakakis [11], Meek and Tan [12], Hsiao and Horng [13]). We use the function of displacement control of V-5 to calculate the load-displacement relation of this frame structure and compare it with the results obtained by previous researchers. It is seen in Fig. 3(b) that the V-5 method can accurately analyze the buckling of space frame with large deformation.

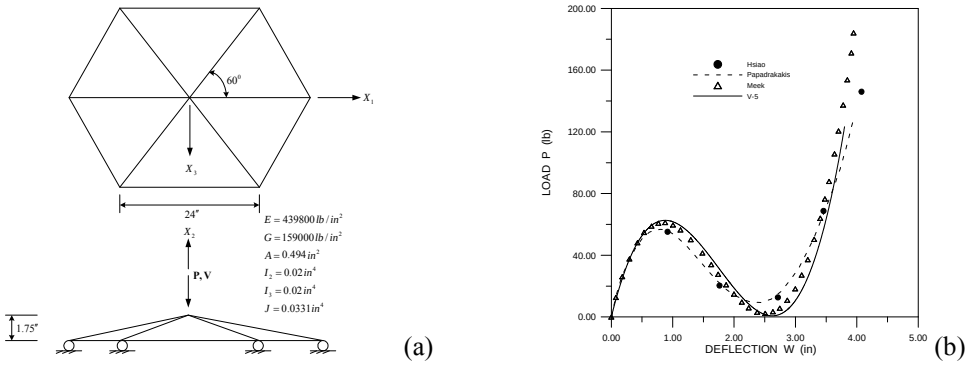

Figure 2: Bucking analysis of reticulated space frame structure composed of 12 members. (a) top view and side view, (b) vertical load- displacement relation of roof tip.

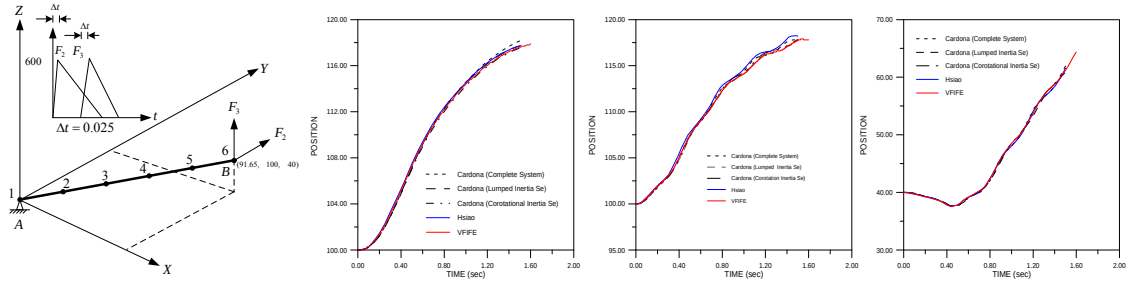

Figure 3: Deformation and rotation of an articulated rod, (a) loading functions, (b) history of the Y coordinate of the tip of rod with $E = 2.1x10^9\ psi$, (c) history of the Y coordinate of the tip of a rod with $E = 6.3x10^6\ psi$, (d)) history of the Z coordinate of rod tip with $E = 6.3x10^6\ psi$.

Example 2: Articulated-free rod

An articulated- free rod subjected to an impulse force F_2 in Y direction and an impulse force F_3 in the Z direction as shown in Fig. 3 was studied. This problem has been investigated by many researchers (Géradin and Cardona [14], Hsiao et al. [15], Crisfield [16]) as a benchmark problem for frame structure having large rotation and large deformation. The rod has length 141.42 inch, cross sectional area 9 in^2 , mass density $\rho = 2.54\times10^{-4}\ lb-s^2in^{-4}$, and Poisson's ratio $\nu = 0.3$. Rods with different Young's modulus were selected to study their difference in motions with large deformation and rotation. Five frame elements were used to model the rod. Figure 3(b) shows the history of the Y coordinate of the tip of a rod with Young's modulus $E = 2.1x10^9\ psi$ and Fig. 3(c) shows the history of the Y coordinate of the tip of a rod with Young's modulus $E = 6.3x10^6\ psi$. These two figures reveal the effect from the rigidity of rod on the deformation of rod. Figure

3(d) shows the history of the Z coordinate of the tip of a rod with Young's modulus $E = 6.3x10^6\ psi$. From Fig. 3, it also find that the V-5 method can accurately analyze the motion of frame structure with large rotation and deformation based on a new concept of computational mechanics.

4. Conclusions

A vastly simple numerical procedure is developed in this paper for motion analyses of the nonlinear response and stability of reticulated space frame structures subjected to large geometrical changes and complicated excitations. Due to the nature of discrete independent particle point, it is not required to set essential boundary conditions of the system. It is very easy to prescribe the displacement and forcing conditions on each particle during the procedure of analysis. Through the numerical analyses of a few benchmark problems of features as large rotation and dynamic instability, the newly proposed method demonstrates its accuracy and superior capability on the nonlinear motion analysis of space frame structure. As well, the vector form nature of the V-5 method allows it to be linked with parallel computation techniques to study the large scale problems that have complicated geometrical variations and loading histories.

References

[1] Argyris JH, Dunne PC and Scharpf DW. On large displacement-small strain analysis of structures with rotational degree of freedom. *Computer Methods in Applied Mechanics Engineering*, 1978; 14: 401-451.

[2] Yang YB, and Kuo SR. *Theory & Analysis of Nonlinear Framed Structures*. Prentice-Hall. 1994.

[3] Ting EC, Shih C, and Wang YK. Fundamentals of a vector form intrinsic finite element: Part I. basic procedure and a plane frame element. *Journal of Mechanics*, 2004; 20: 2. 113-122.

[4] Ting EC, Shih C, and Wang YK. Fundamentals of a vector form intrinsic finite element: Part II. plane solid elements. *Journal of Mechanics*, 2004; 20: 2. 123-132.

[5] Shih C, Wang YK, and Ting EC. Fundamentals of a vector form intrinsic finite element: Part III. Convected material frame and examples. *Journal of Mechanics*, 2004; 20: 2, 133-143.

[6] Wu TY, Wang RZ, and Wang CY. Large deflection analysis of flexible planar frames, *Journal of the Chinese Institute of Engineers*, 2006; 29: 4. 593-606.

[7] Wang CY, Wang RZ, Chuang CC, and Wu TY. Nonlinear Dynamic Analysis of Reticulated Space Truss Structure. *Journal of Mechanics*, 2006; 22: 3. 235-248.

[8] Wang RZ. *Vector Form Motion Analysis of Structure,* Ph. D. Thesis, Department of Civil Engineering, National Central University, Taiwan (in Chinese). 2005.

[9] Wang RZ, Chuang CC, Wu TY, and Wang CY. Vector form analysis of space truss structure in large elastic-plastic deformation. *Journal of the Chinese Institute of Civil & Hydraulic Engineering*, 2005; 17: 4. 633-646.

[10] Wang RZ, Kang LC, Wu SY, and Wang CY. Numerical Simulation of the Whipping Problem of High Pressure Pipe. *Chinese Society of Structural Engineering*, 2005; 20: 4. 120-143 (in Chinese).

[11] Papadrakakis, M. Post-buckling analysis of spatial structures by vector interation methods. *Computers and Structures* 1981; 14; 5-6:393-402.

[12] Meek JL, Tan HS. Geometrically nonlinear analysis of space frames by an incremental iterative technique. *Computer Methods in Applied Mechanics and Engineering* 1984; 47:261-282.

[13] .Hsiao KM, Horng HJ. A corotational procedure that handles large rotations of spatial beam structures. *Computers and Structures* 1987; 27; 6: 769-781.

[14] Géradin M, Cardona A. A superelement formulation for mechanism analysis. *Computer Methods in Applied Mechanics and Engineering* 1992; 100:1-29.

[15] Hsiao KM, Lin JY, Lin WY. A consistent co-rotational finite element formulation for geometrically nonlinear dynamic analysis of 3-D beams. *Computer Methods in Applied Mechanics and Engineering* 1999; 169: 1-18.

[16] Crisfield MA. Dynamic analysis of 3D beams with joints in presence of large rotations. Computer Methods in Applied Mechanics and Engineering 2001; 190: 4195-4230.

Proceedings of the 6th International Conference on
Computation of Shell and Spatial Structures
IASS-IACM 2008: "Spanning Nano to Mega"
28-31 May 2008, Cornell University, Ithaca, NY, USA
John F. ABEL and J. Robert COOKE (eds.)

Dynamic behaviors of two large spatial structures

Jinzhi WU*, Yigang ZHANG, Xiaobing GENG

*Spatial Structures Research Center, Beijing University of Technology
Pingleyuan 100, Chaoyang District, Beijing 100022, P.R. China
kongjian@bjut.edu.cn

Abstract

There are many large spatial structures have been built and more and more are to be built in China these years. The dynamic analysis is very important to the design of large space frames, for the dynamic behaviors can reflect the integrity and the stiffness of the structure. The dynamic behaviors of two large spatial structures we have designed are introduced in this paper, which were analyzed with Midas/Gen.

1. Introduction of the two structures

The first one is a large fanlike roof(Figure 1 and 2) made up of 9 prestressed Beam String Structures(BSSs) connected by pyramid Mero system space frame with the interval of 4.5m. The BSSs are supported by RC columns at the two ends with the span of 148.125m. The BSS roof is half of the roof of the whole structure, and the other part is made up of ordinary three-layer pyramid space frame on the left of the BSS roof with nearly the same area but different height. There are no columns used on the connecting edges of the two parts which are built separately.

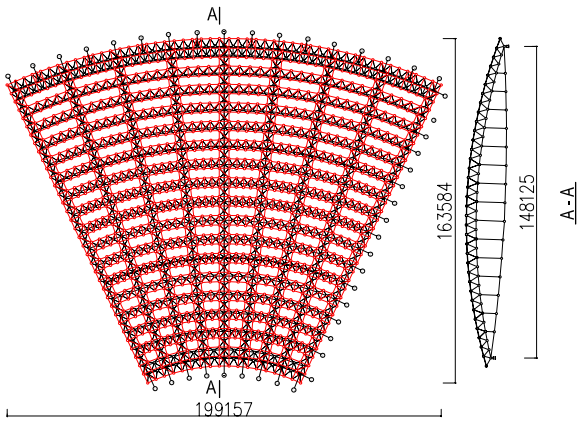

Figure 1 Plan of the BSS roof

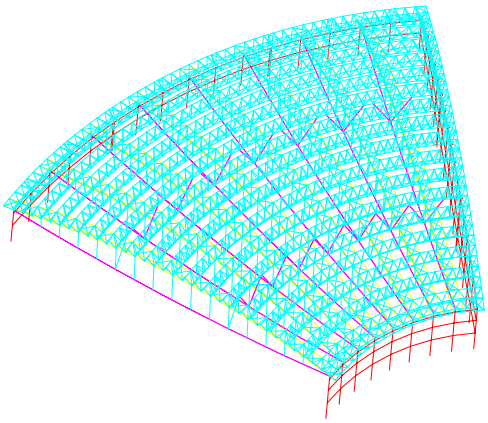

Figure 2 3D view of the BBS roof

The heights of the columns supporting the two ends of the BSSs are 18.86m and 12.77m separately. The thickness of the trigonal truss is 4.5m. The Φ7×337 high strength cable is used with the pretension of 2000kN. The structure is under construction and may be the largest BSS up to now. The area of the roof is about 20,000m^2. The static and dynamic behaviors of the structure are analyzed during its design. It is found that the upward wind load caused greater moment at the bottom of the columns than the dead and live load. To balance the moments with different sign, the BBSs are required to be simply supported during the construction of itself, and fixed to the top of the columns after the pretension. To get a better result, the elastic abutments at top end of the BSSs. The period of the first vibration mode of the structure is 1.05s, longer than 0.94s when the two ends of the BBSs are fixed to the columns. But to the other vibration modes, the periods are only slightly changed and vibration mode shapes are almost the same.

The second one is a large airship assembly factory(Figure 3 and 4), of which the length, width and height are 300m, 100m and 95m separately. Based on the comparing with many different structural types, the space frames are used for the roof, the side and back walls and the 85m high gate finally. The differences of them are that the roof is ordinary three-layer space frame with steel tubes and welded hollow balls, the gate and back wall are space frames with Mero system and the side walls are three-layer space frames with Concrete Filled Steel Tubes(CFST) as the chord members.

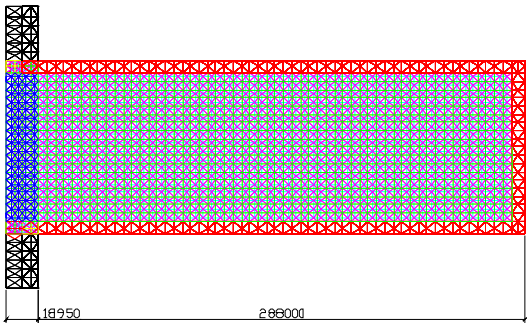

Figure 3 Plan of the airship factory

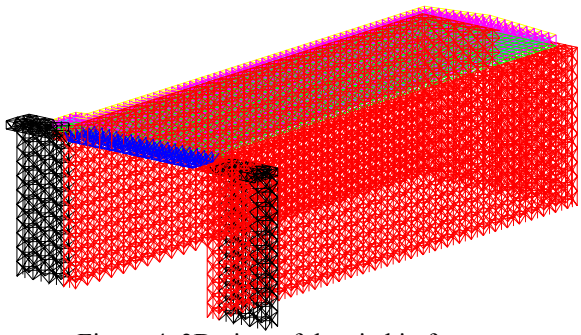

Figure 4 3D view of the airship factory

2. Dynamic behavior of the BBS roof

There are columns at the two ends and only right edge of the BSS roof. So even the BSSs are distributed symmetrically, the mechanical behavior is asymmetrical. The maximum deflection of the whole BSS roof under static vertical load appears at the middle of the left BSS. To obtain the dynamic behavior of the structure, the dynamic analysis has been carried out and the earthquake effect has also been considered in the load combinations. The first ten vibration parameters of the BSS roof are shown in Table 1 and the mode shapes are shown in Figure 5 to 10.

Table 1 The first ten vibration parameters of the BSS roof

Mode	Period /s	Factor of vibration direction / %		
		X	Y	Z
1	1.05	**91.62**	6.46	1.92
2	0.94	2.94	10.62	**86.44**
3	0.86	1.76	10.58	**87.67**
4	0.75	0.31	17.15	**82.54**
5	0.70	2.63	18.17	**79.20**
6	0.66	2.25	7.98	**89.77**
7	0.56	**78.03**	13.25	8.71
8	0.52	11.65	20.57	**67.78**
9	0.50	6.84	30.87	**62.29**
10	0.46	3.55	38.29	**58.16**

From the above table and the figures, we can see that the vibration mode shapes are all asymmetrical, which is because the roof is asymmetrically supported, even the BSSs are distributed symmetrically. That should be taken into the consideration during the design of this kind of structure. The first vibration mode is a horizontal one to the X direction, which indicates the stiffness of the columns at the right edge of the structure is relatively weaker than that the roof itself. But the first period of 1.05s is not a very high value, and that indicates the whole structure is stiff enough. The second to the sixth modes are the vibrations of the BSS roof itself in Z direction with different numbers of the waves, which are the usual cases for long span structures. From the first six mode shapes, we can also see that the integrity of the roof is very good, although it is made up of 9 BSSs, for the BSSs are distributed evenly and the bracing space frames are strong enough. As we know, without the bracing stiff enough in both horizontal and vertical directions, the BBSs will vibrate itself as planar trusses. But this has not appeared in this structure.

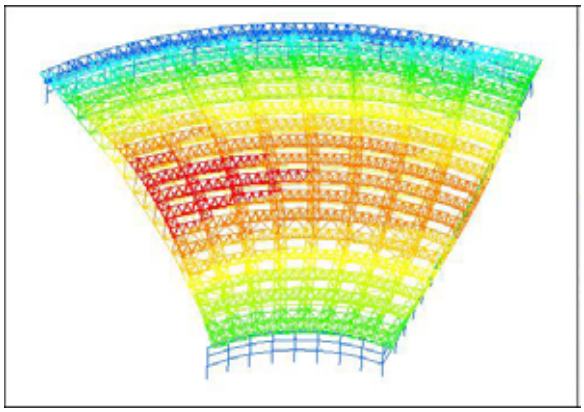

Figure 5 the 1st mode shape of BSS

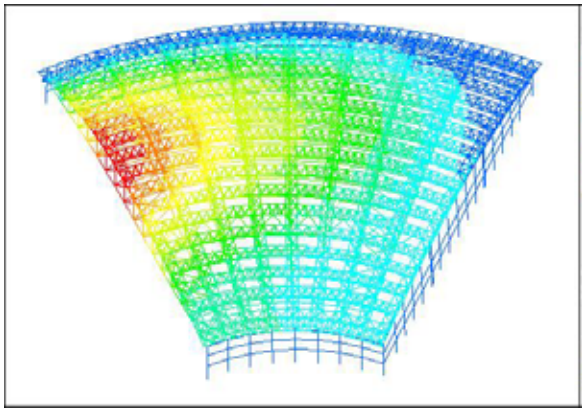

Figure 6 the 2nd mode shape of BSS

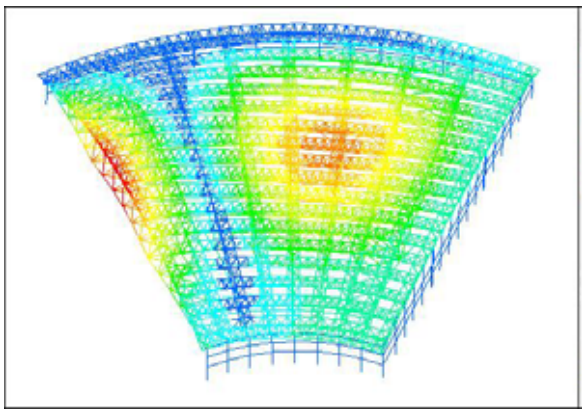

Figure 7 the 3rd mode shape of BSS

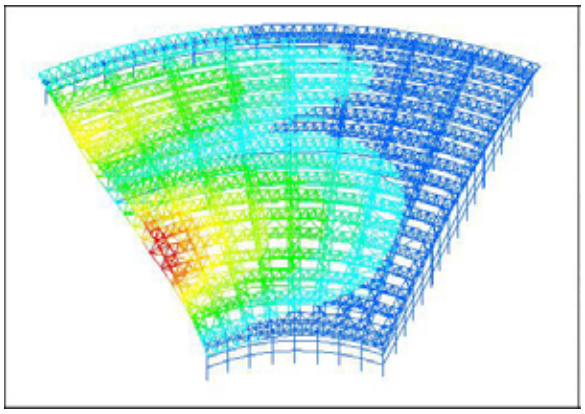

Figure 8 the 4th mode shape of BSS

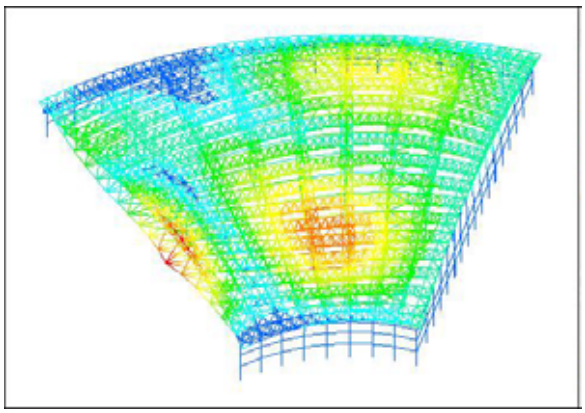

Figure 9 the 5th mode shape of BSS

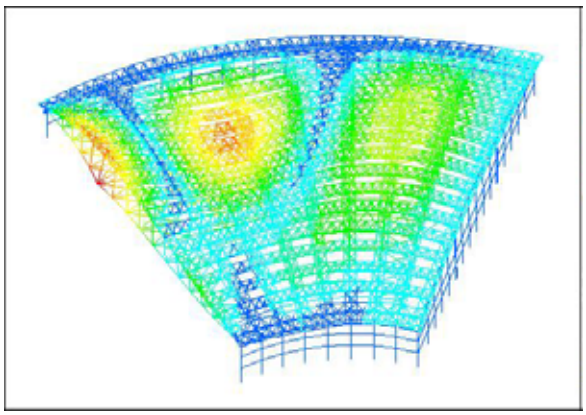

Figure 10 the 6th mode shape of BSS

3. Dynamic behavior of the airship factory

The span of the factory is not very long, but the height of the walls is 85m. And so the transverse stiffness of the structure is relatively weak, like a 30-story tall building. The first six vibration mode shapes are shown in Figure 11 to 16 with the period of 1.36,0.94,0.73,0.69,0.66 and 0.65 second separately. Although the roof space frame and the side walls are stiffened, the first four vibration mode shapes are still horizontal ones, in which the 1st, 2nd and the 4th mode are transverse vibration with 1, 2 and 3 half waves. While the 3rd mode is longitudinal vibration. The 5th and 6th mode shapes are vertical vibration of the roof itself. But the periods of them are very close, even though they have different number of waves, for the length of the factory is about 3 times of its width.

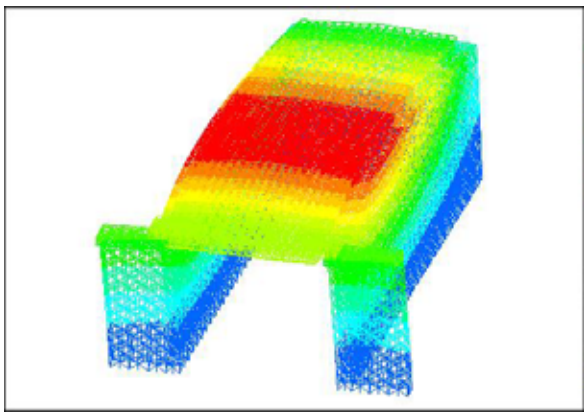

Figure 11 the 1st mode shape of airship factory

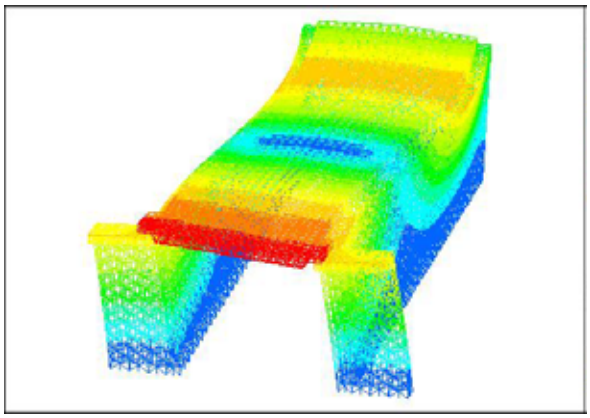

Figure 12 the 2nd mode shape of airship factory

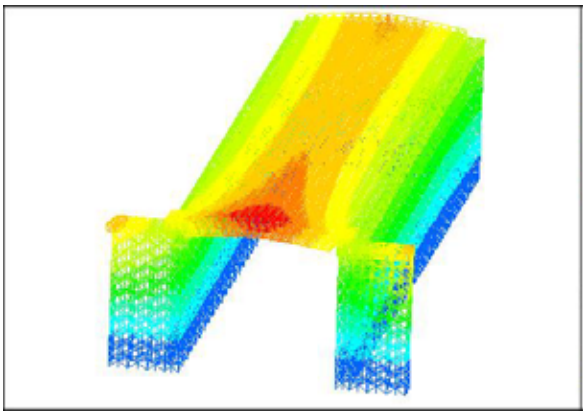

Figure 13 the 3rd mode shape of airship factory

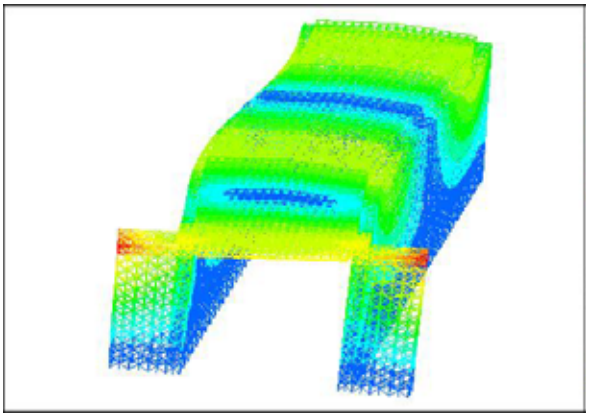

Figure 14 the 4th mode shape of airship factory

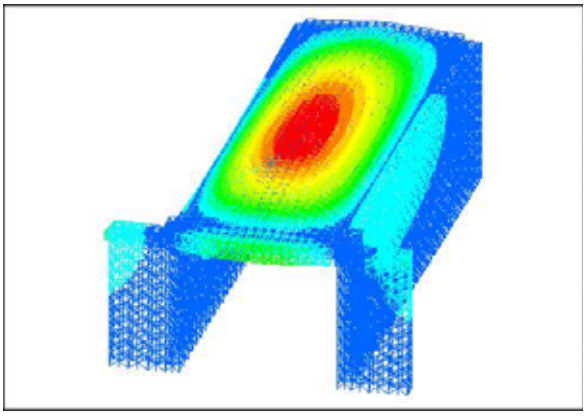

Figure 15 the 5th mode shape of airship factory

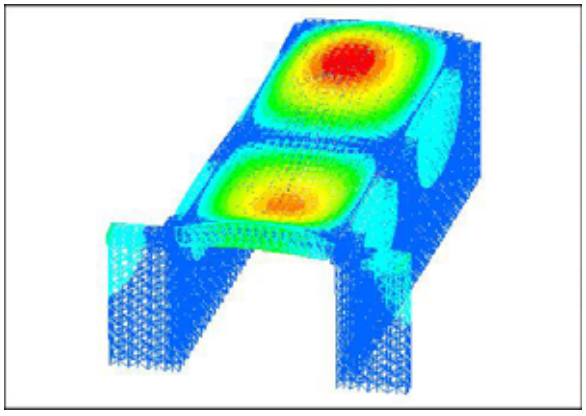

Figure 16 the 6th mode shape of airship factory

4. Conclusions

Based on the analysis above, we can get that it is very important to study their dynamic behaviors during the design of large spatial structures. 1) The dynamic behavior can reveal the integrity and the stiffness of the structure, and this will tell us which part of the structure should be strengthened; 2) The dynamic behaviors of different structures are different distinctly, and the effect of them are different thereby; 3) The period of the first mode is better less than 1.5s, otherwise it will lead to greater wind load effect on the structure.

Acknowledgement

This analysis of the BSS roof is carried out with the help of Mr. Qinggang LU and Mr. Wenfeng LI.

Proceedings of the 6th International Conference on
Computation of Shell and Spatial Structures
IASS-IACM 2008: "Spanning Nano to Mega"
28-31 May 2008, Cornell University, Ithaca, NY, USA
John F. ABEL and J. Robert COOKE (eds.)

Investigation into the dynamic behaviour of double layer tensegrity systems

Behzad SHEKASTEHBAND*, Karim ABEDI

*PhD Student
Sahand University of Technology, Department of Civil Engineering
b_shekastehband@sut.ac.ir, k_abedi@sut.ac.ir

Abstract

Tensegrity systems are systems in a stable self equilibrated (selfstress) states comprising discontinuous set of compressed components inside a continuum of tensioned components. In this paper the dynamic behaviour of double-layer tensegrity systems is investigated taking into account both geometric and material nonlinearities under harmonic loading. The investigation is carried out on the continuous struts tensegrity systems. The structure's frequencies are determined assuming it vibrates about its deflected position under variable load magnitudes. Maximum element force time histories and dynamic amplification factors are computed as a function of variable load frequencies. Results of analyses revealed that resonant responses occurred at frequencies which are not corresponding to that of the lowest mode of vibrations, and caused large forces in some elements of the structures. Also in this study, a dynamic analysis of self-stress levels of tensegrity systems is performed. According to the result, in the case of vibration of the structure about its initial undeflected position and about its deflected position under vertical loading, the frequencies are independent of the selfstress level and dependent on the nonlinear relationship. Based on the obtained results, the first buckling load in these systems can be reached when it is subjected to a harmonic loading having a magnitude too smaller than that of a static load.

1. Introduction

Tensegrity systems are a sub class of reticulated space systems. Their development began at the end of the forties, with the sculptures of Kenneth Snelson and also in the works of Richard Buckminster Fuller and David George Emmerich (Averseng *et al.* [1]). Recently, Rene´ Motro suggested the following definition: "A tensegrity system is a system in a stable self equilibrated state comprising a discontinuous set of compressed components inside a continuum of tensioned components" (Quirant *et al.* [6]). They are stabilized by a selfstress state that is the internal stress state established during assembling. This selfstress state ensures the auto-balance of the system, in the absence of any external action (Averseng *et al.* [1]).
Until recently, some studies have been undertaken on the dynamic behaviour of the small tensegrity systems. Ben Kahla and Moussa have performed a numerical investigation into the effect of sudden rupture of a cable component in the behavior of a tensegrity assemblage using nonlinear dynamic time history analysis (Ben Kahla and Moussa [4]). Ben Kahla *et al.* have investigated the evolution of natural frequencies in tensegrity systems through case study (Moussa *et al.* [5]). Zhang and Chen have carried out dynamic analysis of natural vibration properties and seismic response for a tensegrity tower (Zhang and Chen [7]).
So far few investigation has been carried out to examine nonlinear dynamic behaviour of double layer tensegrity systems, taking into account both geometric and material nonlinearities. The objective of this paper is to investigate the nonlinear dynamic behaviour of double layer tensegrity systems. For this purpose, the implicit dynamic analysis method is used to integrate the equations of motion, together with a Newton-Raphson iterative scheme to insure equilibrium within each time step.

2. Finite element modeling

The studied system is a square grid 9m long constituted of 36 half-cuboctahedron modules which has only 4 struts. For this module, the prism form allows easy assembly by simple juxtaposition of the nodes (Figs. 1 and 2). The height was determined so as to have the bars inclined at 45° with respect to layers. The height of the grid is then 1.15m, giving an aspect ratio of about 1/8. Therefore the assembled grid has 133 nodes and 516 components (144 struts and 372 cables) (Quirant *et al.* [6]).

This system has been analyzed using ABAQUS, a non-linear finite element software package. The analyses consider both geometric non-linearities due to buckling and change of joint coordinates and material non-linearities due to yielding. Figure 2 illustrates the axial strain-axial stress responses of the struts with slenderness ratio of L/r = 100. The strain-stress response of the cables, used in analyses, is illustrated in Figure 4 (Ben Kahla [3]).
The grid is supposed to be resting on the external nodes of the lower layer. The design process proposed by Quirant *et al.* has been used (Quirant *et al.* [6]). According to this method, as for the choice of the selfstress level, it is made according to 50% from the limit recommended by EC3 for the compression of struts. So that, a cross-section design of 3.00 cm^2 for the struts and of 0.80 cm^2 for the cables were obtained.

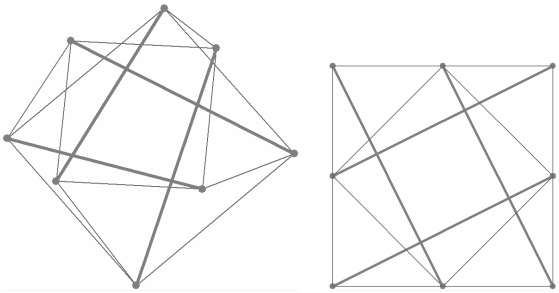

Figure 1: Half-cuboctahedron, perspective view and top view.

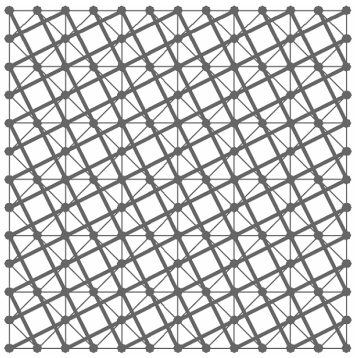

Figure 2: Tensegrity grid formed of 36 half-cuboctahedrons (6 × 6).

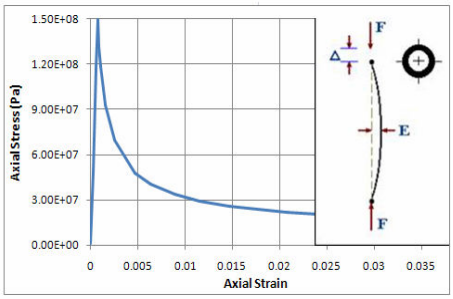

Figure 3: The axial strain-axial stress responses of the struts with the slenderness ratio of L/r=100 (ε=0.001L)

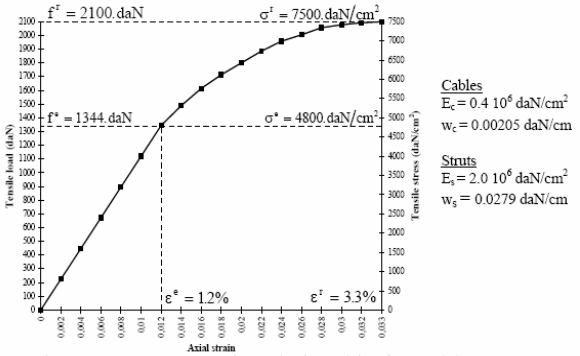

Figure 4: Stress-strain relationship for cable elements (Ben Kahla [3])

The joint co-ordinates and member connectivity data required for the structural analysis has been generated using the configuration processing capabilities of formex algebra.

2.1 Dynamic Analysis

The incremental equation of motion of a tensegrity system written with respect to its configuration at time $t+\Delta t$ is:

$$M\,{}^{t+\Delta t}\ddot{U} + C\,{}^{t+\Delta t}\dot{U} + K\,{}^{t+\Delta t}U = {}^{t+\Delta t}R \qquad (1)$$

Where, M, C and K are the mass, damping and stiffness matrices, respectively; $\ddot{U}$, $\dot{U}$ and U are vectors of nodal acceleration, velocity and displacement, respectively. The damping matrix is formed using Raleigh type damping. The time increment is chosen such that $\Delta t \le \frac{1}{20} T_{co}$, in which $T_{co} = 2\pi/\omega_{co}$ and $\omega_{co} = 4\omega_0$, ω_0 being the system first natural frequency (Bathe [2]).

3. Analysis of natural vibration properties

The first twenty lowest natural frequencies of vibration of this structure were obtained for both vibrations of the structure about its initial undeflected position (no loads applied), listed in Table 1, and about its nonlinear static deflected equilibrium position under equal vertical loads applied to its upper nodes. In Figure 5 the variations of the first twenty lowest frequencies are depicted as a function of the magnitudes of the applied loads. This plot

shows that in the chosen range of amplitude, the fluctuations of the frequencies are not significant for the lower amount of loads; however there are some variations for the upper ones. This behaviour is attributed to the slackening of some cable elements when the system is loaded greater than ± 1500N.

Then a vibration analysis is performed on the stabilized geometry of the system corresponding to the state of self-stress recommended by Eurocode 3 and about its nonlinear static deflected equilibrium position under equal vertical loads applied to its upper nodes (-1000N). Its lowest ten natural frequencies of vibrations about its initial undeflected position are determined for different values of initial strain level and tabulated in table 2. It can be found from table 2, that the frequencies are approximately independent of the self-stress level. Consequently, the level of selfstress has little effect on the rigidity of the system. However, in the case of vibrations of the system about deflected equilibrium position under vertical loading, the frequency, especially in higher modes, varied with the self-stress level (Fig.6). Consequently, under vertical loading, the relationship between the frequency and the self-stress level is nonlinear. In other word, in their evolution when subjected to external loading, the relation between natural frequency and initial stress level is nonlinear, because of the nonlinear behaviour of the tensegrity system.

Mode No.	1	2	3	4	5	6	7	8	9	10
Frequency (Hz)	10.3888	13.6096	13.6096	20.2265	23.9564	23.9564	26.1204	34.1983	34.1983	35.0779
Mode No.	11	12	13	14	15	16	17	18	19	20
Frequency (Hz)	39.4273	40.4633	40.4633	40.5831	42.9299	43.7202	48.1789	48.4978	48.8157	48.8157

Table 1: The twenty lowest frequencies of vibrations of the system about the initial undeflected equilibrium positions

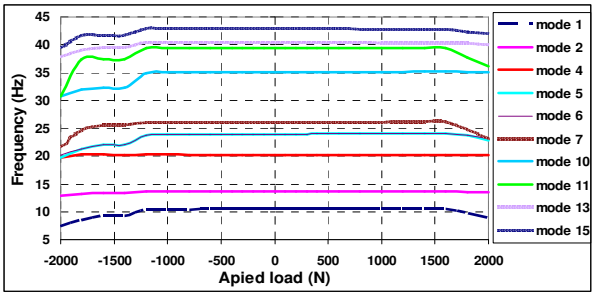

Figure 5: Variations of the first twenty lowest frequencies as a function of the magnitude of the applied load

Initial strain	0	0.0018	0.0027	0.0045	0.0054	0.0081
Mode No.						
1	10.3471	10.3638	10.3721	10.3888	10.3971	10.422
2	13.5414	13.5691	13.5827	13.6096	13.6229	13.6619
3	13.5414	13.5691	13.5827	13.6096	13.6229	13.6619
4	20.1643	20.1899	20.2024	20.2265	20.2382	20.2718
5	23.872	23.9058	23.9227	23.9564	23.9732	24.0233
6	23.872	23.9058	23.9227	23.9564	23.9732	24.0233
7	26.0665	26.0893	26.1001	26.1204	26.13	26.1566
8	34.1682	34.1813	34.1873	34.1983	34.2033	34.2167
9	34.1682	34.1813	34.1873	34.1983	34.2033	34.2167
10	34.8688	34.9548	34.9966	35.0779	35.1175	35.2322

Table 2: Evolution of the first ten natural frequencies as a function of the initial strain (unloaded case)

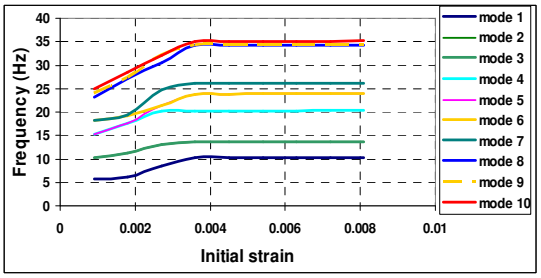

Figure 6: Evolution of the first ten natural frequencies as a function of the initial strain (under load -1000 N)

4. Analysis of dynamic response

For the nonlinear dynamic study, all the upper nodes of this system were loaded by equal vertical loads P(t) = 500.sin(ωt) N. At first, twenty dynamic analyses were carried out. For each of these analyses, the frequency of the applied vertical loads was taken equal to that of the natural frequency of the system assumed to vibrate about its initial undeflected position (no loads applied). The dynamic amplification factors (D.A.F) for the element axial forces of whole system were determined and its average was tabulated in Table 3 for all twenty frequency cases. The dynamic amplification factor for an element axial force is defined as the ratio of the largest element axial force obtained from dynamic analysis to the element initial axial forces obtained statically for the unloaded structure. The maximum D.A.F corresponded to lowest frequency. Next, several dynamic analyses were performed by changing the load frequency from 1 to 12 Hz. In each analysis, the largest element axial force in all elements of the system was obtained. The variations of these forces as a function of load frequency for upper cables and struts of central module are given in Fig.7. This figure demonstrates that resonant responses occurred

at frequencies smaller than that corresponding to the first lowest mode of vibrations, and caused large forces in some elements of the system in a way that few struts were buckled. Although some cables were experienced yielding, none of them exceeded rupture criteria.
By performing nonlinear static analysis (using Arc-Length Type Method) it seems that if this system is loaded by equal vertical loads, the value of load causing first buckling in a strut or in a set of struts is 3904.68 N. These two values (500 in harmonic loading and 3904.68 in static loading) explain that the first buckling load in this system can be reached when it is subjected to a harmonic loading having a magnitude too smaller than that of a static load.

Frequency (Hz)	10.3888	13.6096	13.6096	20.2265	23.9564	23.9564	26.1204	34.1983	34.1983	35.0779	39.4273	40.4633	40.4633	40.5831	42.9299	43.7202	48.1789	48.4978	48.8157	48.8157
Average D.A.F	1.70101	1.16965	1.16965	1.11697	1.05471	1.05471	1.04914	1.04794	1.04794	1.04883	1.06242	1.06888	1.06888	1.06972	1.08841	1.08537	1.07436	1.07448	1.0746	1.0746

Table 3- Average D.A.F. obtained from D.A.F for all elements of the system

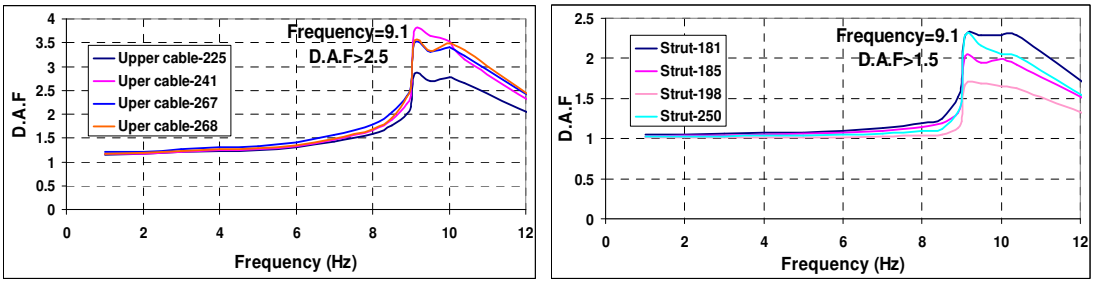

Figure 7: Variations of the largest axial forces in the upper cable and struts of the central module as a function of the load frequency

Conclusion

The study reported herein is concerned with the study of the nonlinear dynamic behaviour of double layer tensegrity system. The analyses revealed that the fluctuations of the first twenty lowest frequencies as a function of the magnitudes of the applied loads are not significant for the lower values and present some variations for the upper ones. Also it was shown that the natural frequencies of vibration of the unloaded tensegrity systems are independent of the self-stress level. However, their stiffness is not constant under loading; and it depends on the magnitude of the applied loads and the nonlinear behaviour of components, thus resulting in non-linear behaviour. It is appeared that resonant responses occurred at frequencies smaller than that corresponding to the first mode. It was also noted that the first buckling load in this particular system can be reached when it is subjected to a harmonic loading having a magnitude too smaller than that of a static load.

Acknowledgement

The authors would like to thank Professor Motro and Dr. Ben Kahla.

References

[1] Averseng A, Kazi-Aoual MN, Crosnier B. Tensegrity Systems Selfstress State Implementation Methodology. In *Space Structures 5*, Park GAR (ed). Thomas Telford: London, 2002; 31-38.

[2] Bathe KJ. Finite Element Procedures. Prentice-Hall, Inc. 1996.

[3] Ben Kahla N. A Study of the Response of a Continuous Tensegrity Beam Under Static Cyclic Loading. In *IASS Symposium*, Montpellier; 2004.

[4] Ben Kahla N and Moussa B. Effect of a Cable Rupture on Tensegrity Systems. *International Journal of Space Structure* 2002, **17**, 51-65.

[5] Moussa B, Ben Kahla N, Pons JC. Evolution of Natural Frequencies in Tensegrity Systems: A Case Study. *International Journal of Space Structures* 2001; **16**, 57-73.

[6] Quirant J, Kazi-Aoual MN, Motro R. Designing tensegrity systems: the case of a double layer grid. *Engineering Structures* 2003; **25**:1121-1130.

[7] Zhang Li-Ping and Chen Zhi-Hua, Dynamic Analysis of Natural Vibration Properties and Seismic Response for a Tensegrity Tower. In *IASS Symposium*, Beijing; 2006.

Proceedings of the 6th International Conference on
Computation of Shell and Spatial Structures
IASS-IACM 2008: "Spanning Nano to Mega"
28-31 May 2008, Cornell University, Ithaca, NY, USA
John F. ABEL and J. Robert COOKE (eds.)

Advances on seismic isolation in spatial structures

Su-Duo XUE*, Xiong-Yan LI

* The College of Architecture and Civil Engineering, Beijing University of Technology, Beijing, 100022, China
sdxue@bjut.edu.cn

Abstract

In order to promote the development of seismic isolation technology in spatial structures, several types of currently used bearings for vibration reduction are reviewed in this paper. To overcome the disadvantages of the in use bearings, a new kind of 3-dimensional seismic isolation bearing (3DSIB) is then developed. The new bearing is combined with friction sliding system in horizontal direction and helical springs or disc springs in vertical direction. Based on the conception model, two practical bearings are designed. Experimental study on their dynamic characteristics is carried out on shaking table. Meanwhile, theoretical model of the bearing is established. Finally, dynamic analysis of a 120m span hangar installed with 3DSIB is conducted in detail. It is shown that the proposed bearing shares very good properties.

1. Introduction

Seismic isolation is an effective means of mitigating earthquake disaster of structures. At present, seismic isolation in spatial structures mainly focused on horizontal directions. It is hard to find reasonable ways for three-dimension seismic isolation. The ideal bearing for spatial structures should possess excellent properties such as three-dimension seismic isolation, enough loading capability in vertical direction, allowing reasonable rotating and being able to resist lifting load.

Two types of commonly used bearings for seismic isolation in spatial structures are reviewed first. To overcome the disadvantages of the in use bearings, a new kind of 3-dimensional seismic isolation bearing is then developed. Based on the conception model, two types of practical bearings are designed. Experimental study on their dynamic characteristics is carried out on shaking table. Meanwhile, theoretical model of the bearing is established. Finally, seismic performance of a 120m span hangar installed with the bearing is analyzed in detail. It is shown that the proposed bearing shares very good properties.

2. Review of seismic isolation in spatial structures

2.1 Rubber bearing system

In earily stages, rubber bearing system was first introduced for seismic isolation devices in spatial structrues. The laminated rubber beaing possesses strong and stiff properties for vertical and flexible deformation under shear stresses. Nowdays, laminated rubber bearings have been used for pratical structures such as Saitama Super Arena, Yamaguchi Kirara Dome (Takeuchi *et al*. [1]). The reduction for the seismic responses and the thermal stesses are expected. In addition, the laminated rubber bearings are also combined with other control devices to satify certain erergy-dissipation functions. For example, in Kyoto Aqua Arena, rubber bearings have been installed along with friction bearings and U-type steel dampers in order to maintain the sways within an allowable range. A type of combined isolator, which consists of one pot-type friction bearing and four rubber bearings, was applied for releasing temperature force and reducing seismic response in the Press Center of the Shanghai International F1 Circuit (Shi *et al*. [2]).

Compared with multistory buildings, the weight of the roof sturctures is light and the space necessary for device defeomantion is insufficient. Therefore, the natural period of the isolated spatial structure tends to be smaller than that of multistory building. However, some problems occurred in the application of laminated rubber bearings, such as the lack of resisting lifting force, permanent deformation under stong ground motions, rather

low energy dissipation capacity, no ability in vertical isolation, and so on. To improve the vibration isolation performance, a type of SMA-rubber bearing is designed by combining SMA with laminated rubber pad (Xue *et al*. [3]).

2.2 Friction sliding system

The friction pendulum system (FPS) is one of the most commonly used sliding systems. It consists of a spherical stainless steel surface, whose geometry generates the self-centering action, and a slider filled with Teflon. Among the most remarkable features of the device are: simplicity of the concept; repeatability of its cyclic behavior; stability of physical properties; durability; independent between restoring and dissipating action; and the control of fundamental vibration period and deformation capacity by simple geometric properties. The FPS has been implemented in some practical structures, such as the terminal roof of the Istanbul Ataturk international Airport, the Seahawks Football Stadium in Seatlle, and others. Another common application for FPS is the use as base isolation, the realized terminal of the San Francisco International Airport is one of this type. Apart from FPS, the purely friction sliding systems are often incorporated with elastic devices such as rubber pad, springs, and so on. The former provides damping, and the latter produces restoring forces.

At present, most of isolation devices can only isolate horizontal earthquake excitations. However, for spatial structures, the seismic responses excited by horizontal and vertical ground motions are nearly at the same level. Therefore three-dimensional seismic isolation has to be considered. In addition, the bearing for spatial structures should possess enough capability to resist lifting force.

3. New developed 3-dimensional seismic isolation bearing (3DSIB)

3.1 Conception model of the 3DSIB

To satisfy the seismic isolation in spatial structures, a new type of 3-dimensional seismic isolation bearing (3DSIB) has been developed by the authors. The bearing shares excellent properties including three-dimensional seismic isolation, enough loading capability in vertical direction, allowing reasonable rotating and being able to resist lifting load. The 3DSIB mainly consists of two parts, i.e. frictional sliding device in horizontal direction and helical springs or disc springs in vertical direction. Figure 1 shows the conception model of the bearing. The horizontal seismic isolation device is combined Teflon-stainless sliding surface with restoring springs. The former is used to limit the transfer of the force across the isolation interface, and the restoring force is provided by the latter. The vertical seismic isolation of the bearing mainly depends on getting reasonable stiffness by vertical springs or disc springs. Being springs utilized in vertical direction, it ensures the 3DSIB shares reasonable rotating capabilities.

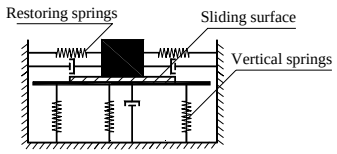

Figure 1: Conception model of the 3DSIB

Suppose the stiffness of the bearing in horzontal and vertical direction is uncopuled, the theoretical model of 3DSIB can be established in horzontal and vertical direction, respectively.

3.2 Theoretical model of the 3DSIB

3.2.1 Vertical model

In vertical direction, the coefficient of isolation effectiveness (*IE*) is introduced first. If the character frequence $\overline{f}$ of the input excitation is determined, the static displacement Δ_{st} caused by vertical gravity loadings of the bearing can be written as

$$\Delta_{st} = \frac{g}{4\pi^2 \overline{f}^2}\left\{(1-2\xi^2)+\frac{2\xi^2}{(1-IE)^2}+\sqrt{\frac{1}{(1-IE)^2}-1+\left[(1-2\xi^2)+\frac{2\xi^2}{(1-IE)^2}\right]^2}\right\} \qquad 0<IE<1 \tag{1}$$

in which ξ is the damping ratio of the spring, for helical steel springs the ξ is 0.02. Once the Δ_{st} being set out, the vertical stiffness of the bearing can be calculated by

$$k_v = W_b / \Delta_{st} \tag{2}$$

where W_b is the gravity loads acting on the bearing. The W_b should be analyzed according to the above structure. Once the stiffness k_v is determined, it is possible to design the vertical helical springs or disc springs. The limit loading capabilities should also be checked.

3.2.2 Horzontal model

In horzontal direction, the sliding device is considered to be subjected to a compressive force W_b and has a general motion in the plane perpendicular to the axis of compression. The total forces caused by the frictional sliding and deformation of the restoring springs may be described by the following equation

$$F_h = F_{h,f} + F_{h,r} \tag{3}$$

where $F_h, F_{h,f}$ and $F_{h,s}$ represent the total force, frictional force and restoring force of the bearing in horizontal direction, respectively.

$$F_{h,f} = \mu_s W_b Z \tag{4}$$

$$F_{h,r} = k_h U \tag{5}$$

In equation (4), μ_s is the coefficient of sliding friction at sliding velocity , and Z is a hysteretic dimensionless quantity. The k_h in equation (5) is the total restoring stiffness of the springs, which should be analyzed according to the horizontal seismic isolation target periods of the structure and the horizontal restoring capabilities of the bearing, and U stands for the sliding displacement. The μ_s can be expressed by an exponential equation, and the relative parameters should be tested by experiments. The hysteretic dimensionless quantity of Z is represented by

$$Y\dot{Z} + \gamma \left|\dot{U}\right| Z \left|Z\right|^{\eta-1} + \beta \dot{U} \left|Z\right|^{\eta} - A\dot{U} = 0 \tag{6}$$

in which $\dot{U}$ stand for the velocity; β, γ, A and η are dimensionless constants; Y represents yield displacement. For Teflon-stainless steel sliding system, the viscoplasticity model is suitable, then $A=1$, $\beta+\gamma=1$ and $\eta=2$.

3.4 Shaking table experiment

Based on the conception model, two practical 3DSIBs were designed and produced. The bearings share same type of horizontal isolation devices. In vertical direction, the helical springs and the disc springs were used respectively. To investigate the performance of the proposed 3DSIB, a series of tests were carried out on the shaking table. The experimental set-up is shown on Figure 2.

Figure 2: Experimental set-up

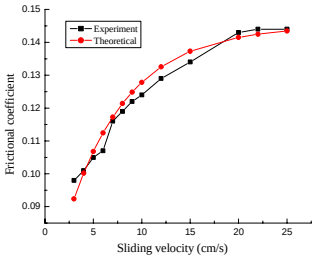

Figure 3: Frictional coefficient

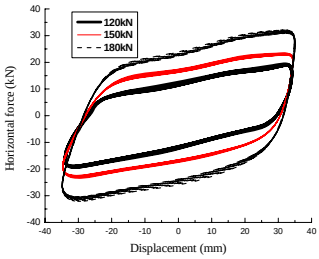

Figure 4: Horizontal hysteretic loops

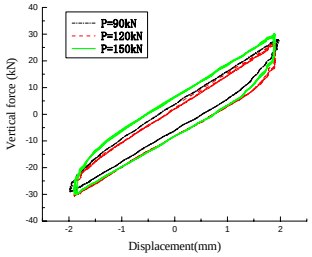

(a) Disc spring

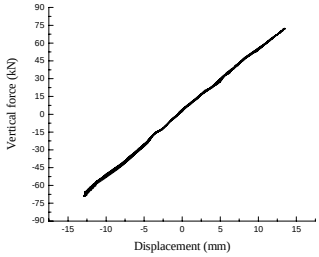

(b) Helical spring

Figure 5: Vertical hysteretic loops

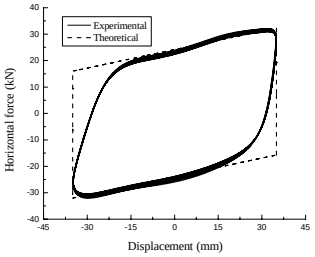

Figure 6: Hysteretic loops comparison between experimental and theoretical

Since frictional coefficient is one of the most important parameters of the 3DSIB, the relationship between frictional coefficient and sliding velocity from experimental and theoretical is compared in Figure 3. Figure 4 and Figure 5 present the typical horizontal hysteretic loops of the two bearings and vertical displacement-force curve. It is seen that the bearings share excellent energy dissipation capability in horizontal direction, and the relationship between vertical displacement and force is nearly linear for helical springs isolation system. However, there exist some hysteretic properties for disc springs device. Figure 6 shows the comparison between the experimental and theoretical results for the bearings. It is indicated that a good agreement is obtained between the theoretical and the measured results.

4. Application of the 3DSIB in spatial structure

The 3DSIB is applied to a maintenance hangar to investigate its control effectiveness under three-dimension seismic excitations (Figure 7). The structure of the hangar is built with a 120m span space frame roof supported on RC columns, and two kinds of 3DSIB are installed on the top of its columns.

In present study, El-centro earthquake waves along X, Y and Z directions are selected as the inputs to the structure. The peak ground acceleration is scaled to 0.20g in the analysis. Some of the results are illustrated in Figures 8 and 9. Figure 9 presents the axial force of up chords of the main truss above the entrance. It is shown that the seismically isolated structure has prolonged periods (Figure 8), and the peak axial forces of the main members are reduced (Figure 9). Furthermore, the sliding displacements of the bearings have been well controlled. The seismic response analysis of the isolated hangar shows that the 3DSIB provides superior performance. In addition, the study has revealed that the seismic isolation effectiveness is mainly related to the frictional coefficient, the restoring stiffness and the vertical stiffness of the bearings.

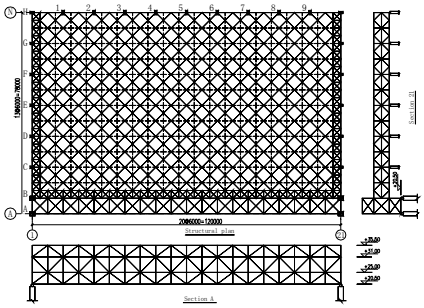

Figure 7: Model of the hangar with 3DSIBs

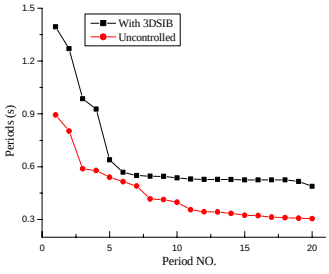

Figures 8: Periods

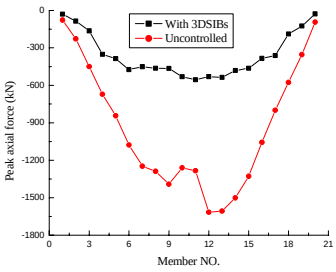

Figures 9: Peak axial force

5. Conclusions

The advances on seismic isolation in spatial structures were reviewed. A new type of 3-dimensional seismic isolation bearing (3DSIB) was introduced. Theoretical models of the 3DSIB were established as well. The experimental results show that the proposed theoretical models can accurately predict the seismic isolation properties of the 3DSIB. Finally, the seismic response of a 120m span hangar roof installed with 3DSIB was analyzed in detail, and some parameters related to seismic isolation performance were discussed. It is shown that the proposed bearing shares very good properties for seismic isolation to spatial structures.

Acknowledgement

The authors gratefully acknowledge the support from the National Natural Science Foundation of China (50778006) and the funding project for academic human resources development in institutions of higher learning under the jurisdiction of Beijing municipality.

References

[1] Takeuchi T, Xue SD, Kato S, *et al*. Recent development in passive control technologies for mental spatial structures. *Proceedings of IASS-APCS Symposium 2006*, DR18, Beijing.

[2] Shi WX, Sun HS, Li ZG, *et al.* High-position isolation of Press Centre at Shanghai International Circuit. *Journal of Tongji University (Natural Science)*, 2005; 12: 1576-1580.

[3] Xue SD, Zhuang P and Li BS. Seismic Isolation of Lattice Shells using a New Type of SMA-Rubber Bearings, *Proceedings of IASS Symposium 2005*, 353-358.

Proceedings of the 6th International Conference on
Computation of Shell and Spatial Structures
IASS-IACM 2008: "Spanning Nano to Mega"
28-31 May 2008, Cornell University, Ithaca, NY, USA
John F. ABEL and J. Robert COOKE (eds.)

Dynamic Analysis of Cable Roof Networks under Transient Wind

S. Ali Ghafari Oskoei (ali.ghafari@mail.mcgill.ca)
Ph.D. Candidate, Department of Civil Engineering and Applied Mechanics, McGill University
Ghyslaine McClure (ghyslaine.mcclure@mcgill.ca)
Associate Professor, Department of Civil Engineering and Applied Mechanics, McGill University
Room 492, Macdonald Engineering Building, 817 Sherbrooke Street West, Montreal, QC, CANADA, H3A 2K6

Abstract

At present, high-speed computing capabilities and advanced nonlinear dynamic finite element procedures enable detailed dynamic analysis of cable structures. Although deterministic approaches require considerable analysis time and effort in relation to modeling, running, and data processing, they seem to be the only alternative to obtain high accuracy. Detailed dynamic analysis of a cable roof network is sophisticated and requires advanced modeling expertise. This paper presents a comparison between detailed nonlinear dynamic analysis and a simplified frequency domain approach to estimate the maximum probable response of weakly nonlinear cable roofs. The approach can be considered as alternative to detailed time-domain analysis in the preliminary design phase, or can be used to validate results obtained from more elaborated numerical models. The proposed method is illustrated with two examples of cable net roofs that were also analyzed in the time domain.

1. Introduction

Large cable roof structures are frequently associated with memorable events. Structurally, they provide an elegant system alternative for large column-free areas. Figure 1 depicts the Olympic Park Stadium of Munich, one of the venues of the Football Word Cup 2006.

Cable roof structures are, in general, lighter and more flexible than most other forms of roof constructions. As a result, they are inherently more resistant to earthquake excitations but also more sensitive to turbulent winds. Moreover, cable roofs with spans exceeding 30 m typically have their dominant lower frequencies within the high-energy range of the wind spectral density function. Hence the need for a dynamic analysis under wind loads should not be readily dismissed for these roof constructions. Also, the nonlinearity of the structure will add to the complexity of the analysis [1].

For highly nonlinear cable networks, dynamic analysis should be performed with a time-marching incremental nonlinear scheme [2]. However, such deterministic approaches for wind analysis are complicated due to modeling of the wind loading. This paper presents a simplified approach that is applicable to weakly nonlinear cable roofs. The proposed procedure combines a linear frequency-domain analysis of the fluctuating component of wind effects and a nonlinear static analysis under mean wind. In this paper, the simplified method is applied to two case studies and the results are compared with those obtained by detailed time-domain nonlinear dynamic analysis.

Figure 1. Olympic Park Munich, Germany. http://www.wikipedia.org/

2. Case Studies

Two saddle-shaped cable roof geometries are studied here, one is rectangular and the other has circular boundaries as illustrated in Figure 2 [3].

In order to define the geometry of the networks and calculate the joint coordinates in the undeformed roof configuration, the general equation of saddle-shaped surfaces is employed:

$$z = \frac{x^2}{a^2} - \frac{y^2}{b^2} \tag{1}$$

where the origin of the coordinate system is placed in the center of the network, and *a* and *b* are the corresponding sags in *x* and *y* directions, respectively.

The circular saddle-shaped roof has a diameter of 120 m and the sag of the pretensioning and the suspension cables is 3% of the roof projected diameter. The net was modeled with 127-mm diameter stranded bridge cable links at 10 mcenter to center. The self weight of the roof, including net and cladding, is taken as 0.6 kN/m^2.

The rectangular roof is 100 m wide and 160 m long with 116-mm diameter stranded bridge cables in a grid of 10 m center to center in the two principal directions. Both networks are prestressed to 30% of the ultimate strain of cables.

Moreover, for both case studies, the mean horizontal wind speed at the average height of the roof is assumed as $U(z)=37\ m/s$. All the loading assumptions regarding the wind effects on the network and the self weight of the roof are also considered to be the same.

3. Modeling Considerations

A nonlinear elastic material model has been used for the cables: a tension-only behaviour is introduced through a bilinear diagram with $E=1.72e11\ N/m^2$ in tension, $\nu=0.3$, and $\rho=7850\ kg/m^3$. The pretension force has been modeled as its corresponding initial strain in each cable element.

Among the truss elements in ADINA, the 3-node parabolic element has been employed for it provides a good compromise in terms of accuracy and numerical effort [4]. Approximately 5 cable elements are required to model the first five transverse modes of a cable segment so a mesh based on 2-m elements is selected.

A nonlinear static analysis under roof self-weight and cable initial strain was performed to obtain the deformed shape of the structures. These deformed configurations were considered as the initial shapes of the structures when applying the external wind forces [5].

4. Dynamic analysis of nonlinear cable networks: time domain approach

The common practice in nonlinear dynamic analysis of structures is to calculate the response using incremental matrix updates and direct integration in time. In this approach, iterations are employed to establish the equilibrium of the forces at the end of each time increment, and algebraic extrapolation is used to evaluate kinematic parameters.

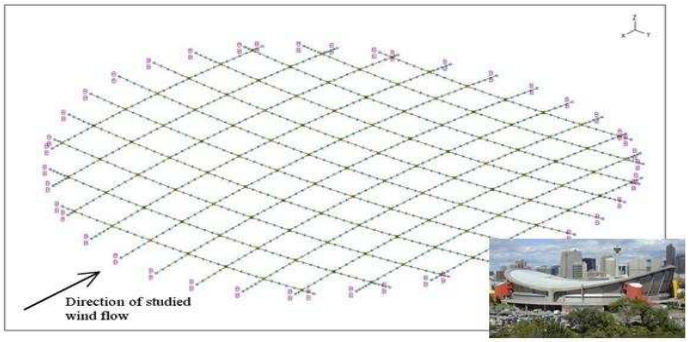

Figure 2. Meshing of a circular saddle-shaped cable network showing cable links and restraints.

4.1. Nonlinear analysis

As an alternative to forms of Newton-Raphson iteration, which are based on the assumption that the solution for the discrete time $t + \Delta t$ is established based on the equilibrium configuration at time t, a class of methods known as matrix update methods has been developed, involving updating the coefficient matrix to provide a secant approximation to the matrix form iteration $(i-1)$ to (i). That is defining a displacement increment

$$\boldsymbol{\delta}^{(i)} = {}^{t+\Delta t}\mathbf{U}^{(i)} - {}^{t+\Delta t}\mathbf{U}^{(i-1)} \tag{2}$$

and an increment in the out-of-balance loads

$$\boldsymbol{\gamma}^{(i)} = \Delta\mathbf{R}^{(i-1)} - \Delta\mathbf{R}^{(i)} \tag{3}$$

the updated matrix ${}^{t+\Delta t}\mathbf{K}^{(i)}$ should satisfy the quasi-Newton equation

$${}^{t+\Delta t}\mathbf{K}^{(i)}\boldsymbol{\delta}^{(i)} = \boldsymbol{\delta}^{(i)} \tag{4}$$

Among The quasi-Newton methods available, the BFGS (Broyden-Fletcher-Goldfarb-Shanno) method was found effective to accelerate the convergence. An energy-based convergence criterion was used [6]. Large displacements but small strains were assumed, which is justified in cable roof applications.

4.2. Dynamic considerations

The constant-average acceleration Newmark-Beta method was selected (with parameters $\gamma = 0.5$ and $\beta = 0.25$) for direct integration of the incremental equilibrium equations. For accuracy considerations, it is recommended to consider $\omega_{co}\,\Delta t \le 0.20$, in which ω_{co} is the highest frequency of interest in the dynamic response [7]. The analyses performed in the current work are based on the assumption that the highest frequency of interest is 30 Hz. Therefore, $\Delta t = 0.001\,\text{sec}$ was selected.

4.3. Modeling of damping

In order to investigate the sensitivity of the structural response to different representations of internal damping, the following three damping models were considered: i) numerical damping introduced by the direct integration scheme, ii) structural viscous damping modelled by individual linear dashpots in parallel with cable elements, and iii) no damping at all.

When no damping was introduced, it was found that the response increased abnormally, presumably due to spurious high frequency contamination from the discrete model. Algorithmic damping was introduced to filter this high frequency noise by setting the parameters of the Newmark method to $\gamma = 0.55$ and $\beta = 0.30$. Surprisingly, the response of structure was further increased and it was concluded that the higher mode vibrations were not spurious. A Fast Fourier Transform (FFT) analysis of the input wind load functions indicated that except for the narrow lowest frequency range, which contains considerable energy, the other parts of the frequency content of the loading had fairly uniform energy. As a result, structural resonance under the wind spectrum was inevitable and it was deemed necessary to introduce a proper structural damping mechanism in the form of viscous dashpot elements in parallel with cable elements.

A parametric study on the sensitivity of the structural response to the amount of equivalent viscous damping was carried out, and it was concluded that varying the damping ratio between 0.5 to 5% critical does not have a significant effect on the total response. Finally, an equivalent translational viscous damper with $2\,\%$ of the critical viscous damping was selected.

4.4. Loading

In this study, five random time histories of horizontal wind pressure are generated through Fourier series. The duration of the generated time histories is taken as $60\,s$. In addition, the delay in the arrival times of the loading in different portions of the roof, following the propagation path of the horizontal wind across the structure, was used to model the correlation of wind histories. The generated horizontal wind pressure histories were projected to the structure according to different angles of attack, and it was found that the worst direction was the

longitudinal direction for the rectangular roof (and corresponding direction for circular network) with the suspension cables experiencing synchronised wind gusts.

4.5. Results and discussion

The results obtained from time history analysis of the circular roof for the maximum vertical displacement of the central point of the roof are listed in the second column of Table 1. It should be mentioned that for calculation of the mean value of the response of different wind histories, which is considered as the design value, RMS is applied as in Equation 5.

$$RMS = \sqrt{\left(x_1^2 + x_2^2 + ... + x_n^2\right)/n} \tag{5}$$

Table 1. Maximum results for the displacements of middle point of circular cable network.

Wind time history Number	X_{max} (middle point) Vertical (m)	RMS	Difference with frequency domain analysis
1	0.47	0.46	24.4 %
2	0.47		
3	0.46		
4	0.45		
5	0.46		

5. Dynamic analysis of nonlinear cable networks: frequency domain approach

It is proposed to determine the dynamic response of weakly nonlinear cable roof structures to wind loading using spectral analysis. In this method, the response of the structure is divided into two parts, the response under mean wind speed, which is obtained through a nonlinear static analysis, and the response due to the fluctuating component of the wind which is estimated by spectral analysis. The fluctuating part is obtained by a statistical approach following the determination of the spectral density function of the response of the structure based on the power spectra of the fluctuating component of loading. The fluctuating response is therefore assumed to vary linearly with the fluctuating component of wind pressure. Adding the two values will result in the total response. Using this approach which is described in more details in [8], we have obtained the maximum vertical displacement of 0.57 m for the circular roof and 0.49 m for the rectangular one (where the detailed nonlinear analysis resulted in 0.46 m), considering the effect of the first mode of excitation only. These values improved while considering more modes in the calculation of the fluctuating portion.

6. Conclusions

The results obtained in the two case studies presented here show that the proposed simplified frequency domain approach provides a capable tool to estimate the maximum probable wind response of the weakly nonlinear cable roof networks. Nevertheless, deterministic approaches remain the only reliable analytical method in the case of highly nonlinear cable networks. However, there should be a reasonable balance between the amount of time and effort invested and the level of the reliability of the results.

References

[1]. Buchholdt, H.A., *An introduction to cable roof structures.* Thomas Telford, 1999.
[2]. Stefanou G. D., (1992): *Dynamic response of tension cable structures due to wind loads.* Computers & Structures, 43(2), 365-372.
[3]. Ghafari Oskoei A., *Analysis of cable roof structure to dynamic loads due to wind and earthquake in frequency domain.* Master's thesis, University of Tehran, July 2006.
[4]. Guevara, McClure, G. (1993): *Nonlinear response of antenna-supporting structures.* Computers & Structures. 47 (4/5), 711-724.
[5]. ADINA R&D Inc., *ADINA User Interface Command Reference Manual*. Watertown, MA, USA, 2004.
[6]. Bathe, K. J., *Finite element Procedure*, Editor, 1996.
[7]. Wilson, E. L., *Static and dynamic analysis of structures*. Computers and structures Inc., USA, 2006.
[8]. Ghafari Oskoei, S.A., McClure, G., Kani, I.M. (2007): *Dynamic analysis of cable roofs under transient wind using a simplified frequency domain approach.* Journal of Engineering Structures, under review.

Proceedings of the 6th International Conference on
Computation of Shell and Spatial Structures
IASS-IACM 2008: “Spanning Nano to Mega”
28-31 May 2008, Cornell University, Ithaca, NY, USA
John F. ABEL and J. Robert COOKE (eds.)

Wind-induced responses of Beijing National Stadium

Qing-Shan YANG and Yu-Ji TIAN

School of Civil Engineering, Beijing Jiaotong University, Beijing 100044

Email: qshyang@bjtu.edu.cn

1 Introduction

The Beijing National Stadium (abbr. BJNS), shown in Fig. 1, is the main stadium for opening and closure ceremony of Beijing Olympic Games. It is located in the center of Beijing Olympic Park in the northern part of the city of Beijing, China. The park is approximately 8 km north of the Forbidden City. The form and appearance of BJNS looks like a nest of birds and it is also called Bird Nest.

The saddle-shaped roof of BJNS has an elliptic plan with main dimension of 320m and 280m along the North/South and East/West axes respectively. It consists of double skins of steel skeleton with translucent ETFE membrane panels on the outer roof, inner roof, inner edge and outer edge providing weather protection, shown in Fig. 2. An elliptic opening with main dimensions of 182m by 124m is located at the roof center. The stadium facades are fully open leading to an open concourse developed in six levels.

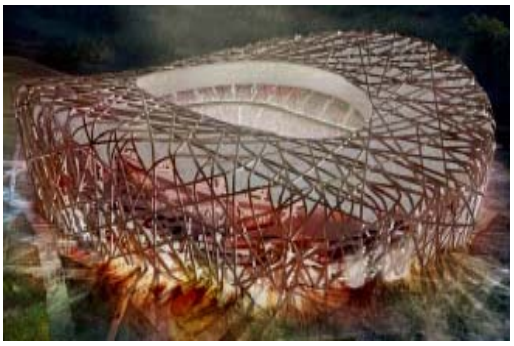

Fig. 1 Beijing National Stadium

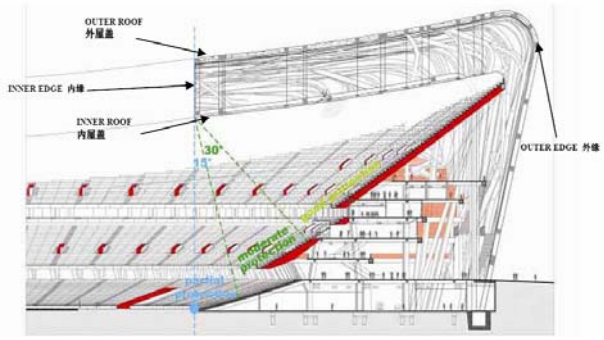

Fig. 2 Profile of BJNS roof

There are several practical methods of calculating the structural responses excited by fluctuating wind, such as the components (mean, background and resonant components) combination method, modal combination methods (modal displacement method and modal acceleration method), Ritz vector combination method and time history analysis method, while the modal displacement method is adopted comprehensively. The key problem of calculating the fluctuation responses is how to select the dominant modes and how to estimate the precision of results. With respect to the large-span roof like BJNS roof, more than one mode contributes to dynamic responses and some dominant modes are perhaps high frequency modes.

In this paper, the mode energy participation coefficients are presented in Section 2. Section 3 gives the detail of wind-induced responses for BJNS roof and Section 4 draws some conclusions.

2 Dominant Modes

The jth mode energy participation coefficient of background response is defined as follows,

$$\gamma_{b,j} = W_{b,j} / W_b \tag{1}$$

in which $W_{b,j}$ is the work expectation of jth mode background response and W_b is the work expectation of total background response.

The jth mode energy participation coefficient of resonant response is defined as follows,

$$\gamma_{r,j} = W_{r,j} / W_r \tag{2}$$

where $W_{r,j}$ is the work expectation of jth mode resonant response, i.e., the expectation of summation of kinetic energy and strain energy; W_r denotes the total energy of the concerned modes.

The mode energy participation coefficient of jth mode is

$$\gamma_j = W_j / W \tag{3}$$

where W is the total energy or work done by fluctuating wind; W_j stands for the jth mode energy.

It is necessary and important for wind-induced responses analysis to identify the dominant modes. For mode displacement method and mode acceleration method, the dominant modes can be selected according to the mode energy participation coefficients shown in Eq. (3). If the components combination method is used to analyze the fluctuating wind-induced responses, the dominant modes for background component and resonant component are identified by Eq. (1) and (2), respectively.

3 Wind-Induced Response of BJNS Roof

All wind loads were determined in accordance with the 100-year design wind pressure stipulated in Chinese Load Code (GB50009-2001) of 0.50kPa. The calculated displacement response under excitation of mean wind is shown in Fig. 3.

Based on the wind pressure time histories of the full-scale structure provided by the tunnel test, the displacement response of the fluctuating wind are calculated using three methods. The following results are the fluctuating wind-induced displacement responses for340 degree, the prevailing wind direction of Beijing city.

The first 100-mode energy participation coefficients of background response and the first 20-mode energy participation coefficients of resonant response are shown in Fig. 4 and Fig. 5, respectively. The first 100-mode energy participation coefficients are given in Fig. 6. The first 500-mode cumulative coefficients of background response and the first 20-mode cumulative coefficients of resonant response are shown in Fig. 7 and Fig. 8, respectively. The first 100-mode cumulative coefficients are given in Fig. 9. It can be seen that the first 150-mode cumulative energy coefficient for background component is greater than 95% while the first 20-mode cumulative energy coefficient for resonant component is greater than 95%; and that the first 70-mode cumulative coefficient is greater than 95%.

Fig. 10 gives the peak displacement of background component using pseudo-static method and Fig. 11 gives the first 20-mode peak displacement of resonant component. Fig. 12 is peak displacement that combines background component and resonant component. Fig. 13 shows the first 70-mode peak displacement using CQC procedure and Fig. 14 is the counterpart using mode acceleration method.

The background responses of higher modes in mode acceleration method are taken into account. If the solution using mode acceleration method is accurate, the relative errors of component combination method and mode displacement method are shown in Fig. 15 and Fig. 16, respectively. It can be indicated that component combination method, which does not consider the correlation between background component and resonant component, cannot be employed in this analysis and that mode acceleration method considering the background responses of the higher modes is more accurate than mode displacement method.

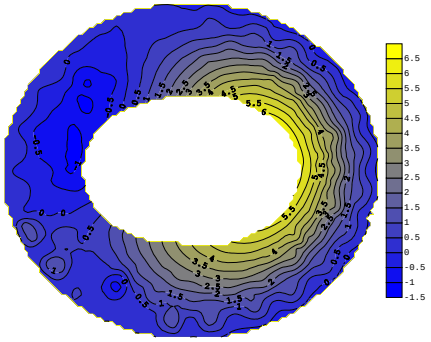

Fig. 3 Displacement under mean wind (mm)

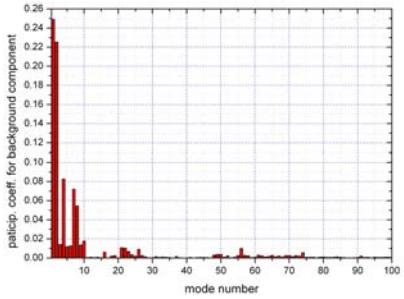

Fig. 4 First 100-mode energy coeff. of background response

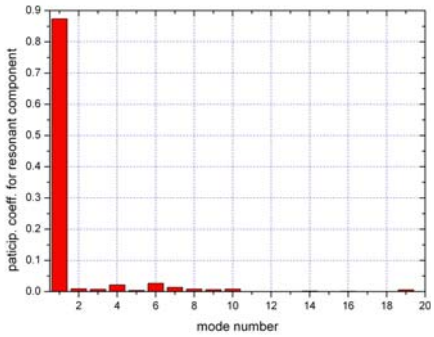

Fig. 5 First 20-mode energy coeff. of resonant response

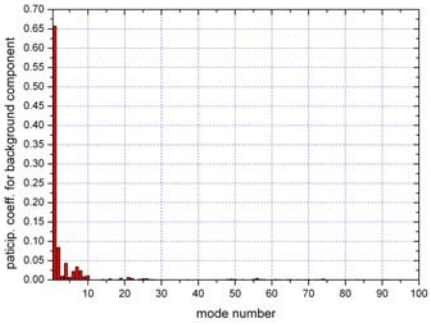

Fig. 6 First 100-mode energy coeff.

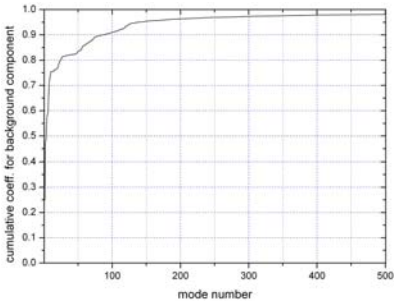

Fig. 7 First 500-mode cumulative coeff. of background response

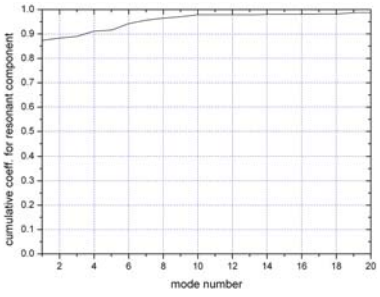

Fig. 8 First 100-mode cumulative coeff. of resonant response

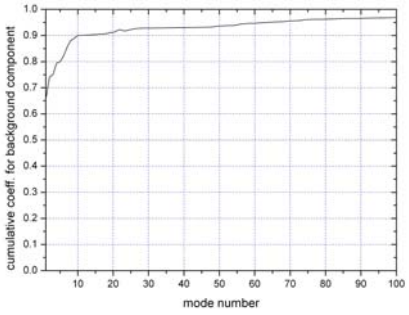

Fig. 9 First 100-mode cumulative coeff.

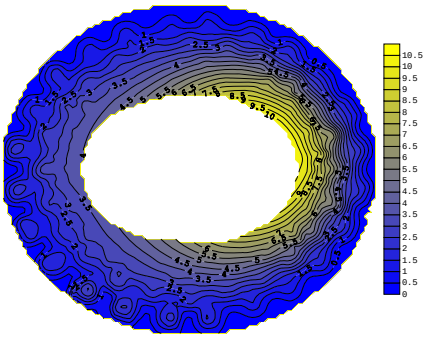

Fig. 10 Peak displ. of background response (mm)

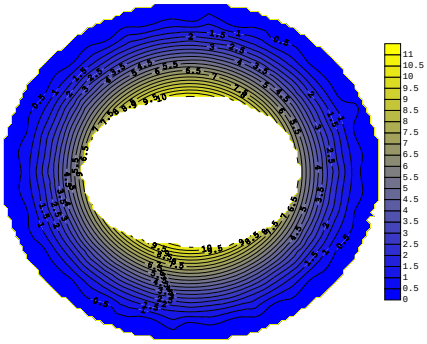

Fig. 11 Peak displacement of resonant response (mm)

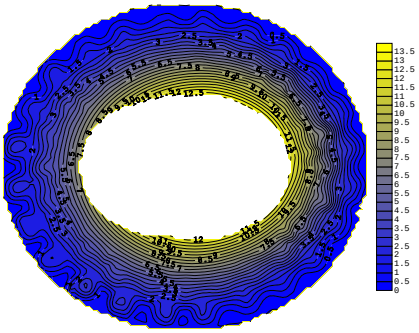

Fig. 12 Peak disp. using componet combination (mm)

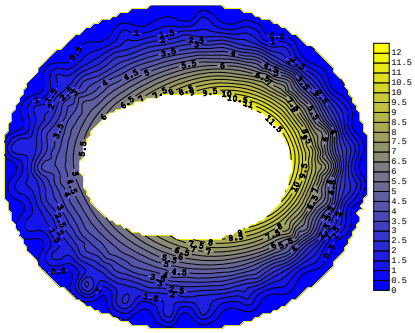

Fig. 13 Peak disp. using mode disp. method (mm)

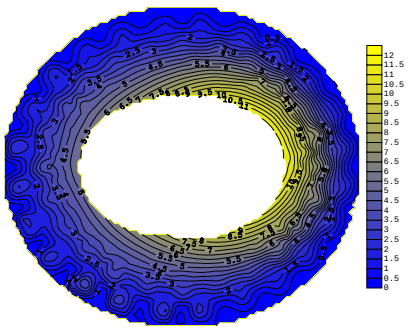

Fig. 14 Peak disp. using mode acce. Method (mm)

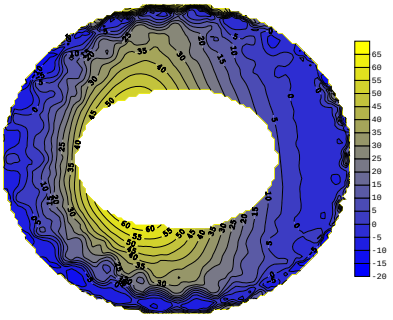

Fig. 15 Relative error between Fig. 12 and Fig. 14 (%)

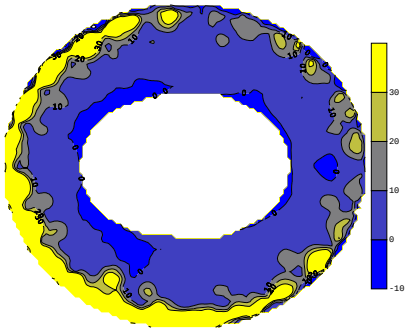

Fig. 16 Relative error between Fig. 13 and Fig. 14 (%)

4 Conclusion

In this paper, the mode energy participation coefficients are investigated to identify the dominant modes of Beijing National Stadium. Three methods of wind-induced responses analysis, component combination method, mode displacement method and mode acceleration method, are employed to analyze the fluctuating wind-induced responses.

The background responses prevail against the resonant responses and the dominant modes of background component are much greater than those of resonant component. However, the prevailing frequency of wind load is so close to the fundamental frequency of BJNS that the correlation between background response and resonant response cannot be neglected. Hence component combination method will be researched when it is used to analyze the responses of long-span space structures.

The mode displacement method is comprehensively employed in wind-induced response analysis while the accuracy of some panels where higher modes prevail may be poor. Sometimes these relative errors are neglected because the responses in these panels are very little. The background responses of the higher modes are considered in mode acceleration method by the sacrifice of the computational efficiency.

Proceedings of the 6th International Conference on
Computation of Shell and Spatial Structures
IASS-IACM 2008: "Spanning Nano to Mega"
28-31 May 2008, Cornell University, Ithaca, NY, USA
John F. ABEL and J. Robert COOKE (eds.)

Theoretical analyses for wind vibration response of reticulated shell structures

De-min WEI *, Jian-feng BIAN

*Department of Civil Engineering, South China University of Technology
Guangzhou Wushan, 510640, Guangdong, P. R. China
dmwei@scut.edu.cn

Abstract

A quasi-mode method, which takes into consideration the effect of the resonance response of the high modes, is used to calculate the wind vibration response of single-layer reticulated shells. Through analysis, it is necessary to consider the contribution of the cross-correlation of modes in order to get accurate enough results. In this paper, through the computation of detailed examples, the number of modes needed for calculating the cross-correlation contribution is determined, and certain useful results and conclusions are obtained.

1. Introduction

Due to the participation of many modes in the wind-induced vibration of reticulated shells, the contribution of two parts must be included in a response analysis of structures: the auto-correlation power and the cross-correlation power of the participating modes. Hence, the crucial problem is to find the main modes contributory to the response, as this determines the effectiveness and accuracy of the response analysis.

In this paper, the induced-wind response of the reticulated shell structures is divided into two parts: the background response and the resonance response. In order to consider the background response of the high modes, a quasi-mode is used. Because the free-vibration frequency values of consecutive tens of modes show almost no difference, it is necessary to include the contribution of the cross-correlation of modes. Through the computation of detailed examples, the number of modes needed for calculating the cross-correlation contribution is determined, and certain useful results and conclusions are obtained.

2. Composition of the wind-vibration response

According to the discretization model in the frequency-domain, the auto-correlation contribution of the ith mode to the total wind-vibration response y_i^2 can be written as:

$$y_i^2(x,y,z) = \phi_i^2(x,y,z)\sum_{k=1}^{N}\sum_{j=1}^{N}\int_0^{\infty}\left|H_i(in)\right|^2 S_{vf}^{kj}(k,j,n)d\mathrm{n} \tag{1}$$

where

$$S_{vf}^{kj}(k,j,n) = \phi_{ki}D_k R_{kj}(k,j,n)D_j S_v(n)\phi_{ji} \tag{2}$$

ϕ_i is orthogonal to the mass matrix, $\left|H_i(in)\right|$ is the modulus of the transfer function of the frequency response, N is the total freedoms of the structure, $[D]$ is the coefficient matrix of the node, R_{kj} is the correlation function of Node k and Node j, $S_v(n)$ is the horizontal component or the vertical component of the fluctuating wind velocity spectrum, n denotes the frequency of the fluctuating wind.

Since $S_{vf}^{kj}(k,j,n)$ is the attenuation function of the frequency n (as shown in Fig.1(a)) and $\left|H_i(in)\right|^2$ is a quick-changing function with a single peak (as shown in Fig.1(b)), the response y_i^2 can be regarded as the sum of the

static component and the narrow bandwidth white noise response component, i.e., the sum of the shaded areas 1 and 2 in Fig.1(c):

$$y_i^2 = \phi_i^2(x,y,z)\left(\left|H_i(0)\right|^2 \int_0^\infty S_{vf}^{kj}(k,j,n)dn + S_{vf}^{kj}(k,j,n_i)\int_0^\infty \left|H(in)\right|^2 dn\right) \tag{3}$$

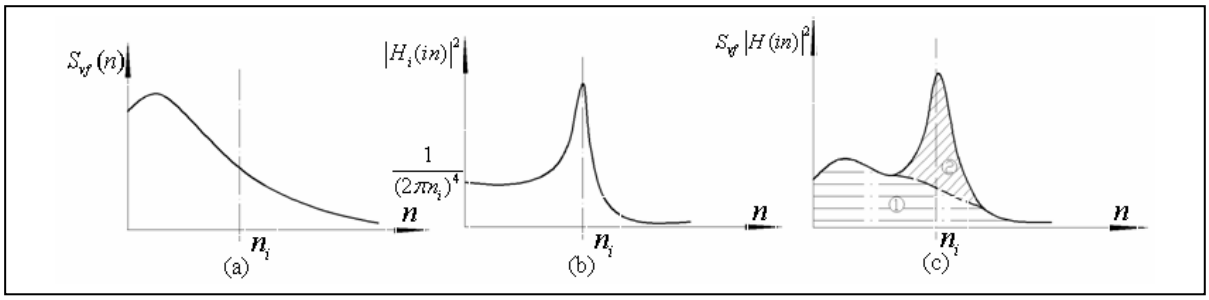

Figure 1: Background response and resonance response

A lot of calculation results show that the error the method may have does not exceed 1%(Simiu E. *et al*. [2]). In consequence, y_i can be decomposed into two parts: the background response y_{iback} and the resonance response y_{ires}:

$$y_i^2 = y_{iback}^2 + y_{ires}^2 \tag{4}$$

And

$$y_{iback}^2 = \phi_i^2 \left|H_i(0)\right|^2 \sum_{k=1}^{N}\sum_{j=1}^{N}\int_0^\infty S_{vf}^{kj}(k,j,n)dn \tag{5}$$

$$y_{ires}^2 = \phi_i^2 \int_0^\infty \left|H(in)\right|^2 dn \sum_{k=1}^{N}\sum_{j=1}^{N} S_{vf}^{kj}(k,j,n_i) \tag{6}$$

3. The background response

Actually, from equation (5), the background response is a quasi-static action on the structure, depending on the geometrical style of the structure and the characteristics of the fluctuating wind. Moreover, owing to its influence, the distribution of the total wind-vibration response is similar to that of the static wind response(Masanao Nakayama *et al*. [1]). So the first tens of consecutive modes and the static wind response can be used to find a quasi-mode, which can be used to solve the background response as an extra mode. Thus, the high modes' contributory to background response can be considered. The quasi-mode's frequency value is somewhere at the point of jump increment of the natural frequencies' values, with its background response being very large and its resonance response close to zero. Therefore, the calculation steps to solve a quasi-mode can be simplified as follows:

1) Given the mean wind load $\{\bar{f}\}$, solve the static wind displacement vector $\{\bar{X}_{st}\}$;

2) Determine the unknown high mode number N_X using $\{\bar{X}_{st}\}$ and the first n modes :

Let $n = n_0$ and then obtain the vector $\{\bar{X}_{sel}\} = \sum_{i=1}^{n_0}\phi_i q_i$, $q_i = \phi_i^T[M]\{\bar{X}_{st}\}/\phi_i^T[M]\phi_i$;

Where, $\{\bar{X}_{sel}\}$ is the displacement vector of the first n_0 modes.

The strain energy solved from (7) and (8), which can judge whether the quasi-mode has accuracy enough:

$$E_{st} = {}^T\{\bar{X}_{st}\}[K]\{\bar{X}_{st}\}/2 \tag{7}$$

$$E_{sel} = {}^T\{\bar{X}_{sel}\}[K]\{\bar{X}_{sel}\}/2 \tag{8}$$

If $E_{sel} \neq E_{st}$, then $n_0 = n_0 + 1$, and computation is to be continued as step 2) until $E_{sel} = E_{st}$. In fact, the above steps may not be necessary, because Mode N_X is located at the jump point of the increment natural frequencies.

3) Determine the selected mode number $n_0 = N_x$ and Solve the quasi-mode and its corresponding frequency f_x;

It can be shown that the response results are accurate enough when the mode number $n \geq N_X / 2$ .Thus, use equation $x = \{\bar{X}_{st}\} - \sum_{j=1}^{n} \phi_j q_j$, get the quasi-mode $\phi_x = \frac{1}{\sqrt{{}^T x[M]x}} x$ and its frequency $f_x = \frac{1}{2\pi}\sqrt{\frac{{}^T x[K]x}{{}^T x[M]x}}$.

It can be found that the natural frequency, the energy contribution and the shape distribution of the quasi-mode are all close to those of the unknown high mode. Thus, we can directly use the quasi-mode and the first n modes to compute the wind-vibration response of the structure.

4. The resonance response

Just as equation (6), the resonance response component can be regarded as a narrow bandwidth white noise response for a low damping ratio ξ, so substitute some parameters into equation (6), the resonance response is solved as equation (9):

$$y_{ires}^2 = \frac{\phi_i^2}{8\omega_i^3 \xi_i} \sum_{k=1}^{N} \sum_{j=1}^{N} S_{vf}^{kj}(k, j, n_i) \tag{9}$$

Where, n_i is the frequency of the ith mode.

5. The total wind-vibration response

Based on the deformation characteristic of single-layer reticulated shells and relevant analysis results, the following steps can be employed to select the participating modes and compute the wind-vibration response:

1) Select the first n_1 ($n_1 \leq N_X / 2$) modes and calculate the quasi-mode;
2) Calculate the auto-correlation and the cross-correlation contributions of the selected modes;
3) Calculate the resonance response of the n_2 ($n_2 > N_X / 2$) modes.

6. Numerical example analyses

Consider the wind-vibration response of a single-layer spherical reticulated shell. The structural parameters are given in Fig.2: the span and the height of the simple supported shell are $L = 40$m/s and $f = 8$m , respectively. The supports height from the ground is $h = 10$m . The damping ratio is $\xi = 0.02$. The horizontal wind velocity spectrum is Davenport Spectrum. The arrangement of the nodes and the elements is shown in Fig.3. The numbers of the nodes and the elements are 217 and 600, respectively.

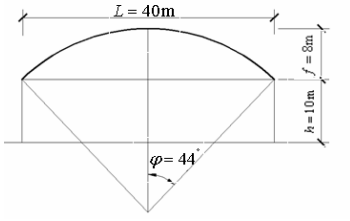

Figure 2: The section line of the shell

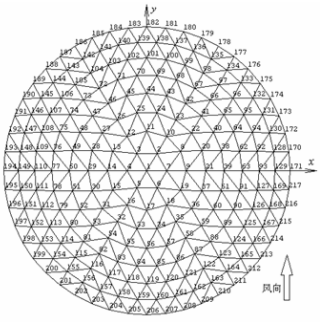

Figure 3: The arrangement of nodes and element

In this example, the first 169 modes are taken in the response analysis of a single-layer reticulated shell, because the frequency jump occurs in the169th mode. The contribution of the first 20 modes is shown in Fig.4. The contribution of the 169th mode is the largest and after the 169th mode, the contribution is close to zero. We have used the quasi-mode method to calculate the wind-vibration response under the following respective cases: 10+quasi-mode, 40+quasi-mode, 70+quasi-mode and 85+quasi-mode; all taking into account the resonance

compensation of modes. The frequencies of the X-mode and the 169th mode for different cases are listed in Table 1. It can be seen that the frequency and the mean strain energy contribution of the quasi-mode(X-mode) approach the true value of the high mode with the increase of the number of mode selected in calculating the quasi-mode. Therefore, as long as enough modes are selected, the quasi-mode can take the place of the real high mode in the computation of the wind-vibration response. Even if modes are selected not enough, the quasi-mode can still express the static response shape better than the real high mode. The vertical displacement response of the nodes along the X-axis is given in Fig.5. If the displacement response in CQC method with the first 169 modes can be regarded as the accurate response, the accuracy of the quasi-mode method rises with the gradually increasing mode number n. When n is equal to 85, there is little difference between the solution by the quasi-mode method and the accurate response.

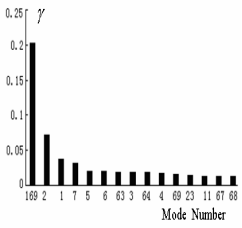

Figure 4: The energy contribution ratio γ_i

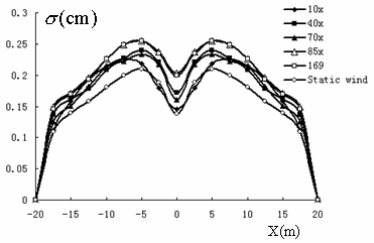

Figure 5: The displacement of nodes along X-axis

Mode number	10+Xmode	40+Xmode	70+Xmode	85+Xmode	169
Natural frequency f / Hz	5.2166	5.4259	5.4505	5.4676	5.48175
Mean strain energy $\bar{E}_i$ / N•m	15.8693	---	---	14.5938	14.1105

Table 1: The difference between the true high mode and the quasi-mode(X-mode)

7. Summary

From the above analyses for the numerical example, the following conclusions are made:

1) The total wind-vibration response is composed of two parts: the background response and the resonance response. There usually exists a mode whose contribution to the total response is the largest. This mode is located at the catastrophic point of the structural frequency.

2) The quasi-mode method adds a quasi-mode to the first n modes in computing the total wind-vibration response. At the same time, it takes into consideration the effect of the resonance response contribution of the high modes.

3) The cross-correlation contribution influences the distribution of the total response, therefore the cross-correlation contribution of the first $N_X / 2$ modes must be considered.

4) The computational results of the nodal displacement, the axial force of elements and the equivalent wind load are accurate enough for the structural design.

Acknowledgement

The authors wish to thank the Natural Science Foundation of Gongdong Province (Project 020940) for providing the financial support for this investigation.

References

[1] Masanao Nakayama, Yasuhito Sasaki, Keiji Masuda, et al. An efficient method for selection of vibration modes contributory to wind response on dome-like roofs. *Journal of Wind Engineering and Industrial Aerodynamics* 1998;73:357-366.

[2] SimiuE, ScanlanRH. Wind effects on structure (3nd edn). New York: John Wiley & Sons, 1996.